Experimental and Theoretical Studies of van der Waals Molecule Photodissociation

Thesis by

Sally Reid Hair

In Partial Fulfillment of the Requirements

for the Degree of

Doctor of Philosophy

California Institute of Technology

Pasadena, California

1988

(Submitted May 3, 1988)

Acknowledgments

Many people have helped me to reach the point of writing this thesis, but I would especially like to thank those involved in the projects described here. My advisor, Ken Janda, has contributed innumerable ideas to the work in this thesis. Both his patience and his impatience deserve my thanks. The calculations in Chapter 2 were performed in collaboration with Alberto Beswick. I would like to thank Alberto for his encouragement, as well as for his patient explanations. The CO_2 laser used in Chapter 3 was cheerfully supplied by Jack Beauchamp. Tom Dunn's assistance was indispensable in completing the experiments of Chapter 3. The work performed in Chapter 4 was a joint effort with Joe Cline and Craig Bieler. Their help was invaluable both in performing and in interpreting the experiment. Rob Coalson kindly allowed me the use of his laser printer to print this thesis. Above all, I thank my husband, Brian, for his unceasing scientific, computational, secretarial, and moral support.

Abstract

Three studies are reported on the vibrational predissociation of polyatomic van der Waals complexes. In the first, the ethylene dimer and rare gas-ethylene complexes are treated theoretically, using a local mode quantum mechanical technique. The ethylene dimer exhibits extensive mixing between the initially excited υ_7 vibration and nearby combinations of the υ_{10} and van der Waals vibrations, while the rare gas-ethylene complexes do not. Mixing is extensive enough in the ethylene dimer to spread the oscillator strength of the υ_7 vibration over a 10 cm^{-1} region of the spectrum, in agreement with the experimentally observed band.

The second study is a low resolution photodissociation experiment on the ethylene-methane complex. The spectra observed by exciting the υ_7 ethylene vibration of C_2H_4-CH_4, C_2H_4-CH_2D_2, and C_2H_4-CD_4 all exhibit the same width. This indicates that the shapes and widths of the observed spectra are not determined by unresolved or power-broadened rotational structure. This result underscores the importance of vibrational coupling in the dissociation process.

The final study is a laser pump-probe experiment on the Ne_2Cl_2 and Ne_3Cl_2 complexes. The Ne_2Cl_2 complex has a distorted tetrahedral geometry, as determined from high

resolution, excitation spectra. Excitation shift arguments suggest a structure for Ne_3Cl_2 with the three neon atoms encircling the Cl_2 bond axis. The total van der Waals bond energy of the Ne_2Cl_2 complex is found to be between 145.6 and 148.6 cm^{-1}. When energetically possible, the Ne_2Cl_2 complex can dissociate by losing a single quantum of Cl_2 stretching energy. This indicates that the two neon atoms do not dissociate by two independent "half-collisions." The Cl_2 fragment rotational excitation is found to depend only weakly on the energy available to the fragments.

Table of Contents

List of Figures

Chapter 2.
A Local Mode Quantum Mechanical Treatment of
Ethylene Complex Infrared Photodissociation Spectra

Chapter 3.
The Infrared Photodissociation of C_2H_4-CH_4

Chapter 4.
The Structure and Dissociation Dyanmics of Ne_2Cl_2

List of Tables

Chapter 2.
A Local Mode Quantum Mechanical Treatment of
Ethylene Complex Infrared Photodissociation Spectra

Chapter 3.
The Infrared Photodissociation of C_2H_4-CH_4

Chapter 4.
The Structure and Dissociation Dyanmics of Ne_2Cl_2

Chapter 1

Introduction

Studies of small molecular complexes can provide detailed information about both the nature of the binding interaction and the process of bond dissociation. In the first instance, the intermolecular forces determine the geometry and binding energy of a complex. In the second instance, learning about the details of weak bond dissociation can aid in understanding the vibrational energy transfer within the complex, which leads to its fragmentation.

The work presented in this thesis examines the dissociation of several weakly bound polyatomic complexes. For the larger molecules discussed in Chapters 2 and 3, information is primarily obtained about the vibrational energy transfer within the complex. Chapter 2 describes a local mode quantum mechanical calculation that models vibrational energy transfer in ethylene dimer and rare gas-ethylene molecules. Chapter 3 reports a low-resolution, infrared photodissociation spectrum of ethylene-methane complexes. Chapter 4 describes an investigation of a smaller molecule, Ne_2Cl_2, using a high-resolution, laser pump-probe technique. For this complex, information is obtained about the structure and bonding, as well as the details of the dissociation process.

van der Waals complexes such as these are bound together by weak forces with electrostatic origins.[1] For molecules that have a permanent dipole or quadrupole moment, dipole-dipole or higher order interactions account for some part of the long-range attraction. In addition, the interaction of a permanent dipole of one component of the complex with the polarizable electron cloud of a binding partner causes attractive induction forces. Finally, dispersion forces contribute to long-range attraction between both polar and nonpolar molecules. This force arises from the correlation of the fluctuating electron density of two molecules. These attractions result in longer bond lengths and smaller bond energies than typical chemical bonds. For example, the attraction between two neon atoms has an energy of 0.3 kJ/mole and a distance of 3.1 Å.[1] The bonding in this case is due entirely to dispersion forces. For the case of the HCl dimer, the bond energy is estimated to be 2.1 kJ/mole, with 86% of the interaction due to dispersion, 4% due to induction, and 10% due to dipole-dipole interaction.[1] A much stronger interaction is observed between two highly polar water molecules, where the dipole-dipole interaction contributes most of the estimated 20 kJ/mole bond energy.[1]

The weakness of the attractive forces that hold van der Waals complexes together makes them interesting systems for studying vibrational energy transfer within

molecules. In most cases, the binding energy of a complex is less than the energy spacing between vibrational levels of the component molecules. Thus, if one component is vibrationally excited, the complex has more than enough energy to dissociate. When enough energy moves from the initially excited vibration to the vibrations of the weak bond, dissociation occurs. Monitoring vibrational predissociation provides a direct probe of the vibrational energy transfer in the complex. The weakness of the van der Waals bond is also advantageous in theoretical work. The large difference in vibrational frequency of the van der Waals and covalent bonds allows them to be treated separately,[2] in a fashion analogous to the Born-Oppenheimer separation of nuclear and electronic motions. A similar separation can also be applied to the different van der Waals vibrations.[3]

Experimental studies of van der Waals complex vibrational predissociation have revealed a tremendous variety of dynamical behavior. The dissociation dynamics of simple triatomic complexes has been investigated in detail and shows effects that include direct vibrational to translational energy transfer,[4] rotational rainbows,[5] and quantum interference.[6] For larger molecules with more than one covalent bond vibrational mode, the complex dissociation time varies, depending on which mode is excited.[7] For complexes containing many atoms or

molecules, liquid-like behavior and phase transitions are observed.[8] The studies in this thesis explore the behavior of intermediate size complexes, containing from four to twelve atoms. While their behavior is perhaps more complicated than that of triatomic complexes, they are small enough that a fairly complete understanding can be achieved.

One of the most controversial polyatomic complexes is the ethylene dimer, studied in Chapter 2. The most recent experimental results firmly establish that the ethylene dimer dissociates on two radically different time scales.[9] Exciting the υ_7 out-of-plane hydrodgen bending motion of ethylene dimer gives an infrared photodissociation spectrum, which contains both very narrow features (3.5-6.5 GHz) and a very broad band (10-12 cm^{-1}). These features correspond to complex lifetimes of 10 ns and $\lesssim$ 1 ps.

In Chapter 2, the dissociations of ethylene dimer and rare gas-ethylene molecules are treated using a local mode quantum mechanical technique. This method includes vibrational relaxation, not previously considered quantitatively, to account for both the rapid and the slow dissociation processes observed for ethylene dimer. By calculating energy levels for the van der Waals vibrations and computing the mixing between them and the initially excited υ_7 vibration, a spectrum can be obtained. For the

rare gas-ethylene molecules, vibrational mixing does not affect the calculated spectrum. For ethylene dimer, however, the mixing between vibrations is extensive and spreads the oscillator strength of the υ_7 vibration over a 10 cm^{-1} region. This agreement with the experiment supports the proposed vibrational mixing and leads to new ideas for explaining the dissociation of ethylene dimer on two very different timescales.

In Chapter 3, the low-resolution, infrared photodissociation spectra of ethylene-methane and its deuterated analogues are measured and compared. By substituting deuterium for hydrogen on the methane component of the complex, the density of vibrational and rotational states of the complex is changed without changing the binding interaction or the coupling terms of the potential energy function. The low-resolution spectra of C_2H_4-CH_4, C_2H_4-CD_4, and C_2H_4-CH_2D_2 are nearly identical in width. This indicates that the ~3 cm^{-1} bandshape observed does not result from unresolved or power-broadened rotational structure. It also suggests that resonances between specific rovibrational states are not responsible for the bandshape. This result supports the importance of vibrational coupling mechanisms proposed in Chapter 2.

Chapter 4 presents experiments on the simpler molecules, Ne_2Cl_2 and Ne_3Cl_2. Using a high-resolution,

laser pump-probe technique, detailed information can be obtained about the complex dissociation on the excited B electronic surface. Energy is added to the Cl_2 stretching vibration of the complex with a pump laser pulse. The rotational and vibrational states of the Cl_2 dissociation fragment are then determined by the probe laser. For Ne_2Cl_2, high-resolution excitation spectra are analyzed to determine a distorted tetrahedral structure for the complex. While a precise structural determination is not possible for Ne_3Cl_2, an excitation band-shift argument predicts a structure with the three neon atoms circling the Cl_2 bond axis. Probing the Cl_2 fragments of the Ne_2Cl_2 dissociation yields a bond energy of approximately 1.8 kJ/mole. Surprisal analysis is applied to the fragment rotational state population distributions, showing that they are "colder" than a random distribution with no dynamical constraints. The Ne_2Cl_2 complex can dissociate by losing a single quantum of Cl_2 stretching energy. This shows that the two neon atoms do not dissociate by independent "half-collisions," each taking one quantum of Cl_2 vibrational energy. Finally, the observation of $NeCl_2$ dissociation fragments illustrates the importance of a sequential reaction mechanism.

References

[1] For a complete description of intermolecular forces see: G.C. Maitland, M. Rigby, E.B. Smith and W.A. Wakeham, *Intermolecular Forces: Their Origin and Determination* (Oxford University Press, Oxford, 1987).

[2] N. Halberstadt, J.A. Beswick, and K.C. Janda, *J. Chem. Phys.* **87**, 3966 (1987); B.P. Reid, K.C. Janda, and N. Halberstadt, *J. Phys. Chem.* **92**, 587 (1988).

[3] S.L. Holmgren, M. Waldman, and W. Klemperer, *J. Chem. Phys.* **67**, 4414 (1977); J.M. Hutson, D.C. Clary, and J.A. Beswick, *J. Chem. Phys.* **81**, 4474 (1984); A.C. Peet, D.C. Clary, and J.M. Hutson, *Chem. Phys. Let.* **125**, 477 (1986); Chapter 2 of this thesis.

[4] D.H. Levy, *Adv. Chem. Phys.* **47**, 323 (1981).

[5] J.C. Drobits, J.M. Skene, and M.I. Lester, poster presentation, Conference on the Dyamics of Molecular Collisions; July, 1987, Wheeling, WV.

[6] J.I. Cline, Ph.D. Thesis, California Institute of Technology, 1988; J.I. Cline, B.P. Reid, D.D. Evard, N. Sivakumar, N. Halberstadt, and K.C. Janda, manuscript in preparation.

[7] M.P. Casassa, A.M. Woodward, J.C. Stephenson, and D.S. King, *J. Chem. Phys.* **85**, 6235 (1986).

[8] See, for example: T.E. Gough, D.G. Knight, and G. Scoles, *Chem. Phys. Let.* **97**, 155 (1983); F.G. Celii and K.C. Janda, *Chem. Rev.* **86**, 507 (1986); J. Bösiger and S. Leutwyler, *Phys. Rev. Let.* **59**, 1895 (1987); D. Eichenauer and R.J. LeRoy, *J. Chem. Phys.* **88**, 2898 (1988).

[9] U. Buck, Ch. Lauenstein, A. Rudolph, B. Heijmen, S. Stolte, and J. Reuss, *Chem. Phys. Let.* **144**, 396 (1988).

Chapter 2

A Local Mode Quantum Mechanical Treatment of Ethylene Complex Infrared Photodissociation Spectra

Abstract

An approximate local mode description of van der Waals vibrations is presented. Using a model atom-atom potential, this calculation examines the mixing of the ethylene υ_7 vibration with a set of background vibrational levels, consisting of combinations of the van der Waals vibrations and the ethylene υ_{10} vibration. The ethylene dimer exhibits extensive vibrational mixing, while the rare gas-ethylene molecules do not. For the ethylene dimer, calculated linestrengths produce a complex spectrum of vibrational lines that span a 10 cm^{-1} region, in agreement with the experimental spectrum. This result suggests new explanations for the coexistence of broad and narrow lines in the ethylene dimer υ_7 dissociation spectrum.

2.1 Introduction

In recent years the vibrational predissociation of ethylene dimer has been a controversial topic of experimental and theoretical research. Low-resolution dissociation spectra of ethylene dimer have been measured by several groups.[1,2] In these experiments the out-of-plane hydrogen bending vibration, υ_7, of one ethylene component is excited by a line-tunable CO_2 laser with a resolution of ~ 2 cm^{-1}. Since the energy of the υ_7 vibration (949 cm^{-1}) is greater than the energy of the van der Waals bond, the complex dissociates. The extent of complex dissociation is monitored by either a mass spectrometer or a bolometer, as a function of the excitation frequency, to obtain a dissociation spectrum. The observed low-resolution spectrum consists of a 10-12 cm^{-1} band (FWHM) that was originally thought to be a single homogeneously broadened line. The lifetime associated with this broad bandshape is less than 1 ps, much shorter than theoretical predictions for the lifetime of the dimer excited in the υ_7 mode[3] and shorter than the linewidth-derived lifetimes of other van der Waals molecules,[4] including other ethylene-containing complexes.[5,6] This observed spectrum is also different from the dissociation spectrum of the ethylene dimer excited in other vibrational modes.[7] It has been

suggested that this rapid relaxation results from efficient coupling to excited rotational channels of the fragments[8,9] or a rapid redistribution of vibrational energy prior to dissociation.[10]

The interpretation of the ethylene dimer spectrum became more controversial with the publication of high-resolution spectra.[11,12] A recent high-resolution study by Heijmen, *et al.*[13] examined changes in the spectrum with beam source pressure and temperature. This experiment used a CO_2 laser that scans 230 MHz about each CO_2 laser transition with 1 MHz resolution. These small, high-resolution sections of the spectrum reveal sharp lines superimposed on the 10 cm^{-1} band. The linewidths range from 3.5 to 6.5 MHz and are observed within the tuning range at six laser transitions, corresponding to a 5 cm^{-1} section of the 10 cm^{-1} band. Structure was also observed in a weak feature 34 cm^{-1} to the blue of the main peak. This feature is attributed to a combination band of the ethylene ν_7 with a stretch or bend of the van der Waals bond.

It has been proposed that the broad background in the ethylene dimer dissociation spectrum arises from dissociation of clusters larger than the dimer.[14] Experiments by Huisken, *et al.*[14] have used crossed molecular beam scattering with helium atoms, to distinguish between dissociation of the dimer and larger

clusters. The low-resolution experiment confirms that the dimer spectrum contains a broad component. The width of the spectrum changes little when contributions from larger clusters are included. Using a high-resolution laser in a crossed molecular beam experiment confirms that both the sharp lines and the broad background arise from the dissociation of the dimer.[15] No sharp lines are observed in the dissociation spectra of larger clusters.

The superposition of sharp lines on a broad background in the ethylene dimer dissociation spectrum has created a stimulus for new theoretical work on this molecule. Quantum mechanical calculations have recently been performed on the ethylene dimer as well as on other systems using several different methods. For smaller molecules, such as triatomics, a fairly complete theoretical description is possible.[16] For larger molecules, only more approximate methods are feasible. Ethylene dimer[3] and the rare gas-ethylene complexes[17] have been modeled using an azimuthal and vibrational close-coupled, rotational, infinite-order sudden method (AVCC-IOS).[18] In this approximation, the low-frequency vibrational motion correlating to end-over-end rotation is fixed, while the higher-frequency azimuthal motion about the C-C axis couples to the van der Waals stretch and the normal mode vibrations of the ethylene monomer. Dissociation spectra of larger complexes have also been

modeled using theory adapted from the field of radiationless transitions. Gentry[19] has used the theory of Bixon and Jortner[20] to discuss dissociation spectra for general cases. Complexes between aromatic compounds and rare gas atoms have also been studied using this approach.[21]

This paper models the ethylene dimer and the rare gas-ethylene complex dissociation spectra, including all van der Waals motions. Treating each motion as a separate local mode, we calculate the energy levels of the resulting one-dimensional potential energy functions. The density of van der Waals states at energies close to the initially excited υ_7 level can be estimated, and matrix elements between the states calculated. Finally, line strengths for transitions to calculated levels can be determined. The following section outlines the method used in the calculation, while Section 2.3 presents the results. Section 2.4 discusses how the results for the dimer compare to those for the rare gas-ethylene complexes and how each compares to the experimental observations. Finally, we use the results of this calculation to suggest possible interpretations of the ethylene dimer spectrum.

2.2 Method

The ethylene-containing van der Waals complexes are initially excited in the υ_7 vibrational mode, with no excitation of the van der Waals vibrations. At this point two different dissociation mechanisms can be considered. In a direct dissociation, the optically prepared state decays directly into a dissociative continuum corresponding to two ethylene fragments, each in the ground vibrational state. The AVCC-IOS calculations on the ethylene dimer indicate that this direct mechanism would not result in fast enough dissociation to produce the broad component of the dimer dissociation spectrum, however.[3] An alternative, indirect mechanism involves an intermediate set of vibrational states, which provides a pathway from the optically prepared level to the dissociative continuum. Figure 2.1 shows the details of an indirect dissociation model similar to that proposed by Gentry.[19] The intermediate states are composed of combinations of low-frequency vibrations involving the van der Waals bond and the lowest-frequency ethylene normal mode, υ_{10}, at 826 cm^{-1}, 123.3 cm^{-1} lower in energy than the υ_7 mode. In this description, only the initially excited υ_7 mode carries oscillator strength from the ground state. The manifold of intermediate vibrational

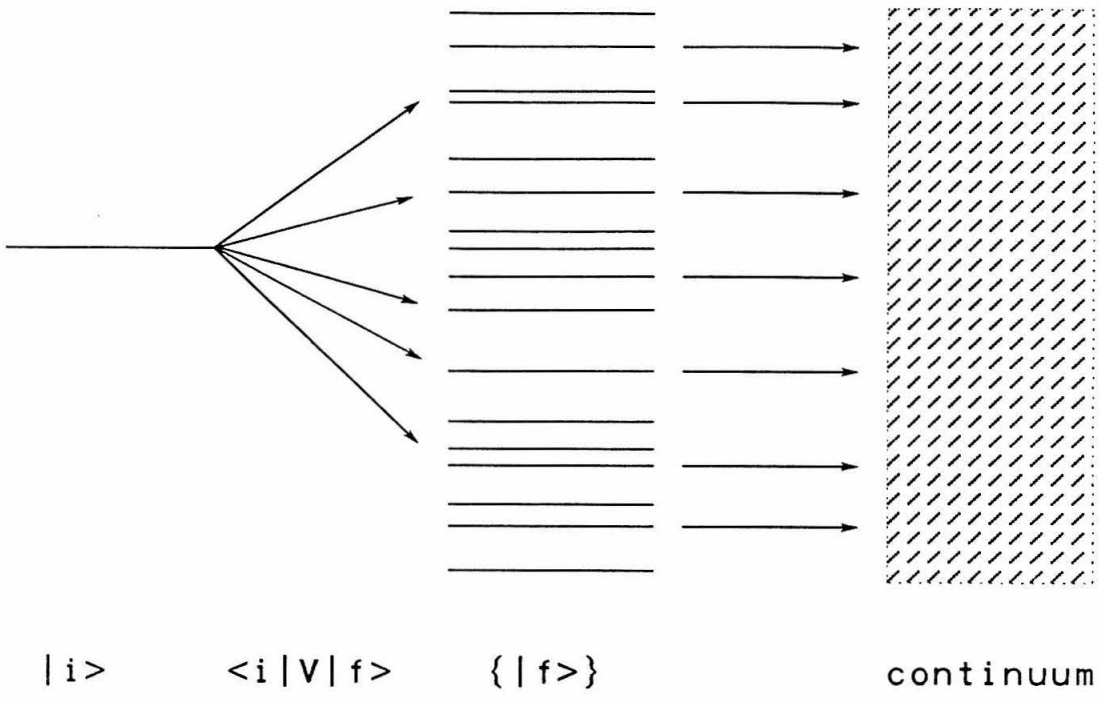

Figure 2.1. Indirect model for complex dissociation. The initial state, $|i\rangle$, is the ethylene υ_7 excitation. The final states, $\{|f\rangle\}$, are combinations of the ethylene υ_{10} mode and van der Waals vibrations. These zero-order states are coupled by the intermolecular potential, V. The coupling between the $\{|f\rangle\}$ states and the continuum results in dissociation.

states cannot be excited directly. This indirect model is used in this calculation.

The potential between the ethylene molecules introduces coupling between the initially excited state, denoted $|i\rangle$, and the manifold of vibrational states, denoted $\{|f\rangle\}$. In Figure 2.1, these couplings are denoted $\langle i|V|f\rangle$. For the indirect mechanism, it is assumed that the couplings between $|i\rangle$ and $\{|f\rangle\}$ are greater than the coupling between $|i\rangle$ and the dissociative continuum. Termed zero-order states, $|i\rangle$ and $\{|f\rangle\}$ are eigenfunctions of the zero-order Hamiltonian, which does not include the intermolecular coupling. The system can also be described as a set of linear combinations of $|i\rangle$ and $|f\rangle$ states. These linear combinations are eigenfunctions of the full Hamiltonian (see Section 2.2.4). The terminology best used to describe this mechanism is discussed in Section 2.4.2.

The first step of the calculation is to determine the energies of the $|f\rangle$ states. The large number of van der Waals degrees of freedom of the ethylene dimer precludes a calculation that includes the interactions among all the vibrational modes. Instead, each vibration involving the van der Waals bond is treated separately, while holding the other coordinates fixed at equilibrium. Solving the Schrödinger equation, using each of the resulting one-dimensional potentials, yields the local

mode energy levels. The energy levels for the different van der Waals coordinates are then combined with the energy of the ethylene monomer υ_{10} vibration to estimate the number of vibrational states available in the 12 cm^{-1} range of the observed υ_7 dissociation spectrum. Next, the coupling between the initially excited υ_7 vibration and the combinations of the calculated van der Waals vibrational levels and the υ_{10} vibration are calculated to obtain line strengths for individual transitions. This section discusses the different van der Waals vibrational modes, the potential energy functions and energy level calculations, the matrix element calculations, and finally, the calculation of the dissociation spectra.

2.2.1 Vibrational Modes

Representations of the υ_7 and υ_{10} normal modes of ethylene monomer are illustrated in Figure 2.2. Figure 2.3a depicts the rare gas-ethylene coordinate system. In this figure, the upper case axis labels refer to the coordinate frame of the complex and the lower case labels denote the principal axes of the uncomplexed ethylene molecule. The two frames are related by a coordinate transformation using the angles θ, φ, and ζ.[22] The angles φ and ζ range from 0 to 2π, while θ ranges from 0 to π. For the rare gas-ethylene equilibrium structure,

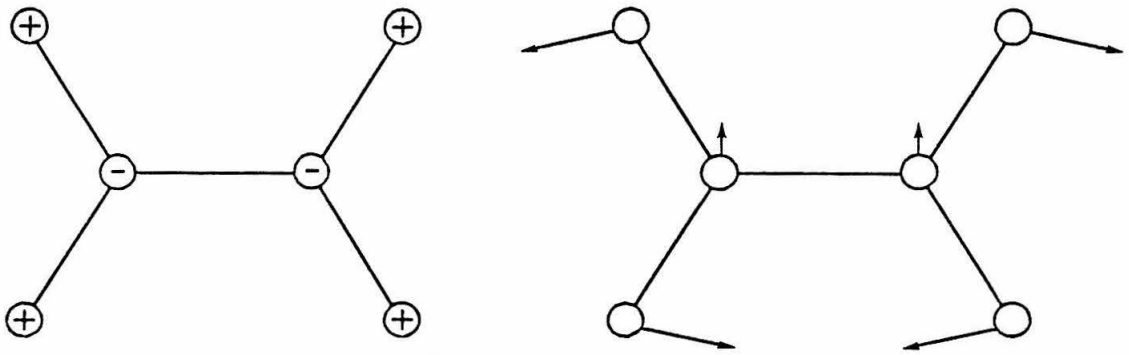

Figure 2.2. Ethylene υ_7 and υ_{10} normal mode vibrations.

Figure 2.3. Coordinate system and vibrations for rare gas-ethylene molecules. In (a), the θ, φ, and ζ angles describe the transformation between the reference frame of the complex (XYZ) and the reference frame of the ethylene molecule (xyz). The three vibrations involving the van der Waals bond are shown in (b).

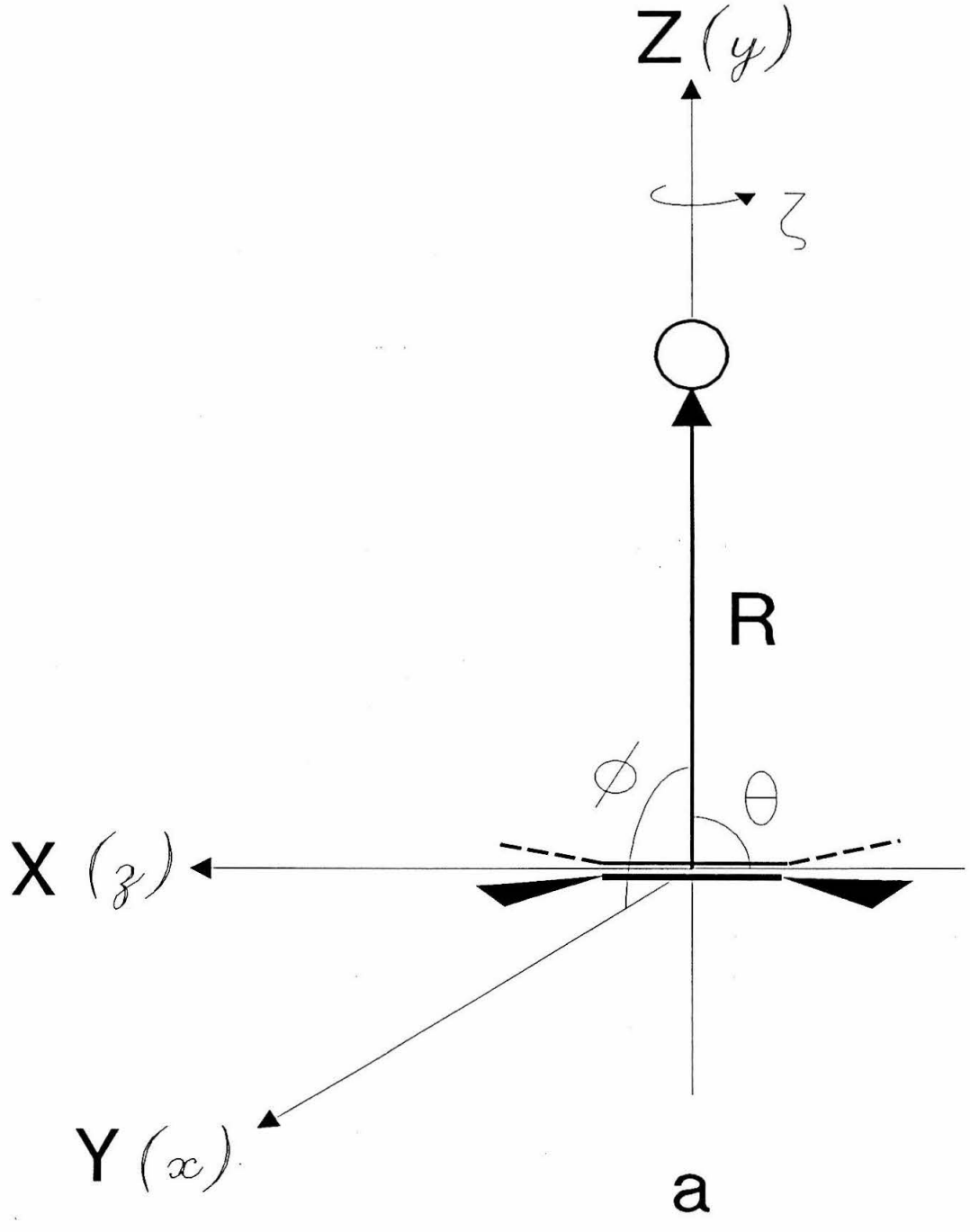
Z (y)
ζ
R
ϕ
θ
X (z)
Y (x)
a

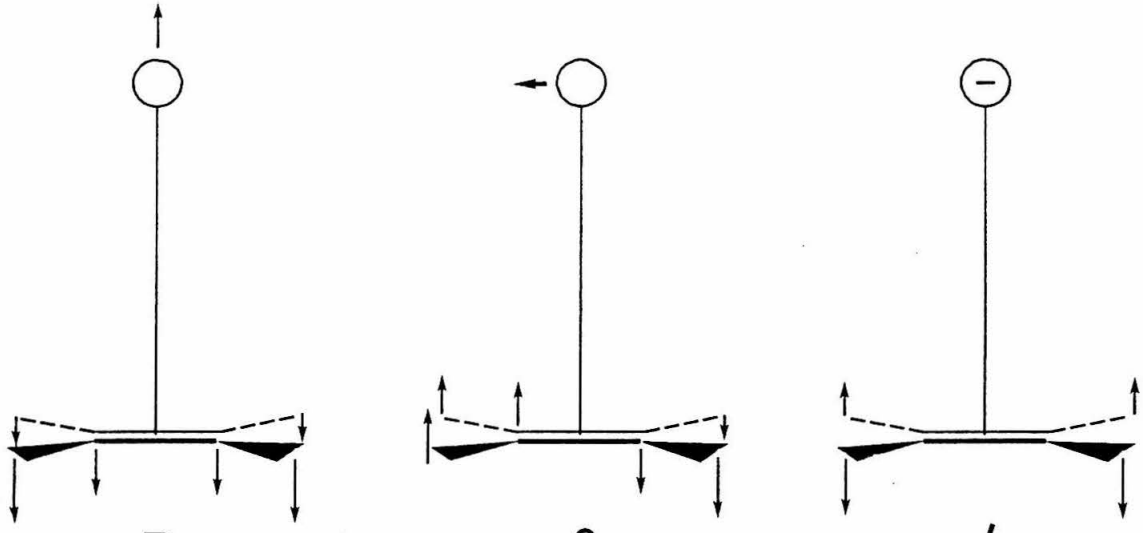

b

θ and φ are both 90°. Change in ζ corresponds to overall rotation of the complex in this case, and is not considered here. The three vibrational modes involving the van der Waals bond are shown schematically in Figure 2.3b. These are the stretch along R and bends associated with θ and φ.

The coordinate system and vibrational modes of the ethylene dimer are shown in Figure 2.4. In Figure 2.4a, the upper case axis labels refer to the reference frame of the complex, while the lower case labels refer to the two ethylene reference frames. θ_1, θ_2, φ_1, and φ_2 are the angles between each ethylene reference frame and the reference frame of the complex; ζ describes the twist between the two ethylene frames. There are six vibrational modes involving the van der Waals bond, as shown in Figure 2.4b. In addition to the stretch along R, there are four bending modes, θ_a, θ_s, φ_a, and φ_s, and a torsional motion about R, ζ. In the symmetric θ and φ modes,

$$\theta_s = \tfrac{1}{2} (\theta_1 + \theta_2)$$
$$\varphi_s = \tfrac{1}{2} (\varphi_1 + \varphi_2),$$

both ethylene units rotate in the same direction. In the

Figure 2.4. Coordinate system and vibrational modes of ethylene dimer. In the coordinate system shown in (a), θ_1 and φ_1 relate the frame of one ethylene monomer ($x_1 y_1 z_1$) to the complex frame (XYZ). Similarly, θ_2 and φ_2 relate the frame of the second ethylene monomer to the complex frame. The angle ζ describes the twist between the two monomer reference frames. For clarity, the x_1, x_2, y_1, y_2, X, and Y axes are not shown. Figure 2.4(b) shows the six dimer vibrations involving the van der Waals bond.

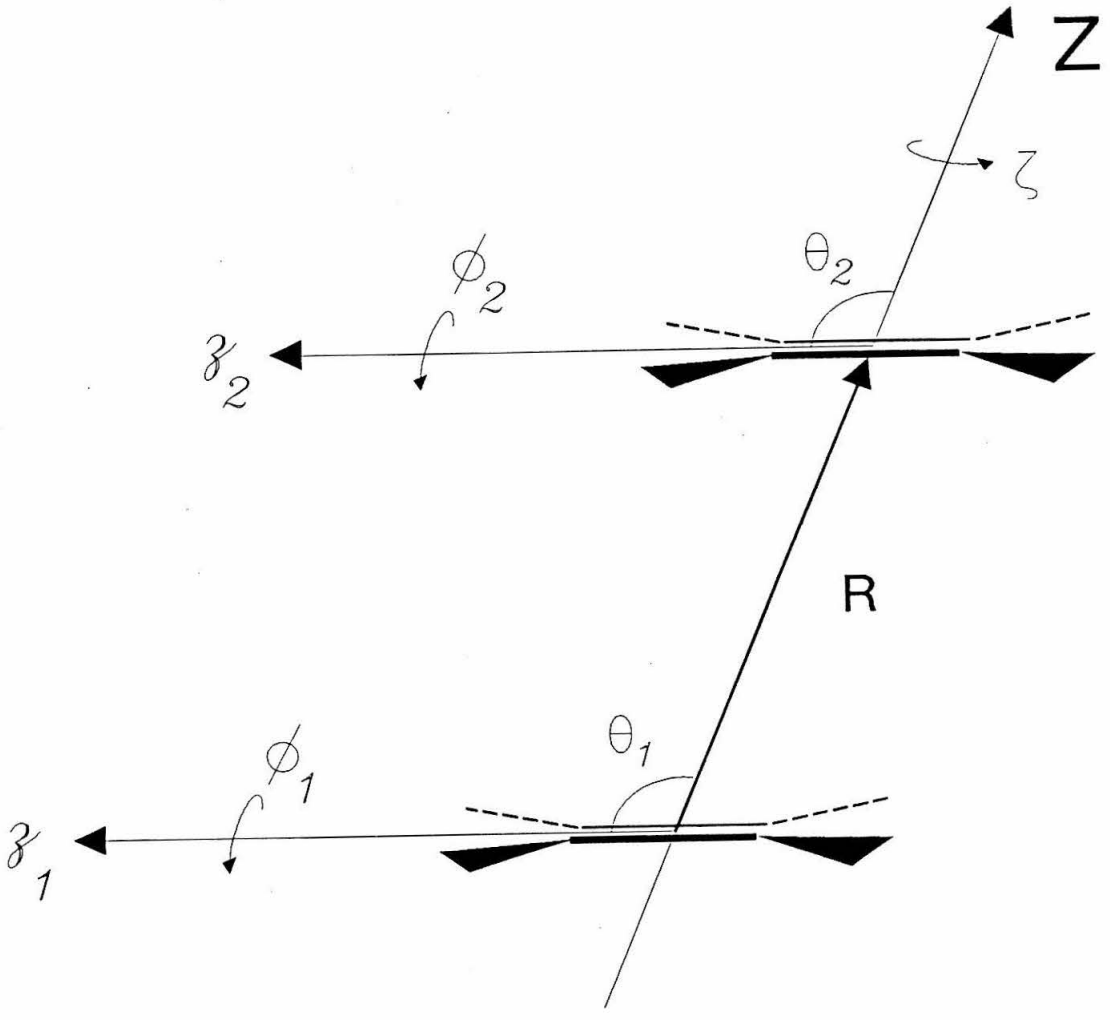

a

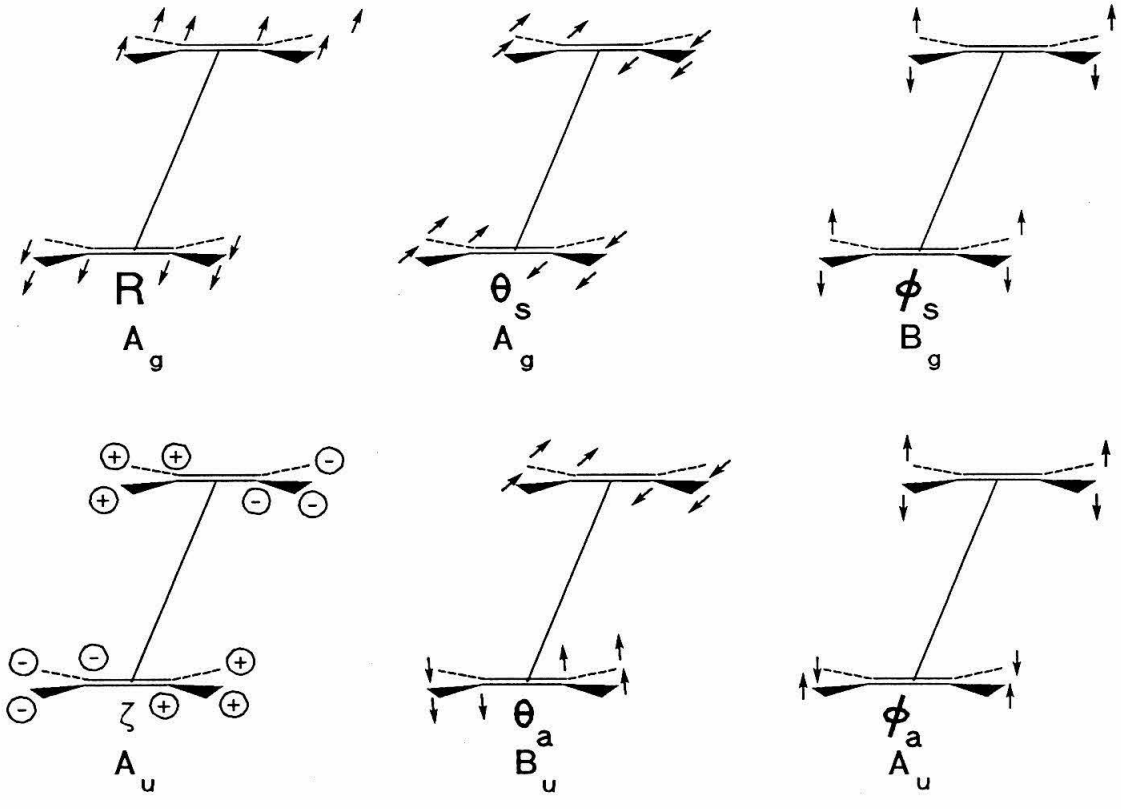

b

asymmetric modes,

$$\theta_a = \tfrac{1}{2} (\theta_1 - \theta_2)$$
$$\varphi_a = \tfrac{1}{2} (\varphi_1 - \varphi_2),$$

the ethylene monomers rotate in opposite directions.

The symmetry of the vibrations is important in the calculation of the coupling matrix elements (see Section 2.2.3). The rare gas-ethylene molecules have C_{2v} symmetry. In this point group, the ethylene υ_7 vibration is in the A_1 representation, while the υ_{10} mode is in the B_2 representation. The symmetry species of the three van der Waals vibrations are given in Figure 2.3b. The ethylene dimer equilibrium structure has C_{2h} symmetry. In this point group, the υ_7 vibration transforms as B_u, while the υ_{10} mode transforms as A_u. The symmetry species of the six van der Waals vibrations of the dimer are given in Figure 2.4b.

2.2.2 Potential Form and Energy Level Calculation

For the ethylene dimer molecule, an atom-atom potential energy function is chosen following Peet, *et al.*[3]:

$$V = \sum_i \sum_j \left[A_{ij} \exp(-B_{ij} R_{ij}) - \frac{C_{ij}}{R^6} \tanh(R_{ij} - R^0_{ij}) + \frac{q_i q_j}{R_{ij}} \right] + \sum_i \frac{q_i q_0}{R_{i0}} + \sum_j \frac{q_j q_0}{R_{j0}} \quad . \qquad (1)$$

In this equation, i refers to the atoms of one ethylene molecule and j refers to the atoms of the other ethylene molecule. R_{ij} is the distance between the ith and jth atoms. R_{i0} (R_{j0}) is the distance from the ith (jth) atom to the center of mass of the opposite ethylene subunit. The constant R^0_{ij} controls the rate of damping of the $1/R^6$ term by the hyperbolic tangent. The two final summation terms represent additional point charges, q_0, at the center of mass of each ethylene subunit. These charges are chosen to mimic the long-range, quadrupole-quadrupole interaction. The constants used for the potential are listed in Table 2.1. The potential minimum for the dimer has an energy of $-425\ cm^{-1}$ relative to the dissociated fragments, and occurs at $\theta_1=\theta_2=112.3^\circ$, R=3.97 Å, $\varphi_1=\varphi_2\sim45^\circ$. The structure at the minimum of this potential agrees with the structure observed in an ethylene crystal.[23]

For the rare gas-ethylene molecules, an atom-atom potential is used, which excludes the electrostatic terms. Following Hutson *et al.*,[17] we use the potential parameters

Table 2.1
Constants for ethylene dimer and rare gas-ethylene atom-atom potentials in atomic units.

	A_{ij}	B_{ij}	C_{ij}	R^0_{ij}
C-C[a]	43.21	1.672	63.57	3.7
C-H[a]	10.16	1.815	9.58	3.4
H-H[a]	2.39	1.958	1.98	2.9
Ne-C[b]	19.0229	2.0137	11.3689	3.78
Ne-H[b]	75.1042	2.3252	5.9661	3.78
Ar-C[b]	80.3928	2.0062	29.1495	4.54
Ar-H[b]	276.3214	2.2379	18.2061	4.54
Kr-C[c]	216.591	2.017	44.670	4.91
Kr-H[d]	1024.83	2.333	25.506	4.91

$q_C = -0.596$ $q_H = 0.218$ $q_O = 0.320$

[a]From reference 3
[b]From reference 17
[c]From reference 24
[d]From reference 25

of rare gas-rare gas interactions to approximate those of the rare gas-carbon interaction. The Ne-, Ar-, and Kr-C well depths and equilibrium positions are taken as those of the Ne-, Ar-, and Kr-Ne[24] interactions. Similarly, the Ne-, Ar-, and Kr-H well depths are taken as half those of Ne-, Ar-, and Kr-H_2;[25] the equilibrium distances are taken as those of Ne-, Ar-, and Kr-H_2.[25] The values of the potential constants are given in Table 2.1. Table 2.2 lists the values of the minima for each rare gas-ethylene potential.

The above potential form is used to calculate one-dimensional potential energy functions for each van der Waals vibration by separately varying each coordinate while holding the others fixed at their potential minima. Energy levels and wavefunctions are calculated for each of these one-dimensional potentials. The Schrödinger equation is solved for these one-dimensional potentials, using the method of finite differences.[26] This method, which assumes boundary conditions of infinite potential, is not appropriate for the φ_a motion of the ethylene dimer, because of its nearly free rotation. In this case, a basis set of sine and cosine functions is used to diagonalize the Hamiltonian and to determine the wavefunctions and eigenvalues. Because the φ_a potential is symmetric about both π and $\pi/2$, the Hamiltonian matrix

Table 2.2
Rare gas-ethylene potential minima.

	R_0 (Å)	ϵ (cm^{-1})
$Ne-C_2H_4$	2.91	-113.28
$Ar-C_2H_4$	3.24	-192.12
$Kr-C_2H_4$	3.48	-205.32

factors into four submatrices with basis sets: sin $m\varphi_a$, m even; sin $m\varphi_a$, m odd; cos $m\varphi_a$, m even; and cos $m\varphi_a$, m odd.

2.2.3 Matrix Elements

To determine the extent of mixing between the initially excited υ_7 state and combination levels involving the υ_{10} mode close in energy, we calculate the matrix elements $\langle i|V|f\rangle$. Here the state $|i\rangle$ is a product wavefunction made up of the first excited υ_7 wavefunction and the ground vibrational wavefunctions of the υ_{10} and van der Waals modes. For the ethylene dimer we can write explicitly:

$$|i\rangle = |\Psi(n_{\upsilon_7}=1)\rangle\ |\Psi(n_{\upsilon_{10}}=0)\rangle\ |R(n_R=0)\rangle\ |\theta_s(n_{\theta s}=0\rangle$$
$$\times\quad |\theta_a(n_{\theta a}=0)\rangle\ |\phi(n_{\varphi s}=0)\rangle\ |\phi(n_{\varphi a}=0)\rangle\ |\chi(n_\zeta=0)\rangle$$

For each final state, the product wavefunction is composed of the ground state υ_7 wavefunction, the first excited state υ_{10} wavefunction, and various combinations of van der Waals vibrational quantum numbers:

$$|f\rangle = |\Psi(n_{\upsilon_7}=0)\rangle\ |\Psi(n_{\upsilon_{10}}=1)\rangle\ |R(n_R)\rangle\ |\theta_s(n_{\theta s})\rangle$$
$$\times\quad |\theta_a(n_{\theta a})\rangle\ |\phi(n_{\varphi s})\rangle\ |\phi(n_{\varphi a})\rangle\ |\chi(n_\zeta)\rangle\quad .$$

These product wavefunctions are formed using numerical wavefunctions obtained from the energy level calculation for the van der Waals modes and harmonic oscillator wavefunctions for the υ_7 and υ_{10} vibrations. Finally, the matrix elements are evaluated numerically using trapazoid rule quadrature. For the rare gas-ethylene molecules, the integration over the υ_7, υ_{10}, R, and θ coordinates is performed using a ten point grid of values. For the φ integration a fifteen point grid is used in order to cover the double well potential adequately. For the ethylene dimer, a ten point integration over υ_7 and υ_{10} is performed, but due to the large number of modes involved, more limited integrations are performed over the van der Waals coordinates. Because all integrals include each of the ground state wavefunctions, a minimum number of points needed to outline the basic features of this state are used. In the cases of the R, θ_a, and ζ coordinates, three point integrations are adequate. For θ_s, five points are used and for φ_a six points are used. For the φ_s integration, a 9 point grid is needed. Matrix elements calculated in this manner are only approximate; however, their accuracy should be sufficient to evalutate qualitatively the feasibility of the proposed mechanism.

The number of integrations performed is greatly reduced by considering the symmetry selection rules

governing transitions between the $|i\rangle$ and $|f\rangle$ states. For integrals of the form $\langle i|V|f\rangle$ to be nonzero, the integrand must be a totally symmetric function. By examining the symmetry of each vibration, the symmetry-allowed combinations of final states can be determined for the two different point groups. The symmetry representations of the van der Waals vibrations are given in Figures 2.3b and 2.4b.

First, consider the rare gas-ethylene complexes in the C_{2v} point group. The initial state has A_1 symmetry, since the excited υ_7 vibration has this representation and all other modes are in their ground vibrational states. The potential term in the integrand will also have A_1 symmetry because the molecular potential is always totally symmetric in the point group of the molecule. Thus, final states must also have A_1 symmetry for nonzero coupling matrix elements.

The final state is a product of the ground state υ_7 wavefunction, the first excited υ_{10} wavefunction and three van der Waals wavefunctions. Since the excited υ_{10} vibration is in the B_2 representation, the van der Waals modes must combine to form a wavefunction of B_2 symmetry, for $|f\rangle$ to be totally symmetric. The B_2 representation can be formed by the products $A_1 \times A_1 \times B_2$ or $A_2 \times B_1 \times A_1$. This can be accomplished by combining any R level (A_1) with even θ levels (A_1) and odd φ levels (B_2).

The selection rules for rare gas-ethylene molecules are summarized in Table 2.3.

For ethylene dimer, in the C_{2h} point group, the initial excited υ_7 state has B_u symmetry. The final state must also have B_u symmetry for the matrix element integral to be nonzero. The van der Waals vibrations must combine to have B_g symmetry, since the υ_{10} mode has A_u symmetry and, in the C_{2h} point group, $A_u \times B_g = B_u$. The representations combine to form the B_g representation in two ways: $B_g = A_g \times B_g$ and $B_g = A_u \times B_u$. These conditions can be met by four different combinations of the van der Waals vibrations. Since the R and θ_s modes are totally symmetric (A_g), all levels are allowed. The four allowed combinations for the remaining modes are listed in Table 2.3.

2.2.4 Lineshape Calculation

Once the matrix elements which couple the initial and final states are determined, line intensities can be calculated using a time-independent, quantum mechanical treatment. A linear combination of zero-order $|i\rangle$ and $|f\rangle$ states describes the system, forming a set of

Table 2.3
Symmetry selection rules for rare gas-ethylene molecules (C_{2v}) and ethylene dimer (C_{2h}). Even quantum numbers are denoted by + and odd by -.

C_{2v}	R	θ	φ	Symmetry
	+/-	+	-	$A_1 \times A_1 \times B_2$

C_{2h}	R	θ_s	θ_a	φ_s	φ_a	ζ	Symmetry
	+/-	+/-	+	-	+	+	$A_g \times A_g \times A_g \times B_g \times A_g \times A_g$
	+/-	+/-	-	+	+	-	$A_g \times A_g \times B_u \times A_g \times A_g \times A_u$
	+/-	+/-	-	+	-	+	$A_g \times A_g \times B_u \times A_g \times A_u \times A_g$
	+/-	+/-	+	-	-	-	$A_g \times A_g \times A_g \times B_g \times A_u \times A_u$

wavefunctions Ψ_n:

$$|\Psi_n\rangle = a_n|i\rangle + \sum_f b_{nf}|f\rangle \ . \qquad (2)$$

$\{|\Psi_n\rangle\}$ are eigenfunctions of the full Hamiltonian, which includes the interaction between $|i\rangle$ and $\{|f\rangle\}$ states.[27] Substituting the Ψ_n wavefunction into the time-independent Schrödinger equation $(H-E_n)|\Psi_n\rangle = 0$ and left multiplying by $\langle i|$ and $\langle f|$ give two equations:

$$(E_i-E_n)a_n + \sum_f V_f b_{nf} = 0 \qquad (3)$$

$$V_f a_n + (E_f-E_n)b_{nf} = 0 \ , \qquad (4)$$

where $V_f=\langle i|V|f\rangle$. Rearranging Equation 4 yields an expression for b_{nf}:

$$b_{nf} = \frac{-V_f}{(E_f-E_n)} \ a_n \ . \qquad (5)$$

Substituting this expression into Equation 3 gives:

$$\left[E_i-E_n-\sum_f \frac{V_f^2}{E_f-E_n}\right] a_n = 0 \ . \qquad (6)$$

Equation 6 can be solved numerically to give the E_n eigenvalues for the exact molecular eigenstates.

In the zero-order description, the problem is described as the decay of a single optically prepared state, $|i\rangle$, into a set of $\{|f\rangle\}$ "dark" states. In the exact molecular eigenstate description, there are optical transitions to f+1 molecular eigenstates, $\{|n\rangle\}$, all having different amounts of $|i\rangle$ character, or "brightness." The amount of $|i\rangle$ character of each $|n\rangle$ state will be given by a_n^2. Using Equation 5 and the normalization condition for each $|n\rangle$ state,

$$a_n^2 + \sum_f b_{nf}^2 = 1,$$

we can solve for a_n^2:

$$a_n^2 = \left[1 + \sum_f \frac{V_f^2}{(E_f - E_n)^2} \right]^{-1} . \qquad (7)$$

The intensity of a transition to a given $|n\rangle$ state is proportional to a_n^2. Thus, a plot of a_n^2 vs. E_n will yield a spectrum of lines corresponding to excitation of individual $|n\rangle$ states.

2.3. Results

The results of the calculation for the rare gas-ethylene molecules are presented first, followed by the results for the ethylene dimer. For the three rare gas-ethylene complexes studied, the results are very similar. As the mass of the rare gas atom increases, the well becomes deeper and supports more bound levels. For the purpose of describing the potential energy function and the energies of the calculated levels, we take the energy zero to be the dissociated fragments in the ground vibrational state. For the three molecules, the potential minima for the R coordinate are given in Table 2.2. The potential along the θ coordinate consists of a single well with a minimum at 90°. The sides of the well are quite steep, crossing the energy zero at $\theta \sim 60\text{-}65^{\circ}$. These barriers to internal rotation are very high when the R and φ coordinates are fixed at their equilibrium positions. The potential for the φ coordinate consists of a double well with minima at $\varphi = 90^{\circ}$ and 270°. These wells are also very steep and cross the dissociation energy at $\varphi \sim 45^{\circ}$. The steepness of these potentials probably indicates that the calculated van der Waals vibrational energies are higher than their true values. An interaction between the stretch and bend, for example, would lower the bending frequency.

The calculated energy levels for the rare gas-ethylene complexes are tabulated in Table 2.4. In the stretching coordinate, neon-ethylene has six bound states, argon-ethylene has 10, and krypton-ethylene has 12. In the θ bending mode, the neon-, argon-, and krypton-ethylene molecules have three, four, and four levels below the dissociation energy, respectively. For the φ coordinate, the double well with a high barrier causes all levels to be nearly doubly degenerate. Including these near degenerate states, the neon-, argon-, and krypton-ethylene complexes have four, six, and six φ levels, respectively. The vibrational frequencies of the R and θ modes for the three different molecules are also given in Table 2.4. The zero-point energies for the three molecules are 66.52 cm^{-1} for $Ne-C_2H_4$, 74.41 cm^{-1} for $Ar-C_2H_4$, and 66.07 cm^{-1} for $Kr-C_2H_4$.

The calculated energy levels of the rare gas-ethylene complexes are shown graphically in Figure 2.5. Here, the zero of energy is taken to be the energy of the lowest level, the zero-point energies given above. The vibrational states which have energies near the υ_7 excitation at 949.3 cm^{-1} combine the υ_{10} vibration at 826 cm^{-1} with van der Waals excitation totaling 123.3 cm^{-1}. Taking into account the ~18 cm^{-1} width of the observed spectra,[6] a range from 114.3 to 132.3 cm^{-1} should

Table 2.4
Calculated energy levels for rare gas-ethylene complexes. υ is the number of vibrational quanta and ω is the fundamental vibrational frequency. Values are in cm^{-1}.

Neon-Ethylene			
υ	R	θ	φ
0	-93.95	-94.21	-85.16
1	-59.54	-53.26	-85.16
2	-33.94	-7.09	-21.26
3	-16.50		-21.26
4	-6.16		
5	-1.34		
ω	34.41	40.95	

Argon-Ethylene			
υ	R	θ	φ
0	-169.90	-171.42	-160.63
1	-130.20	-126.98	-160.63
2	-96.61	-76.93	-89.49
3	-68.90	-22.19	-89.49
4	-46.74		-5.03
5	-29.72		-5.03
6	-17.31		
7	-8.89		
8	-3.74		
9	-1.07		
ω	38.70	44.44	

Krypton-Ethylene			
υ	R	θ	φ
0	-185.08	-186.46	-178.35
1	-148.32	-146.31	-178.35
2	-116.39	-100.41	-116.24
3	-89.09	-49.78	-116.24
4	-66.20		-40.00
5	-47.46		-40.00
6	-32.54		
7	-21.07		
8	-12.64		
9	-6.81		
10	-3.12		
11	-1.07		
ω	36.76	40.15	

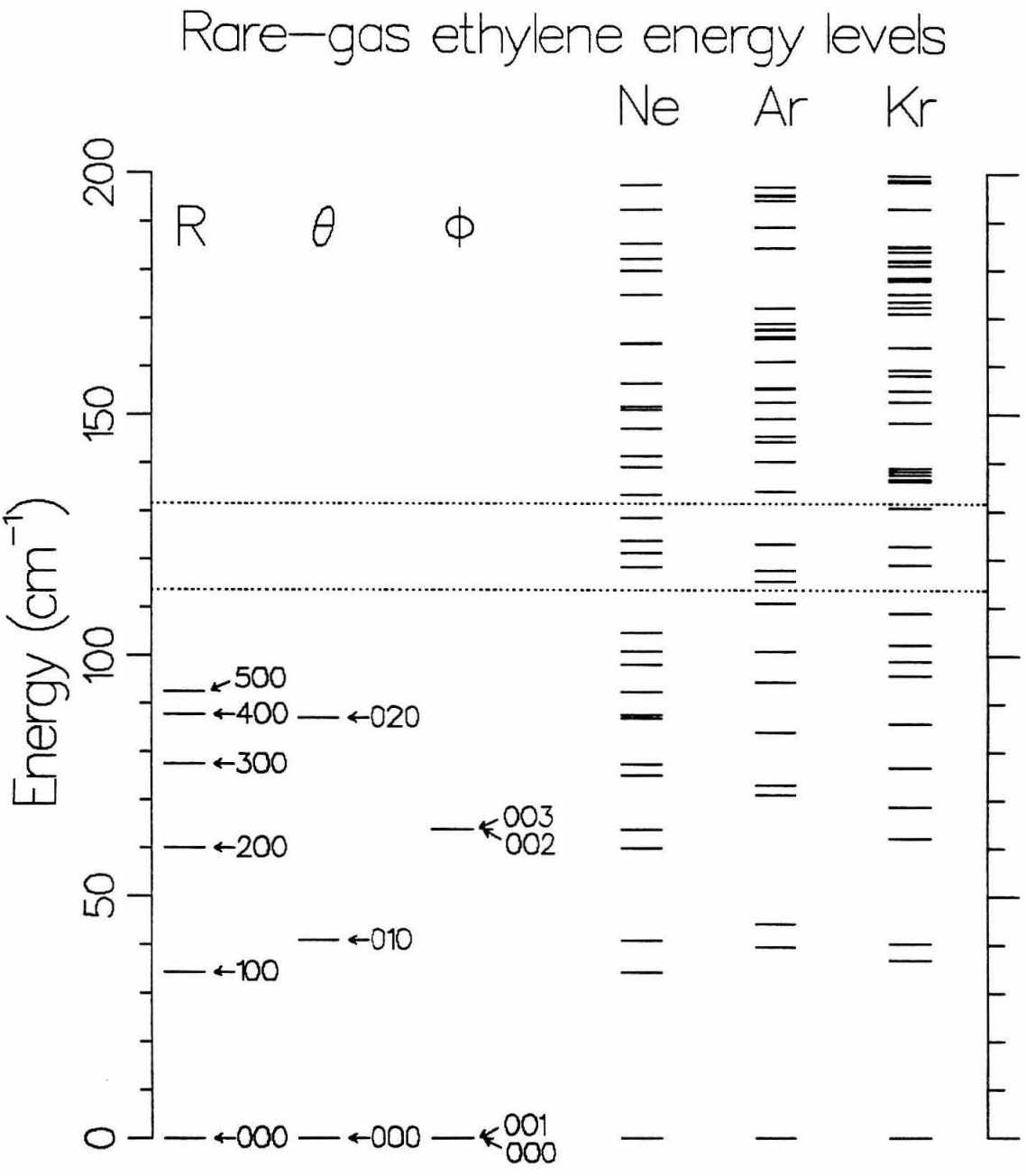

Figure 2.5. Energy levels for rare gas-ethylene molecules. On the left, the neon-ethylene R, θ, and φ energy levels are displayed separately. The labels correspond to quantum numbers n_R, n_θ, and n_φ. On the right, all combination levels are displayed for the neon-, argon-, and krypton-ethylene molecules. The dotted lines denote the energy range of the experimental spectrum.

be considered. This range is highlighted in Figure 2.5. The neon-, argon-, and krypton-ethylene molecules have eight, six, and six combination levels in this range, respectively. Of these states, the neon-ethylene complex has two, which are allowed by symmetry, while the argon and krypton complexes have one and three symmetry-allowed states, respectively.

The coupling matrix elements for these allowed combination levels are given in Table 2.5. Line strengths and energies for the transitions given by Equation 7 are also listed in Table 2.5. The greatest amount of level mixing is observed for the neon-ethylene complex. However, the largest minor peak has only ~6% of the intensity of the main peak. For the rare gas-ethylene molecules, the essentially unmixed υ_7 excitation dominates the spectra.

For the ethylene dimer, the density of vibrational states at the υ_7 energy is much greater. The six potential energy functions, with energy levels and wavefunctions, are shown in Figures 2.6-2.11. The energy levels and zero-point energies are given in Table 2.6. The potential for the stretching mode (Figure 2.6) has been described in Section 2.2.2. This coordinate has 16 bound levels, some of which are shown in Figure 2.6. The potential for the torsional motion, ζ, is shown in

Table 2.5

Energies, matrix elements and line strengths for rare gas-ethylene molecules. E_f denotes energies of the zero-order $|f\rangle$ states and V_f are matrix elements between zero order initial and final states, $\langle i|V|f\rangle$. E_n is the energy of the molecular eigenstate $|n\rangle$, with relative line strength I_n. Note that the number of $|n\rangle$ states is one greater than the number of $|f\rangle$ states listed, because of the inclusion of the state $|i\rangle$ in the linear combination. Energies and matrix elements are in cm^{-1}.

	vdW state			E_f	V_f	E_n	I_n
	n_R	n_θ	n_φ				
$Ne-C_2H_4$	1	2	1	947.53	6.847×10^{-4}	947.53	1.51×10^{-7}
						949.25	0.93760
	2	0	3	949.91	1.686×10^{-1}	949.95	0.06240
$Ar-C_2H_4$						949.30	0.99997
	4	0	1	949.15	8.723×10^{-4}	949.15	3.38×10^{-5}
$Kr-C_2H_4$	4	0	1	944.87	9.143×10^{-4}	944.87	4.26×10^{-8}
	1	2	1	948.80	1.888×10^{-3}	948.80	1.45×10^{-5}
						949.29	0.99936
	2	0	3	956.80	1.879×10^{-1}	956.80	6.26×10^{-4}

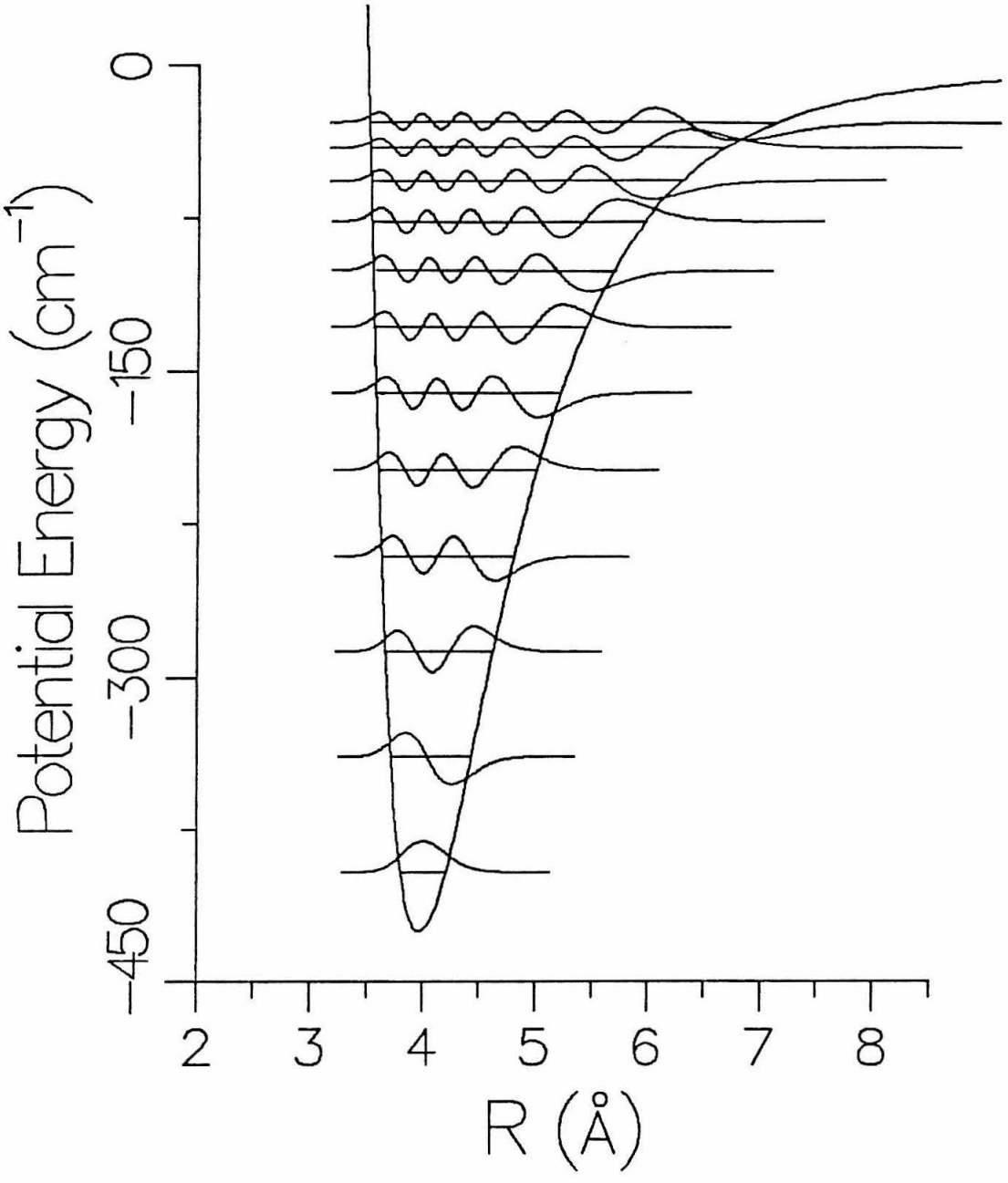

Figure 2.6. Ethylene dimer one-dimensional R potential with calculated energy levels and wavefunctions. For clarity, the four highest energy levels are not shown.

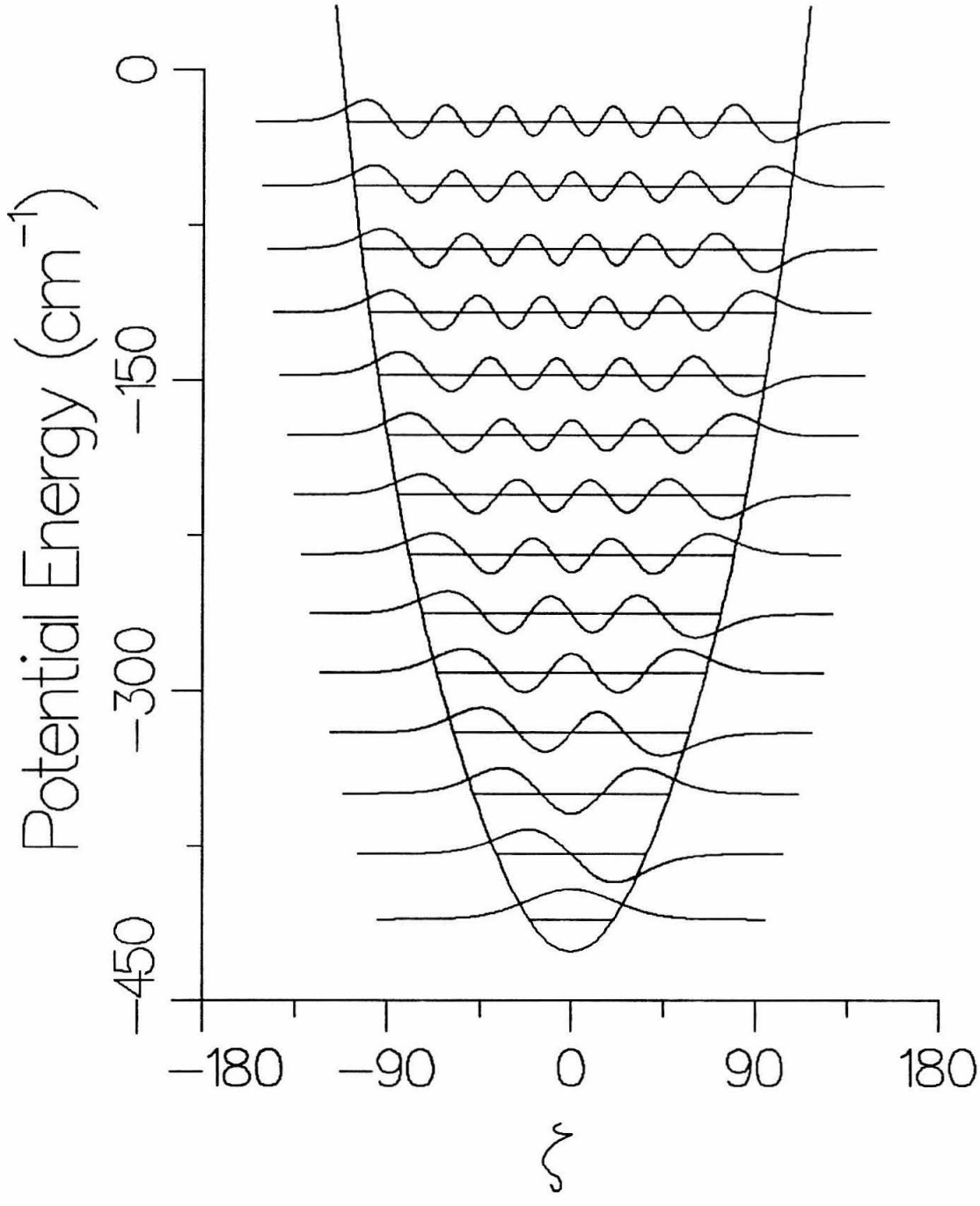

Figure 2.7. Ethylene dimer one-dimensional ζ vibrational potential. Energy levels and wavefunctions are shown for the fourteen calculated states.

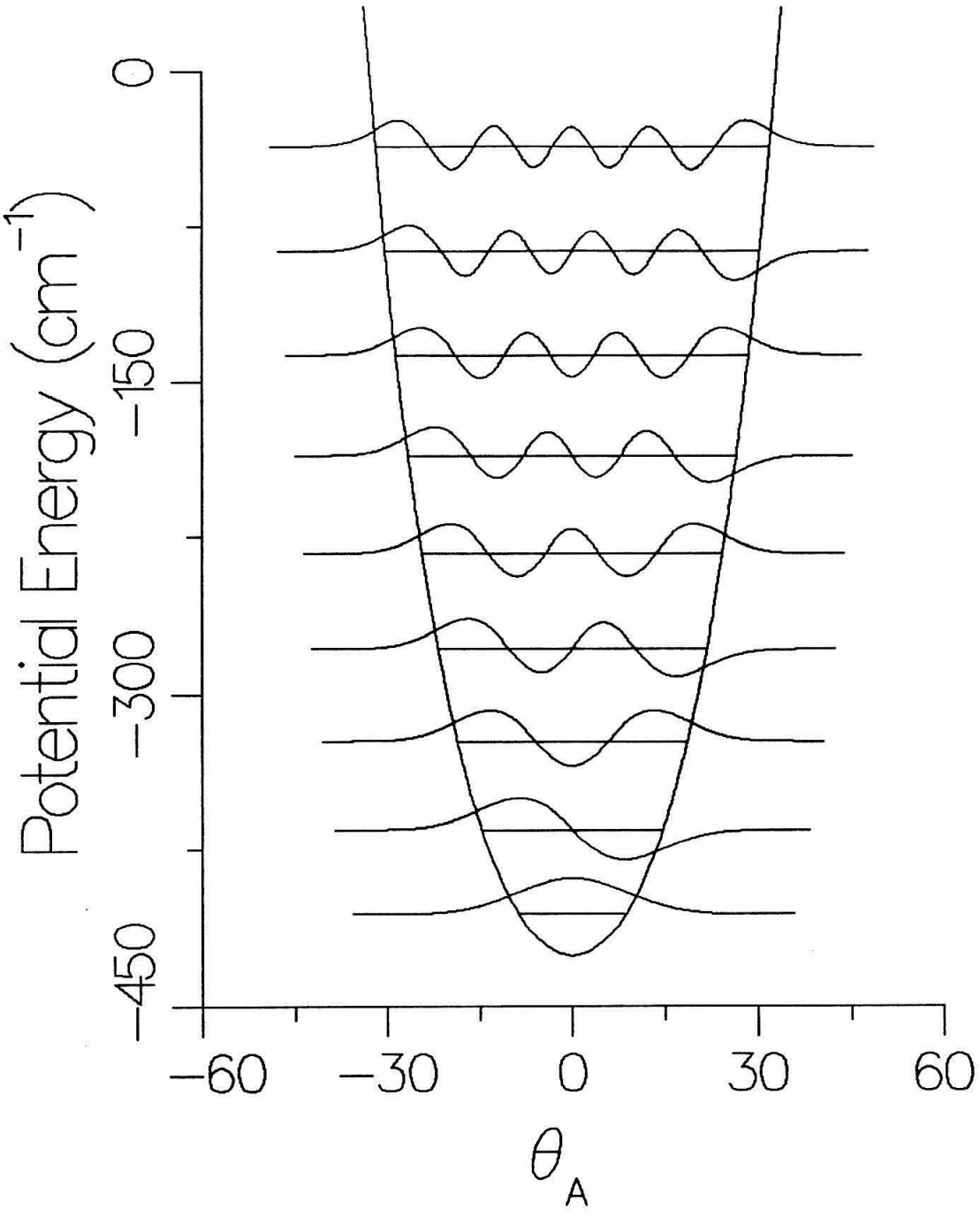

Figure 2.8. Ethylene dimer one-dimensional θ_a vibrational potential. The nine calculated levels and wavefunctions are illustrated.

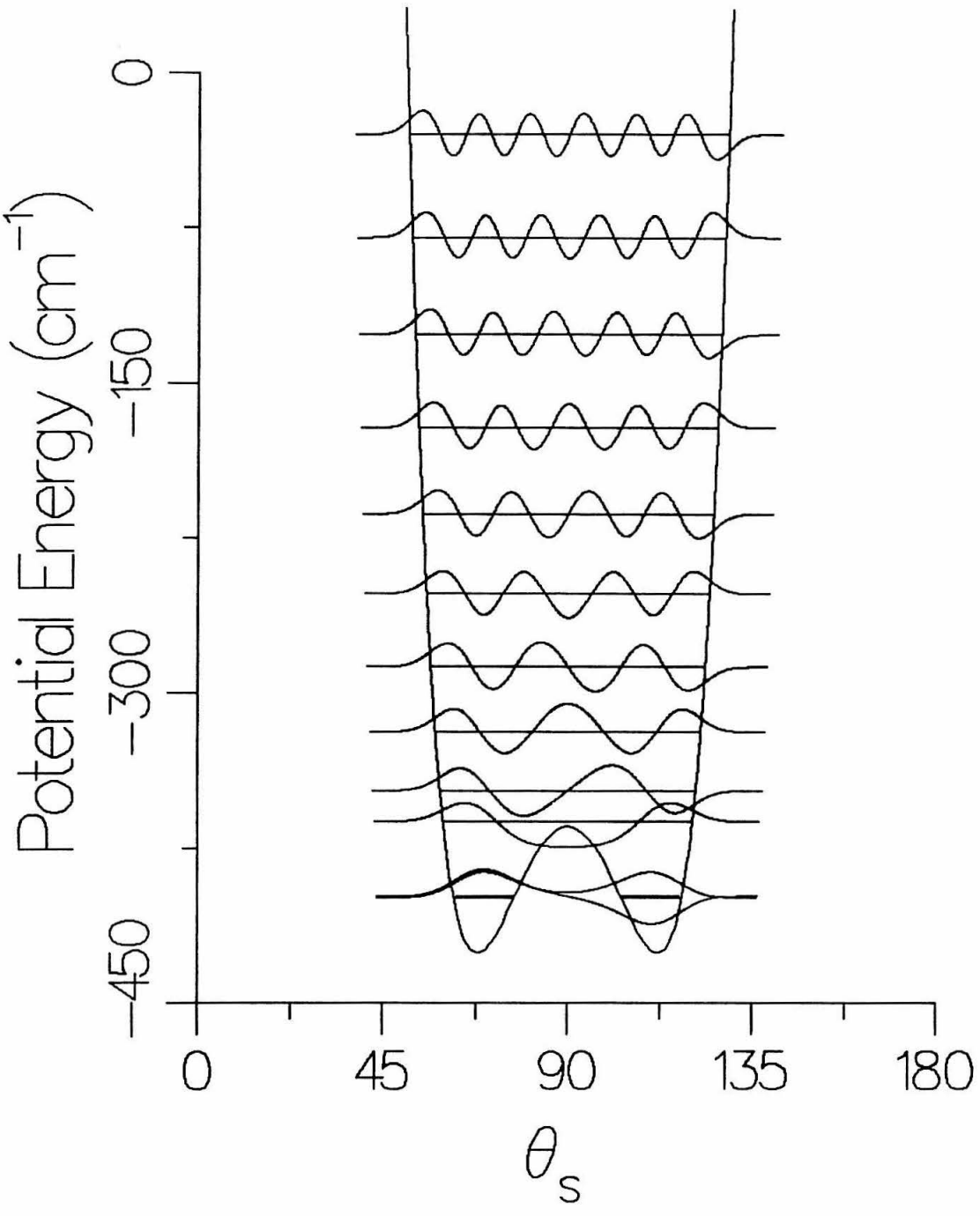

Figure 2.9. Ethylene dimer one-dimensional θ_s vibrational potential. The twelve calculated levels and wavefunctions are shown.

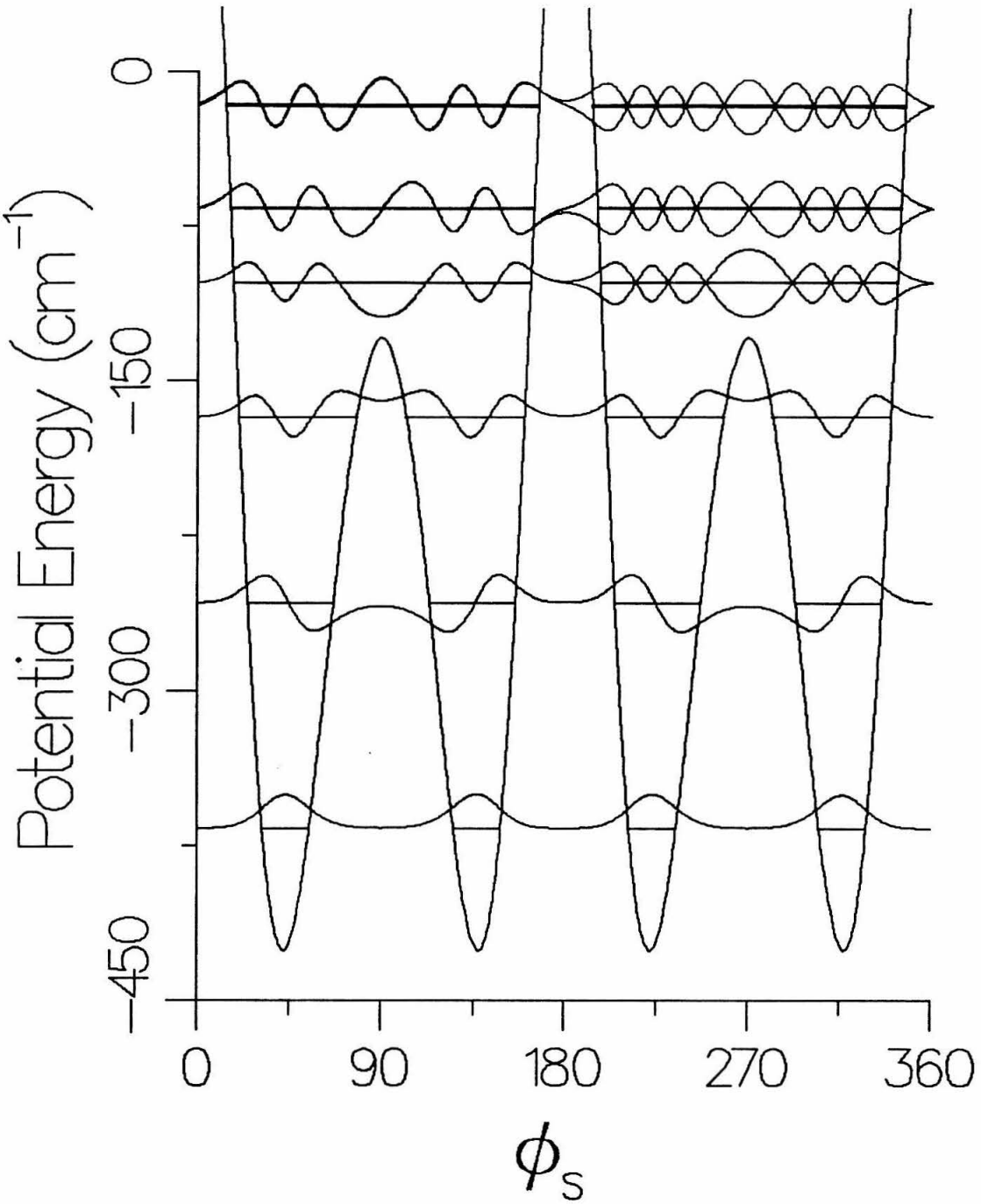

Figure 2.10. Ethylene dimer one-dimensional φ_s potential. Wavefunctions and energy levels are displayed for the calculated vibrational states, including levels one, five, nine, and thirteen through eighteen.

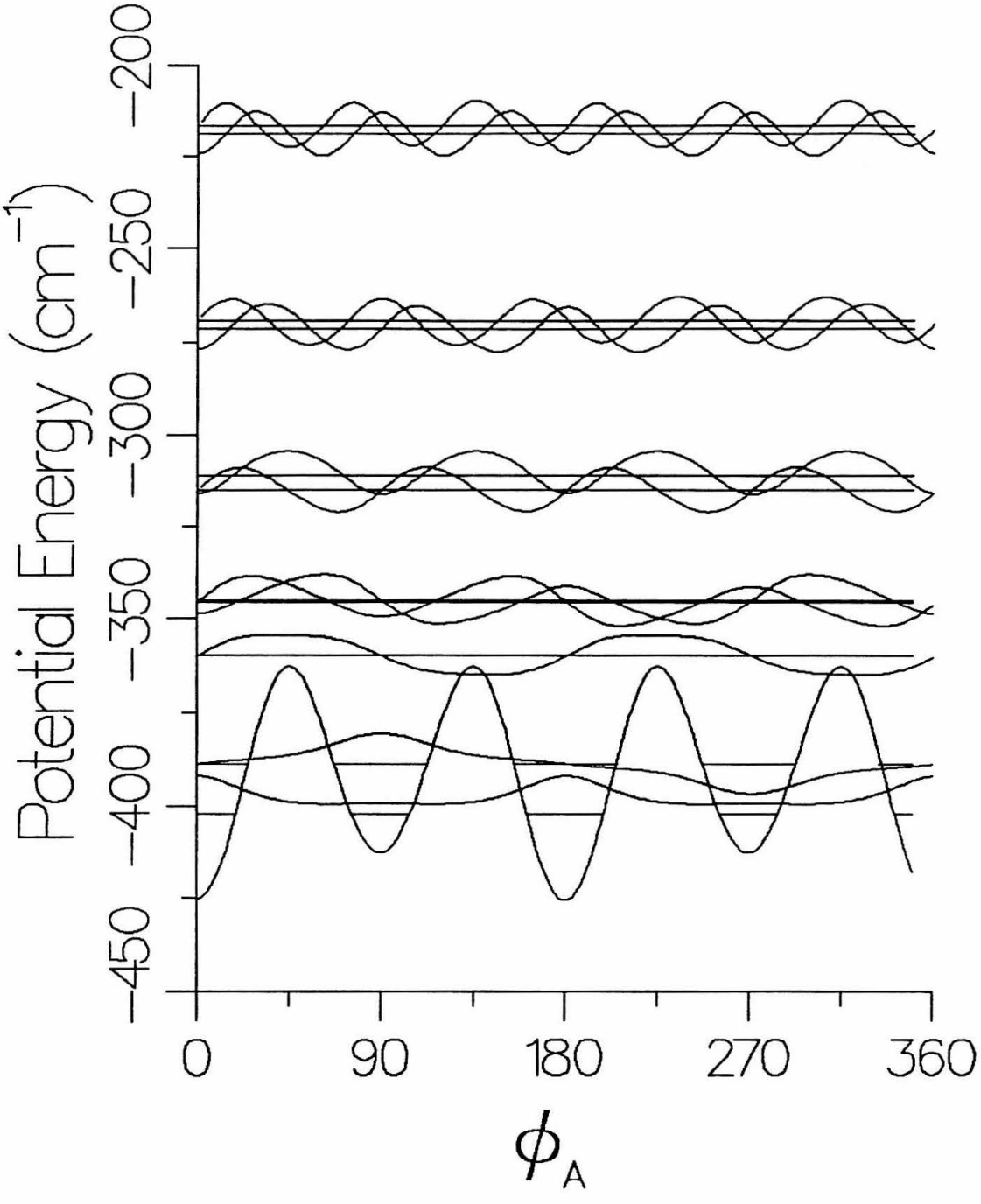

Figure 2.11. Ethylene dimer one-dimensional φ_a vibrational potential with calculated energy levels and wavefunctions. For clarity, states two, four, and fourteen through seventeen are not shown.

Table 2.6

Ethylene dimer calculated energy levels in cm^{-1}.

v	R	θ_s	θ_a	φ_s	φ_a	ζ
0	-395.77	-398.94	-405.87	-367.15	-402.45	-410.08
1	-339.27	-398.12	-365.06	-367.15	-401.87	-379.25
2	-287.39	-361.55	-322.37	-367.15	-388.76	-349.37
3	-240.44	-346.91	-278.07	-367.15	-386.52	-320.22
4	-198.41	-318.52	-232.32	-257.52	-359.50	-291.55
5	-161.13	-287.45	-185.25	-257.52	-345.22	-263.08
6	-128.45	-252.11	-136.98	-257.17	-344.70	-234.59
7	-100.24	-213.38	-87.49	-257.17	-315.04	-205.88
8	-76.27	-171.58	-36.74	-167.70	-311.31	-176.84
9	-56.33	-126.97		-167.67	-271.30	-147.39
10	-40.12	-79.78		-159.82	-269.33	-117.48
11	-27.33	-30.17		-159.77	-218.64	-87.09
12	-17.59			-102.70	-216.16	-56.21
13	-10.51			-102.59	-155.72	-24.85
14	-5.67			-67.04	-153.53	
15	-2.62			-66.73	-83.18	
16				-17.48	-80.98	
17				-16.65		
Zero point energy	29.82	26.65	19.72	58.44	23.14	15.51
Total	173.28					

Figure 2.7, with some of the 14 levels calculated. The θ_a potential consists of a single well with a minimum at 0° and steep walls. This potential supports nine energy levels below the dissociation energy, shown in Figure 2.8. The symmetric θ_s bend has a small potential barrier at 90°, with minima at 70° and 110°. This potential supports 12 states (Figure 2.9). The first two levels are split by $\sim 1\ cm^{-1}$. The φ bending vibrations each have four wells, as shown in Figures 2.10 and 2.11. The φ_s potential has high barriers at 0° and 180° and intermediate barriers ($300\ cm^{-1}$) at 90° and 270°. This motion has 18 levels as listed in Table 2.6. The φ_a motion has four low barriers, as shown in Figure 2.11. Seventeen levels are calculated for this potential. The upper levels correspond to essentially free rotation of the ethylene monomers about their φ axes.

As expected, the density of combination states in the region of the υ_7 vibration is much larger for the dimer than for the rare gas-ethylene molecules. In this case, we consider a $12\ cm^{-1}$ region from 117.3 to $129.3\ cm^{-1}$. The 264 states falling in this range are shown graphically in Figure 2.12. Also shown are the 68 symmetry-allowed combinations. The matrix elements for these states are given in Table 2.7. The matrix elements were used to calculate a spectrum with the treatment given

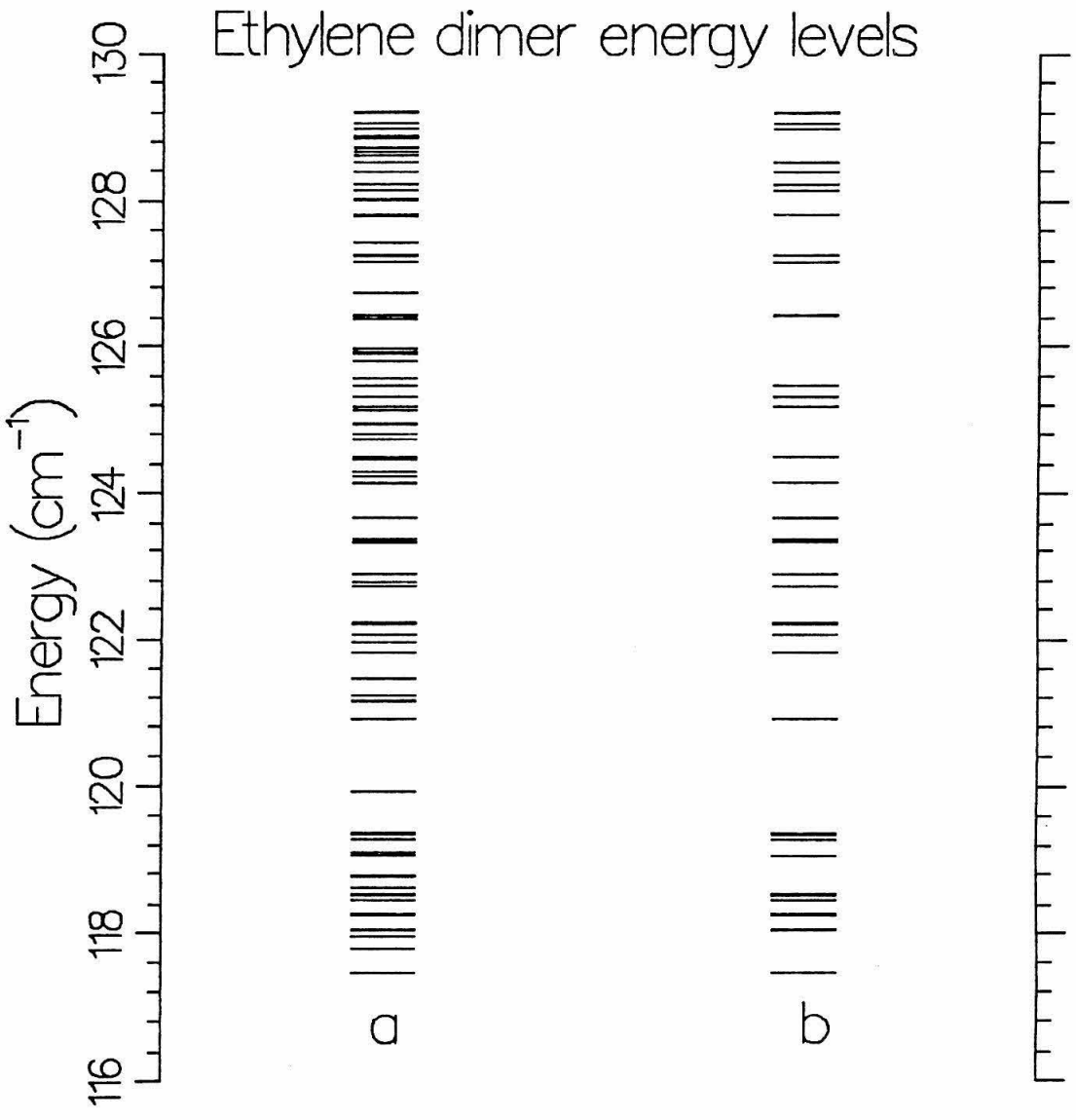

Figure 2.12. Energy level diagram for ethylene dimer. All vibrational combinations falling in the 12 cm^{-1} width of the spectrum are shown in column a. Column b shows the combinations allowed by symmetry.

Table 2.7

Ethylene dimer matrix elements tabulated by symmetry of the final state. V is the matrix element between the initially excited υ_7 and the listed final vibrational state. Even quantum numbers are designated + and odd are designated -.

van der Waals levels						V
R	θ_s	θ_a	φ_s	φ_a	ζ	cm^{-1}
Symmetry						
+/-	+/-	+	-	+	+	
0	0	0	1	0	4	7.274×10^{-2}
0	0	0	1	6	2	-5.739×10^{-10}
0	0	0	3	0	4	1.603
0	0	0	3	6	2	3.978×10^{-10}
0	0	0	5	2	0	8.350×10^{-10}
0	0	0	7	2	0	-2.010×10^{-10}
0	0	2	1	4	0	-5.967×10^{-5}
0	0	2	3	4	0	-1.180×10^{-3}
0	1	0	1	0	4	$2\ 994 \times 10^{-5}$
0	1	0	1	6	2	-7.422×10^{-12}
0	1	0	3	0	4	6.720×10^{-4}
0	1	0	3	6	2	-1.530×10^{-11}
0	1	0	5	2	0	$1\ 492 \times 10^{-12}$
0	1	0	7	2	0	-2.705×10^{-12}
0	1	2	1	4	0	8.013×10^{-6}
0	1	2	3	4	0	2.381×10^{-5}
0	2	0	1	8	0	3.938×10^{-2}
0	2	0	3	8	0	9.934×10^{-1}
0	2	2	1	0	0	-1.757×10^{-2}
0	2	2	3	0	0	-4.312×10^{-1}
0	3	0	1	2	2	-1.177×10^{-12}
0	3	0	3	2	2	$2\ 783 \times 10^{-12}$
0	4	0	1	4	0	$6\ 001 \times 10^{-5}$
0	4	0	3	4	0	1.259×10^{-3}
0	5	0	1	2	0	2.340×10^{-13}
0	5	0	3	2	0	1.725×10^{-12}
1	1	0	1	0	2	-8.843×10^{-7}
1	1	0	3	0	2	-3.864×10^{-13}
1	3	0	1	2	0	3.880×10^{-13}
1	3	0	3	2	0	-1.230×10^{-13}
2	0	0	1	2	0	-9.397×10^{-11}
2	0	0	3	2	0	-1.557×10^{-11}
2	1	0	1	2	0	-1.095×10^{-12}
2	1	0	3	2	0	-2.259×10^{-13}

Table 2.7
Ethylene dimer matrix elements by symmetry, continued.

van der Waals levels						V
R	θ_s	θ_a	φ_s	φ_a	ζ	cm^{-1}
Symmetry						
+/-	+/-	+	-	-	-	
0	0	0	1	7	1	4.331×10^{-9}
0	0	0	3	7	1	7.611×10^{-7}
0	1	0	1	7	1	2.192×10^{-3}
0	1	0	3	7	1	6.148×10^{-2}
0	2	0	1	1	3	8.186×10^{-12}
0	2	0	1	5	1	3.839×10^{-12}
0	2	0	3	1	3	-1.508×10^{-12}
0	2	0	3	5	1	3.035×10^{-12}
0	4	0	1	3	1	-4.919×10^{-5}
0	4	0	3	3	1	-1.218×10^{-3}
1	2	0	1	1	1	-6.032×10^{-13}
1	2	0	3	1	1	6.388×10^{-13}
Symmetry						
+\-	+\-	-	+	+	-	
0	2	1	0	2	1	2.307×10^{-13}
0	2	1	2	2	1	-3.039×10^{-12}
0	3	1	0	0	1	9.861×10^{-4}
0	3	1	2	0	1	-1.324×10^{-6}
1	0	1	0	0	1	-1.107×10^{-2}
1	0	1	2	0	1	2.513×10^{-4}
1	1	1	0	0	1	1.192×10^{-4}
1	1	1	2	0	1	-7.169×10^{-7}
Symmetry						
+/-	+/-	-	+	-	+	
0	0	1	0	3	2	4.328×10^{-6}
0	0	1	0	7	0	4.064×10^{-4}
0	0	1	2	3	2	-6.650×10^{-7}
0	0	1	2	7	0	-3.400×10^{-6}
0	0	3	0	1	0	-4.664×10^{-11}
0	0	3	2	1	0	-6.047×10^{-12}
0	1	1	0	3	2	4.223×10^{-4}
0	1	1	0	7	0	1.122×10^{-1}
0	1	1	2	3	2	6.691×10^{-6}
0	1	1	2	7	0	-5.615×10^{-4}
0	1	3	0	1	0	4.819×10^{-10}
0	1	3	2	1	0	-6.921×10^{-10}
0	4	1	0	1	0	-1.741×10^{-12}
0	4	1	2	1	0	-1.977×10^{-12}

in Section 2.2.4. This result is shown in Figure 2.13. The calculated linestrengths and transition energies are listed in Table 2.8.

2.4 Discussion

In the first part of the discussion, we summarize and compare the results of the calculation for the rare gas-ethylene molecules and the ethylene dimer. The results for both types of molecules are compared with those of other calculations and experiments. The limitations of the method used and the accuracy of the results are also considered. In the second subsection, we discuss the ethylene dimer spectrum and possible explanations for the coexistence of broad and sharp lines. The section begins by discussing terminology and outlining the experimental observations that must be accounted for in a model. We review the previously proposed models and use the results of our calculation to suggest new ideas.

2.4.1 Summary of Results

The results of this calculation suggest that the ν_7 dissociation of the rare gas-ethylene molecules is quite different from that of the ethylene dimer. The ethylene

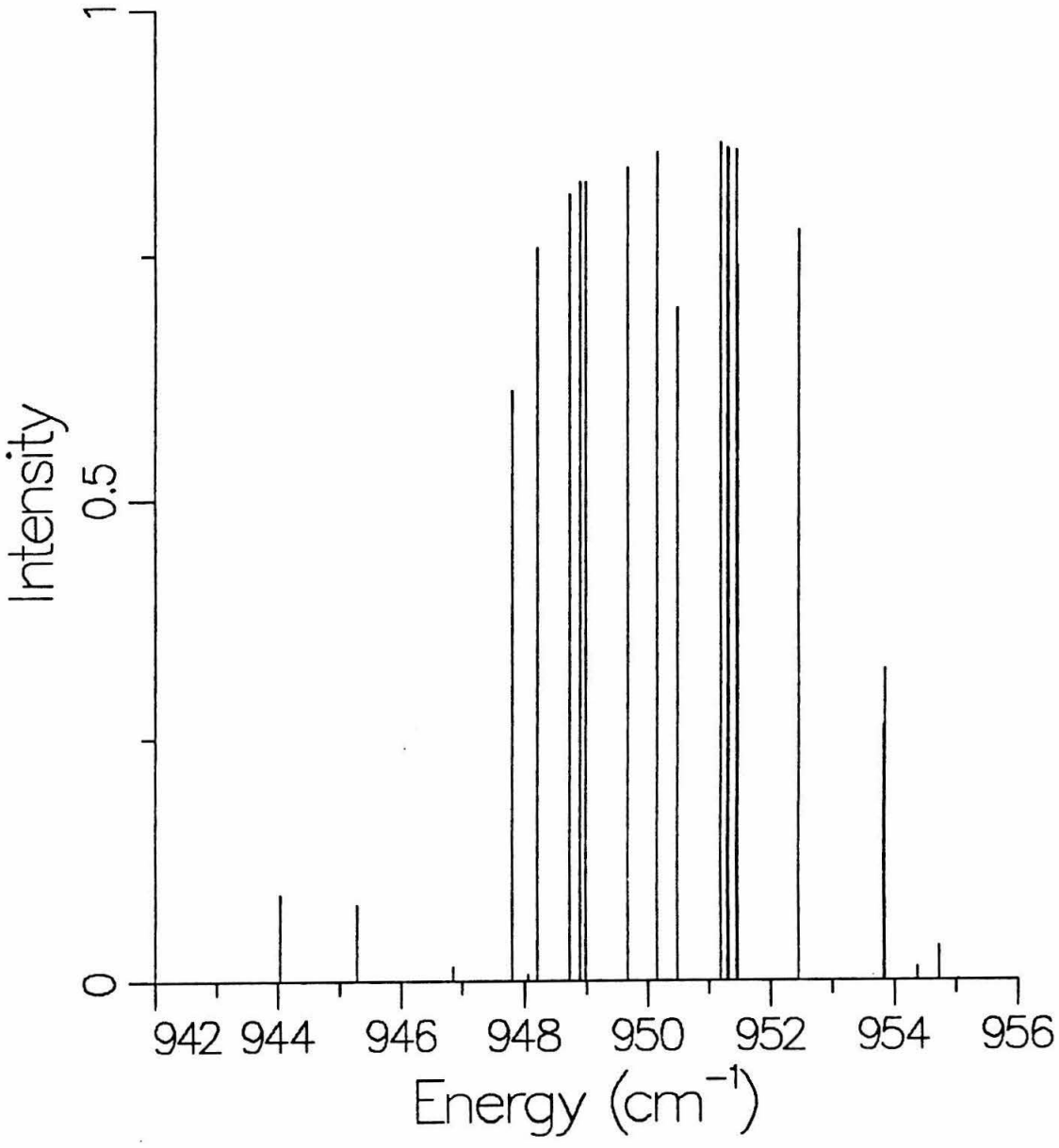

Figure 2.13. Calculated line intensities in the ethylene dimer υ_7 spectrum.

Table 2.8
Line strengths for vibrational transitions of ethylene dimer. E_n is the energy of the molecular eigenstate $|n\rangle$, with relative line strength I_n. Energies are in cm^{-1}.

E_n	I_n
944.03	0.0895
944.24	2.601×10^{-6}
944.46	1.271×10^{-4}
945.06	4.779×10^{-5}
945.28	0.0782
946.84	0.0153
947.81	0.6109
948.07	0.0063
948.22	0.7564
948.72	0.8110
948.72	0.7153
948.89	0.8239
948.90	0.8239
949.33	5.6782×10^{-5}
949.37	3.0367×10^{-8}
949.38	1.3810×10^{-5}
949.66	0.8373
949.67	1.4288×10^{-8}
949.67	0.0217
950.15	0.8522
950.49	0.6953
951.18	0.8639
951.19	0.8132
951.30	0.8583
951.31	0.8566
951.45	0.8554
951.46	0.7392
952.43	0.7759
952.44	0.7320
952.46	1.2933×10^{-7}
953.19	8.0119×10^{-8}
953.83	0.2648
953.84	0.3235
954.14	2.4792×10^{-6}
954.38	0.0146
954.53	1.4373×10^{-7}
954.73	0.0351
955.04	0.0010
955.20	1.219×10^{-4}

dimer has a deeper potential well and twice as many vibrational modes as the rare gas-ethylene molecules. This dramatically increases the density of vibrational states for the dimer in comparison to the rare gas-ethylene complexes, as evidenced in the increased number of lines in the calculated dimer spectrum. The calculated spectra of the rare gas-ethylene complexes contain a single strong line that is due to transitions to the essentially unmixed initial state, $|i\rangle$. The great difference between the rare gas-ethylene molecule and dimer results suggests that the two types of complexes dissociate by different mechanisms. The small well depths of the rare gas-ethylene potentials may allow these complexes to dissociate, leaving the ethylene fragment excited in the υ_{10} mode, for example (*vide infra*).

The results of this calculation can be compared to both experimental and theoretical studies. For the neon- and argon-ethylene molecules, dissociation spectra have been measured and analyzed using a hindered internal rotor model by Western, *et al.*[6] Although high resolution spectra have not been recorded for the rare gas-ethylene complexes, the $\sim$1 cm^{-1} resolution of the experiment revealed structure in the dissociation profiles that was due to excitation of hindered internal rotations. Rare gas-ethylene complex dissociation has also been the

subject of a theoretical study using AVCC-IOS techniques.[17] In this work, Hutson, *et al.*[17] calculated lifetimes ranging from 5 ns to 260 ps for neon-ethylene. The short lifetime occurred for the case of dissociation to an ethylene molecule with excitation in the υ_{10} mode. The longer time results from dissociation to an ethylene molecule in the ground vibrational state. We cannot compare our calculation directly with the results of the experimental or theoretical study. Our model does not explicitly include dissociation to vibrationally excited ethylene, which is the most likely dissociation mechanism for neon- and argon-ethylene. In addition, this calculation considers only states with zero total angular momentum and cannot correctly reproduce the experimentally observed structure. Our results indicate that the mechanism assumed in our calculation is not important for the rare gas-ethylene molecules, confirming the accuracy of the previous analysis.

Several experimental and theoretical results for the ethylene dimer can be compared to our calculation. The lines of our calculated spectrum cover a 10 cm^{-1} region, like the broad background observed in the experiment. The calculated transitions will be broadened by coupling to the dissociative continuum, possibly giving both broad and narrow spectral features (*vide infra*). A further test of the accuracy of our calculation is a comparison with the

observed combination band to the red and blue of the main peak.[13] This feature is attributed to a combination of the υ_7 mode and a van der Waals bend with a frequency of 34 cm^{-1}. This frequency has been confirmed by the spectra of collisionally "hot" dimers.[14] The AVCC-IOS method was used to calculate a φ bending frequency of 40 cm^{-1}.[28] These values compare well with our calculated θ bending frequencies (see Table 2.6). Unfortunately, the near degeneracy in the φ_s levels that is due to artificially high barriers prevents us from assigning a vibrational frequency to this motion. Our calculated φ_a frequency (13.7 cm^{-1}) is lower than these values.

The accuracy of the results presented here is limited by the assumptions used in the calculation. The van der Waals vibrational motions are each treated one-dimensionally, and the interaction among the modes is neglected. This results in high barriers in the angular potentials, which cause the energy levels to shift from the values obtained in the case of a more realistic barrier. These shifts cause our vibrational frequencies for the various angular modes to differ from the estimates of other calculations.[3,28] A second factor affecting the accuracy of the calculation is the approximate atom-atom potential used. Future refinements in the calculation might include varying potential parameters or forms,[29] adding interaction between some of the van der Waals

motions, including bending levels above the dissociation limit, and also including angular momentum coupling. The approximate method used in this calculation is sufficient to evaluate the indirect dissociation model qualitatively, however.

2.4.2 Understanding the Ethylene Dimer Spectrum

The theoretical results presented here may help in understanding the experimental observations for the ethylene dimer outlined in Section 2.1. Before discussing possible explanations for the coexsistence of sharp and broad lines, it is expedient to review and clarify the terms used in describing complex dissociation. Three terms are used to describe the coupling between one state carrying oscillator strength and a manifold of dark states. The most general term is "radiationless transition." This term applies to any type of transition or coupling, including electronic relaxation such as intersystem crossing, as well as vibrational relaxation. Intramolecular vibrational relaxation (IVR) implies a vibrational radiationless transition within a single molecule. In general, the potential couples the interacting levels; however, kinetic effects such as Coriolis coupling can also be important. Fermi resonance also describes an intramolecular vibrational relaxation.

In this case, the coupling is induced by anharmonicity in the potential. All three terms can be applied correctly to the mechanism we assume in this calculation. The first two terms, however, imply a dynamic process, and are perhaps best used to describe a time-resolved experiment. For the case of an experiment in the frequency domain, such as the ethylene dimer dissociation, it is more accurate to speak of the redistribution of oscillator strength induced by the potential. The term Fermi resonance is used to describe this sharing of oscillator strength, generally for a small number of levels. IVR has become the most popular term in the literature, although Fermi resonance is equally accurate.

In addition to the existence of both sharp and broad lines, several more specific experimental observations must be accounted for in a model of the dissociation. First, the spectrum consists of only very sharp lines (3.5-6.5 GHz) and very broad background (10 cm^{-1}). No intermediate linewidths are observed, possibly because of limitations of the experimental technique. The sharp lines are present in the middle 5 cm^{-1} of the main peak and in the combination band. No significant broad background is observed in the combination band, possibly because the background transitions are too weak to observe with the laser power of the experiment. Second, the broad background appears to be homogeneous, while the sharp

lines are inhomogeneous. Finally, studies of the ratio of the background to sharp lines as a function of source pressure, temperature, and concentration indicate that the background is due to warmer dimers.

Three explanations have been proposed for the coexistence of sharp lines and a broad band. First, a high density of final states spread over the 10 cm^{-1} region could produce the observed homogeneously broadened band. However, the number of states having 3.5 MHz widths required to agree with the experiment is unrealistically large (10^5).[13] The broad band results from transitions between a ground state level and the 10^5 excited state levels, while the sharp peaks are due to transitions between single ground and excited levels. In this case, one would expect some ground state levels to reach a number of final levels between one and 10^5, giving rise to lines of intermediate width.

The second explanation for the coexistence of sharp lines and broad background in the dimer spectrum was suggested by Heijmen, *et al.*[13] They hypothesized that the two types of spectral features result from excitation to final states lying below and above the υ_{10} dissociation threshold. According to this model, the background arises from transitions of warmer dimers, with final states above the υ_{10} dissociation threshold. In this case, dissociation occurs on a subpicosecond time scale. The

sharp lines result from transitions of colder dimers to final states below the υ_{10} threshold. Here, dissociation occurs much more slowly. This model is supported by the source pressure and temperature dependence of the spectral features. However, the most probable value of the van der Waals well depth is too large for this model to be applicable. The observation of sharp lines in the combination band is also a counter argument to this explanation. In this model, transitions in the main peak can occur to states both above and below the υ_{10} dissociation threshold; *i.e.*, a 12 cm^{-1} range is sufficient to overcome this threshold. If this is the case, the 34 cm^{-1} of additional energy in the combination band would be more than enough to overcome the threshold, and sharp lines should not be observed.

The final explanation for the sharp lines and broad band of the dimer spectrum relies upon rapid IVR. In this model, proposed by Gentry,[19] the broad band is the result of vibrational energy transfer between the initially excited υ_7 mode and combinations of the υ_{10} and van der Waals vibrations close in energy. The sharp lines result from the longer decay time of these combination levels into the translational continuum of the dissociated fragments. In the model developed by Gentry, both the sharp and the broad components of the spectrum would be homogeneous, with any inhomogeneity arising from different

initial states. In the two laser experiments of Heijmen, *et al.*, however, no correlation was observed between any of the sharp lines or between the sharp lines and broad background; *i.e.*, depletion of one line by a second laser did not change the intensity of any of the other sharp lines.

Our results suggest the possibility of another explanation for the experimental results. The redistribution of oscillator strength that is due to potential coupling between zero-order vibrational states gives vibrational structure that mimics the sharp lines of the experiment. Including rotational structure would greatly multiply the number of lines in the spectrum. The various couplings between these rovibrational states and the continuum will broaden the spectrum. For different initial rotational states, a separate manifold of vibrational states will exist, with the same angular momentum as the initial state. The magnitude of the couplings to the continuum may vary with this angular momentum, thus broadening transitions originating from some initial rotational states more than others. If Coriolis coupling becomes important for nonzero total angular momentum or if an angular momentum selection rule applies, one set of vibrational levels could be very strongly coupled to the continuum and another weakly coupled. This could give rise to a spectrum of both

broadened and narrow lines. This model remains consistent with the experimental observation that the sharp and broad features result from different initial states of the complex. Such angular momentum constraints on IVR processes have been observed for other systems[30], including electronically excited benzene.[31] This hypothesis could be tested by examining the effect of angular momentum coupling on the calculated spectrum.

While the results presented here suggest some new ideas for understanding the ethylene dimer spectrum, none of the proposed explanations for the sharp and broad lines resolve the problem conclusively. Before final conclusions can be made, more sophisicated calculations and new experiments must be performed.

2.5 Conclusions

We have presented calculated local mode energy levels for the van der Waals vibrations of rare gas-ethylene molecules and the ethylene dimer obtained, using one-dimensional, atom-atom potentials. Using these vibrational states, we calculate matrix elements and line strengths for excitation to individual vibrational levels. For the rare gas-ethylene molecules, Fermi resonance is not important, confirming previous results for these systems.[6,17] For the ethylene dimer, Fermi resonance

redistributes the oscillator strength of the υ_7 excitation into many vibrational states over a 10 cm^{-1} region. Based on the results of this calculation, we suggest that the broad and narrow features of the dimer spectrum result from different couplings to the dissociative continuum for vibrational manifolds originating from different initial rotational states.

2.6 References

1 M.P. Cassasa, D.S. Bomse, and K.C. Janda, *J. Chem. Phys.* **74**, 5044 (1981).

2 M.A. Hoffbauer, K. Liu, C.F. Geise, and W.R Gentry, *J. Chem. Phys.* **78**, 5567 (1983).

3 A.C. Peet, D.C. Clary, J.M. Hutson, *Chem. Phys. Let.* **125**, 477 (1986); A.C. Peet, D.C. Clary, J.M Hutson, *Faraday Disc. Chem. Soc.* **82**, 327 (1986).

4 For several examples, see F.G. Celii and K.C. Janda, *Chem. Rev.* **86**, 507 (1986).

5 M.P. Casassa, C.M. Western, F.G. Celii, D.E. Brinza, and K.C. Janda, *J. Chem. Phys.* **79**, 3227 (1983).

6 C.M. Western, M.P. Casassa, and K.C. Janda, *J. Chem. Phys.* **80**, 4781 (1984).

7 W.-L. Liu, K. Kolenbrander, and J.M. Lisy, *Chem. Phys. Let.* **112**, 585 (1984).

8 G.E. Ewing, *Faraday Disc. Chem. Soc.* **73**, 325 (1981).

9 M.P. Casassa, C.M. Western, and K.C. Janda, *ACS Symposium Series* **263**, 305 (1984).

10 W.R. Gentry, *ACS Symposium Series* **263**, 287 (1984).

11 M. Snels, R. Fantoni, M. Zen, S. Stolte, and J. Reuss, *Chem. Phys. Let.* **124**, 1 (1986).

12 K.G.H. Baldwin and R.O. Watts, *Chem. Phys. Let.* **129**, 237 (1986).

13 B. Heijmen, C. Liedenbaum, S. Stolte, and J. Reuss, *Z. Phys. D* **6**, 199 (1987).

14 F. Huisken, H. Meyer, Ch. Lauenstein, R. Sroka and U. Buck, *J. Chem. Phys.* **84**, 1042 (1986); F. Huisken and T. Pertsch, *J. Chem. Phys.* **86**, 106 (1987); U. Buck, F. Huisken, Ch. Lauenstein, H. Meyer, and R. Sroka, *J. Chem. Phys.* **87**, 6276 (1987); U. Buck, F. Huisken, Ch.

Lauenstein, T. Pertsch, and R. Sroka, *Structure and Dynamics of Weakly Bound Molecular Complexes*, ed. A. Weber (Reidel, Dordrecht, 1987), p. 477.

[15] U. Buck, Ch. Lauenstein, A. Rudolph, B. Heijmen, S. Stolte, and J. Reuss, *Chem. Phys. Let.* **144**, 396 (1988).

[16] J.M. Hutson, C.J. Ashton, and R.J. LeRoy, *J. Chem. Phys.* **87**, 2713 (1983); I.F. Kidd and G.G. Balint-Kurti, *Chem. Phys. Let.* **105**, 91 (1984); J.M. Hutson, *J. Chem. Phys.* **81**, 2357 (1984); N. Halberstadt, J.A. Beswick, and K.C. Janda, *J. Chem. Phys.* **87**, 3966 (1987).

[17] J.M. Hutson, D.C. Clary, and J.A. Beswick, *J. Chem. Phys.* **81**, 4474 (1984).

[18] D.C. Clary, *J. Chem. Phys.* **81**, 4466 (1984).

[19] W.R. Gentry, *Structure and Dynamics of Weakly Bound Molecular Complexes*, ed. A. Weber (Reidel, Dordrecht, 1987), p. 467.

[20] M. Bixon and J. Jortner, *J. Chem. Phys.* **48**, 715 (1968).

[21] G.E. Ewing, *J. Phys. Chem.* **90**, 1790 (1986).

[22] E.B. Wilson, J.C. Decius, and P.C. Cross, *Molecular Vibrations* (Dover, New York, 1980), p. 285. The angle φ (ζ) of Figures 2.3a and 2.4a corresponds to the angle χ (ϕ) in this reference.

[23] G.J.H. van Nes and A. Vos, *Acta Chrys. B* **33**, 1653 (1977).

[24] R. Candori, F. Pirani, F. Vecchiocattavi, *Mol. Phys.* **49**, 551 (1983).

[25] R.J. LeRoy and J.M. Hutson, *J. Chem. Phys.* **86**, 837 (1987).

[26] D.G. Truhlar, *J. Computational Phys.* **10**, 123 (1972).

[27] See, for example: K.F. Freed and J. Jortner, *J. Chem. Phys.* **50**, 2916 (1969); K.F. Freed and A. Nitzan, *J.*

Chem. Phys. **73**, 4765 (1980); P.R. Stannard and W.M. Gelbart, *J. Chem. Phys.* **85**, 3592 (1981).

[28] A.C. Peet, *Chem. Phys. Let.* **132**, 32 (1986).

[29] H.J. Böhm, R. Ahlrich, P. Scharf, and H. Schiffer, *J. Chem. Phys.* **81**, 1389 (1984).

[30] T.K. Minton, H.L. Kim, and J.D. McDonald, *J. Chem. Phys.* **88**, 1539 (1988), and references therein.

[31] U. Schubert, E. Riedle, H.J. Neusser, and E.W. Schlag, *J. Chem. Phys.* **84**, 6182 (1986).

Chapter 3

The Infrared Photodissociation of C_2H_4-CH_4

Abstract

Infrared photodissociation spectra of C_2H_4-CH_4, C_2H_4-CH_2D_2, and C_2H_4-CD_4 were observed by exciting the υ_7 vibration of ethylene. Spectral bandwidths were found to be nearly the same for all three complexes, despite their different rotational state densities. This result indicates that the observed widths are not due to unresolved or power-broadened rotational structure. Vibrational coupling, which should be similar for the three complexes, may be important in determining the lifetime.

3.1 Introduction

Study of the vibrational predissociation of van der Waals molecules has raised many interesting questions about the nature of intramolecular vibrational energy transfer.[1] In particular, the vibrational predissociation of ethylene-containing clusters has been intensively studied by exciting vibrations of the ethylene component and observing dissociation with mass spectrometers and bolometers.[1-12] The out-of-plane hydrogen bend of ethylene, ν_7, can be excited by a line-tunable CO_2 laser, and a low-resolution band profile can be recorded.[2-6,10] By using a high-resolution, waveguide CO_2 laser, a small frequency range surrounding each laser line can be observed at high resolution.[11,12] It has proved difficult to record the entire band of the ethylene ν_7 vibration at high resolution, and as a result the nature of vibrational relaxation in these molecules remains uncertain. The photodissociation spectrum of $(C_2H_4)_2$ has proved particularly difficult to interpret, since sharp lines[11-13] are observed within a broad band profile.[2,6,10,11,13] The most recent ethylene dimer experiment combines a cluster size selective scattering technique with the high-resolution CO_2 laser.[13] The results show conclusively that both the sharp and broad

components arise from the dissociation of the ethylene dimer.[14]

Ideally, one would like to study the ethylene ν_7 vibrational dynamics by both high-resolution spectroscopy and state-to-state pump-probe techniques. Neither of these experiments has been performed because of their technical difficulty. Instead, a series of molecules has been studied to observe changes in the low-resolution ν_7 band profile as a function of bonding partner.[2-5] The density of van der Waals states for C_2H_4-Ne is low enough to observe rotational structure with a line-tunable CO_2 laser.[4] For C_2H_4-HF, no structure was observed, but the band profile is asymmetric, reflecting rotational state inhomogeneity.[5] The ethylene dimer band is three times as broad as that of C_2H_4-HF and is well described by a symmetric Lorentzian profile.[2] These studies clearly show that the ν_7 bandwidth is influenced by the nature of the bonding partner. A drawback of the above studies is that each molecule is quite different, both in terms of the coupling between the ν_7 excitation and the van der Waals modes and in terms of the density of the vibrational and rotational states.

To try to separate the effects of vibrational coupling from those of density of states, we have studied the isotopically substituted set of molecules formed by adding CH_4, CH_2D_2, and CD_4 to the C_2H_4 chromophore. The

different rotational constants of the isotopically substituted methane partners change the density of states of the cluster without affecting the bonding interaction or coupling strength. Any differences in the spectra would indicate that the different energy level spacings of the three molecules influence the dynamics. The observed spectra are very similar, indicating that the υ_7 bandwidth is independent of the density of states for this set of molecules.

3.2 Experimental Procedure

Ethylene-methane spectra were measured using a molecular beam apparatus described previously.[2-5] Dilute gas mixtures were expanded through a 50 μm metal pinhole at room temperature. The beam was first skimmed and then traveled 60 cm through two stages of differential pumping to a mass spectrometer, where the clusters were detected. The mechanically chopped beam of a line-tunable CO_2 laser passed through the chamber antiparallel to the molecular beam. As cluster dissociation occurs, fragments fall out of the molecular beam. Loss of cluster mass spectrometer signal was measured as a function of laser frequency to obtain a dissociation spectrum. Laser power was monitored inside the vacuum chamber with each data point and was maintained at 10 W/cm^2.

Gases were obtained commercially and used without further purification. Methane (99.99% purity) was obtained from Matheson, and isotopic methanes were obtained from MSD Isotopes (CH_2D_2, 98% and CD_4, 99% isotopic purity). A commercial mixture containing 90% neon and 10% helium was used as a carrier gas.

To characterize the formation and dissociation of the complexes in the molecular beam, several different types of experiments were performed. The intensities of different ion masses were monitored as a function of stagnation pressure. In addition, dissociation spectra were measured by detecting different ions. Finally, extensive concentration studies were performed. Gas mixtures were repeatedly diluted until the spectrum no longer changed with further dilution. Using very dilute mixtures required fairly high stagnation pressures to observe the dissociation spectra, but each spectrum was measured at the lowest stagnation pressure possible without loss of signal. For the case of the CH_4-containing cluster, the parent ion has the same mass as the CO_2 background in the mass spectrometer chamber. Higher stagnation pressures and longer signal averaging were necessary in this case.

3.3 Results

The photodissociation spectra of the three isotopically substituted ethylene-methane van der Waals molecules are shown in Figure 3.1. The curves are calculated using a two-level homogeneous lineshape model described previously.[15] Fitting the spectra with this model indicates that all three spectra have a FWHM of approximately 2.8 cm^{-1} and are shifted 1 cm^{-1} from the υ_7 band origin of the ethylene monomer.

Clusters such as these have been shown to fragment extensively in the electron impact ionizer of the mass spectrometer.[16] In order to insure that the spectra measured are those of the dimer, without contributions from larger clusters, pressure and concentration studies were performed. In some cases, higher-order dependence of mass spectrometer ion signal on stagnation pressure implied contribution from larger clusters. For example, the pressure dependence of $C_3H_5^+$ (m/e 41) and $C_3H_6^+$ (m/e 42) was higher order than that observed for the parent ion of the complex, $C_3H_8^+$ (m/e 44).

The dissociation spectra measured by detecting different ions were useful in eliminating some contributions from clusters other than the ethylene-methane dimer. The dissociation spectra observed at some masses showed clear contributions from the 10 cm^{-1}

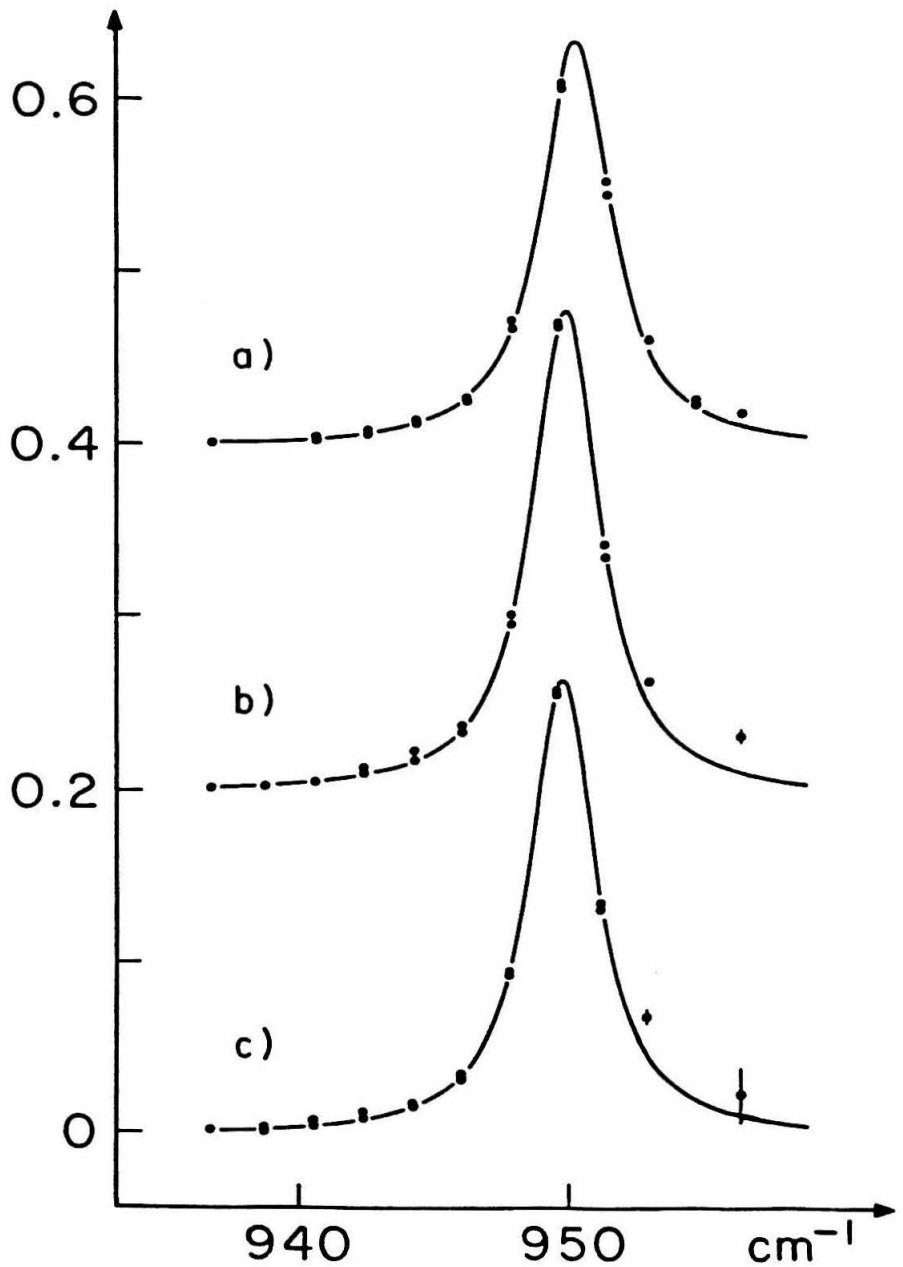

Figure 3.1. Photodissociation spectra of isotopically substituted C_2H_4-CH_4 complexes. a)Photodissociation spectrum of C_2H_4-CD_4 with FWHM of 2.9 cm^{-1}; b)C_2H_4-CH_2D_2 spectrum with FWHM of 2.8 cm^{-1}; c)C_2H_4-CH_4 spectrum with FWHM of 2.8 cm^{-1}. The circles represent the data points, and statistical error is indicated by vertical error bars. The curve is calculated using a two-level lineshape formula.[12]

wide ethylene dimer spectrum. Figure 3.2 compares two spectra measured using the same sample mixture and detecting either $C_3H_6^+$ (m/e 42), a fragment of the ethylene dimer,[7] or $C_3H_8^+$ (m/e 44), the parent ion of ethylene-methane. As shown in Figure 3.2, the spectrum measured by detecting $C_3H_6^+$ (m/e 42) exhibits the 10 cm^{-1} bandwidth of the ethylene dimer spectrum. The bandwidth of spectrum measured by detecting $C_3H_8^+$ (m/e 44) is narrower, indicating that this mass is not contaminated by ethylene dimer nor presumably by larger clusters containing two or more ethylene molecules. The width of the lower spectrum in Figure 3.2 is due to large clusters of the form $(CH_4)_nC_2H_4$. This result could be predicted from the known fragmentation pattern of the ethylene dimer[10] as well as the very low concentration of ethylene and the relatively high concentration of methane in this particular sample.

Contributions from large clusters containing many methane molecules were minimized in the extensive dilution studies. Figure 3.3 shows the spectra measured by detecting $C_3H_8^+$ (m/e 44) for successively more dilute concentrations of methane. The width of the spectrum decreased with dilution until a limiting value was reached, as shown in the upper spectra of Figure 3.3. The final gas mixtures, shown in Table 3.1, contained from

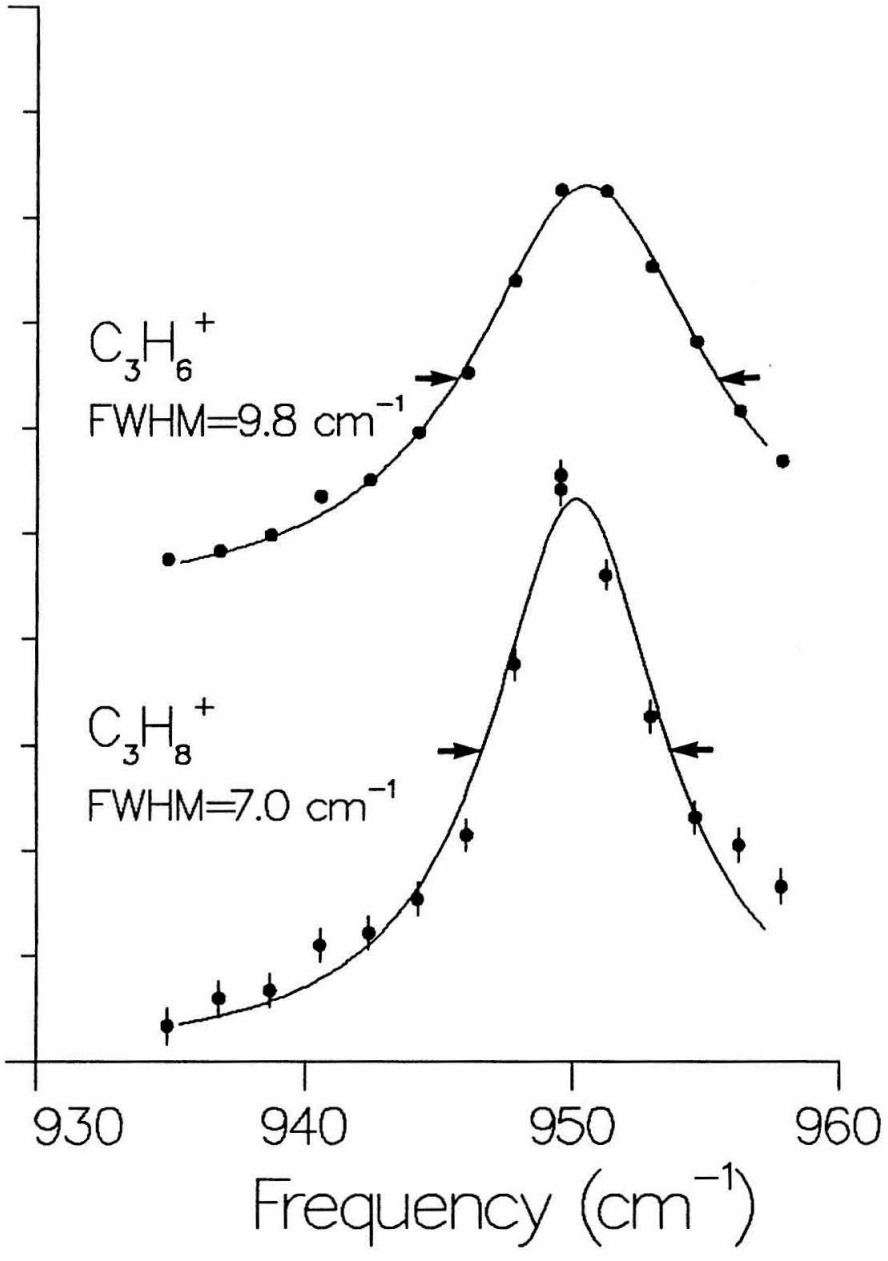

Figure 3.2. Dissociation spectra recorded by monitoring two different ion masses. The upper spectrum was measured by detecting $C_3H_6^+$ (m/e 42) and has a FWHM of 9.8 cm^{-1}, characteristic of the ethylene dimer dissociation spectrum. The lower spectrum was measured by detecting $C_3H_8^+$ (m/e 44) and has a FWHM of 7.0 cm^{-1}, indicating that the cluster contains a single ethylene molecule. In both cases the gas mixture contained 0.05% ethylene, 10.0% methane, 9.0% helium, and 80.95% neon.

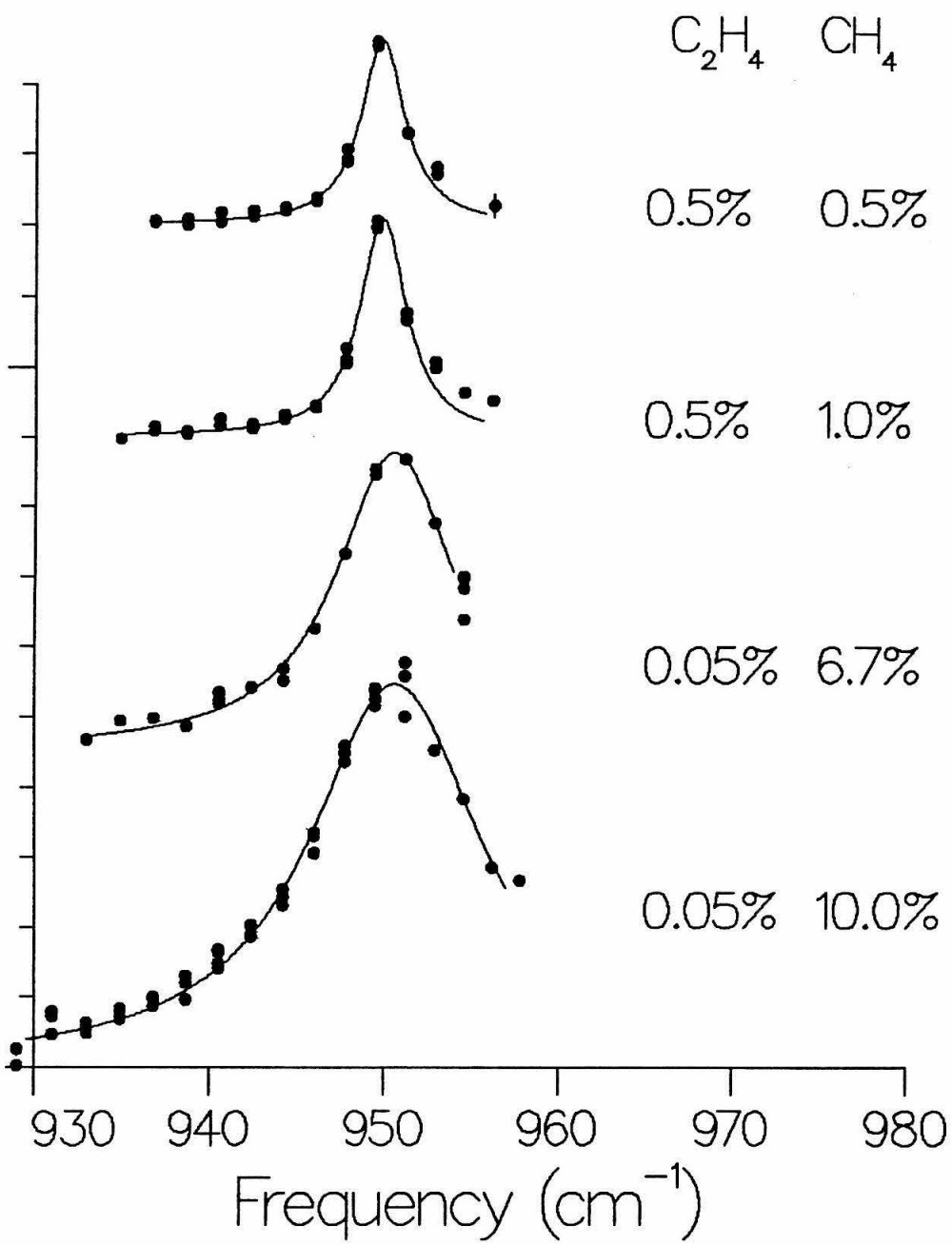

Figure 3.3. Dilution study of ethylene-methane gas mixtures. The spectrum, measured by monitoring $C_3H_8^+$ (m/e 44), becomes narrower as the concentration of methane in the mixture is reduced, until it reaches a limiting value. The ethylene concentration is slightly higher in the upper spectra to improve signal levels; the observed linewidths were not sensitive to this concentration. The range of the lower spectra is limited by the available CO_2 laser frequencies.

Table 3.1: Ethylene-methane molecular beam conditions. The listed gas mixtures and stagnation pressures were used to measure the spectra shown in Figure 3.1.

	C_2H_4	CH_4	He	Ne	P_0(psig)
C_2H_4-CH_4	0.5	0.5	9.9	89%	280
C_2H_4-CH_2D_2	0.5	0.3	9.8	89%	180
C_2H_4-CD_4	0.4	0.2	9.9	89%	180

0.2% to 0.5% methane and ethylene. This is from 5 to 25 times more dilute than the mixtures used by Snels, *et al.*[11] and from 5 to 50 times more dilute than those of Huisken, *et al.*[10] in their cluster size selective experiments. Similar concentrations were used to observe the uncontaminated spectrum of benzene dimer by Kolenbrander and Lisy with a cluster size selective isotopic technique.[17]

The spectra shown in Figure 3.1 were measured by monitoring the parent ions to avoid interference from the ethylene dimer spectrum, which is present at all smaller masses. Although cluster fragmentation makes detection of the parent ion a less than ideal method for observing dimer spectra, the results shown in Figure 3.1 appear to be the true ethylene-methane dimer spectra for several reasons. First, clusters containing two or more ethylene monomers do not contribute to the dissociation spectra measured at the parent ion masses. Second, the careful concentration studies have minimized contributions from clusters containing more than one methane molecule. Finally, even if the results do contain some contribution from larger clusters, they still provide information about the dimer spectrum. The spectra we report do not change with further dilution of the gas mixture. This indicates that either we are observing only the ethylene-methane

dimer spectra, or that the spectra of higher cluster contaminants are very similar to that of the dimer. Thus, even though large cluster contamination cannot be ruled out absolutely, the spectra can be unambiguously associated with the ethylene-methane dimer.

3.4 Discussion

The results in Figure 3.1 show that the spectra of the three isotopically substituted van der Waals molecules have nearly the same bandwidth, despite the difference in the density of states of the molecules. To understand this result, the homogeneity of the spectrum of C_2H_4-CH_4, as well as that of other ethylene-containing van der Waals molecules is considered. The results for C_2H_4-CH_4 are then compared to those of $(C_2H_4)_2$. We conclude by suggesting further theoretical and experimental work on these molecules.

The low-resolution ν_7 predissociation spectra of the ethylene dimer was initially thought to be dominated by homogeneous broadening.[2,6] This was supported by the large fraction of molecules that dissociate with low laser power[2,6] and the broad (10-15 cm^{-1}) Lorentzian lineshapes observed. The inhomogeneous spectrum of C_2H_4-HF, in contrast, does not exhibit the symmetric shape of the C_2H_4-CH_4 and $(C_2H_4)_2$ spectra, and it is well fit by a

multilevel model, which includes rotational state inhomogeneity.[5]

Recently, the closer examination of the ethylene dimer spectrum with a high-resolution CO_2 laser has revealed structure in the broad Lorentzian.[11,12] In this experiment, first performed by Snels, *et al.*[11] and confirmed by Baldwin and Watts,[12] the CO_2 laser was tuned over a 75 MHz range about each laser line. In addition to the broad Lorentzian peak of the ν_7 vibration, two side bands were observed, corresponding to combination bands of the ν_7 excitation and a van der Waals mode, ν_{vdW}, at 36 cm^{-1}.[11] Structure was observed in a small region about laser lines of the $\nu_7 + \nu_{vdW}$ combination band and the main ν_7 peak.[11] The width of this structure corresponds to a 10 ns lower limit for the lifetime.[11]

Another result germane to the question of spectral homogeneity of ethylene complexes has been presented by Huisken, *et al.*[10] In these experiments, scattering collisions with helium separate clusters of different masses spatially. Thus, the predissociating laser can interact with a sample that is purely $(C_2H_4)_2$ without contributions from larger clusters. This eliminates problems of sample inhomogeneity and cluster fragmentation in electron impact ionizers. At low resolution, the same broad Lorentzian spectrum (FWHM=10-12 cm^{-1}) was observed for the dissociation of ethylene dimer, trimer, and

tetramer.[10] Combining the high resolution laser with this scattering technique confirmed that both broad and narrow components in the spectrum are due to the ethylene dimer.[13]

Several explanations for the observed ethylene dimer spectrum of narrow lines within a broad band profile have been detailed in Chapter 2. One possiblity is that a very dense set of states is broadened to form the observed Lorentzian at low resolution or high laser power. The density required to account for the observed spectrum is unrealistically large, however.[11] A second explanation, as proposed in Chapter 2, is a dissociation mechanism with a strong dependence on the nature of the initially populated level. An example of this would be a strong dependence of the dissociation rate on the rotational quantum number.

The low-resolution spectra of isotopically substituted ethylene-methane molecules shown in Figure 3.1 are similar to those of the ethylene dimer, in that the bandshape is symmetrical. The width of the bands is broader than one would expect in the absence of significant coupling between the ethylene υ_7 mode and other vibrations. At the center of each spectrum, approximately 20% of the dimers in the molecular beam are dissociated with a laser fluence of 10 W/cm^2. This indicates significant inhomogeneity in the spectrum, since

for a homogeneously broadened line with the same oscillator strength as the ethylene υ_7 mode, the sample would be more completely dissociated. These results lead to the hypothesis that the description of ethylene-methane dissociation will be analogous to that of ethylene dimer.

It is of particular interest that the isotopic substitution has no effect on the symmetrical band shape of the ethylene-methane spectrum. The three clusters studied differ in density of states, both in the excited complex and in the dissociated fragments. The bonding interaction and strength of coupling between the initially excited state and the van der Waals vibrations would not be expected to change upon isotopic substitution, however. Since the three spectra are nearly identical in width, we conclude that the band shape does not reflect underlying rotational structure. It also suggests that the coupling between the ethylene υ_7 mode and the background vibrational states does not depend on specific resonances within the van der Waals energy levels. The results of Chapter 2 for the ethylene dimer suggest that the band width reflects the coupling between the initially excited level and "dark" vibrational levels of the van der Waals vibrations. The narrower band of the ethylene-methane spectrum indicates that the coupling is less extensive in this case than in that of the ethylene dimer.

3.5 Summary

The results presented here reinforce the hypothesis that some ethylene clusters undergo vibrational mixing prior to dissociation. The low resolution dissociation spectra of isotopically substituted ethylene-methane complexes all consist of a ~2.8 cm^{-1} wide symmetrical band. This indicates that the observed widths do not reflect underlying rotational structure. Clearly, high-resolution spectroscopy and time-resolved studies are necessary to evaluate the extent of coupling in these molecules. The ethylene-methane molecule may be more amenable to high-resolution study than the ethylene dimer because the band is only one-third as broad, indicating less extensive vibrational coupling. Finally, theoretical analysis to determine the extent of coupling between the ethylene υ_7 vibration and the background density of states would be very helpful.

3.6 References

[1] K.C. Janda, *Adv. Chem. Phys.* **60**, 201 (1985); F.G. Celii and K.C. Janda, *Chem. Rev.* **86**, 507 (1986), and references therein.

[2] M.P. Casassa, D.S. Bomse, J.L. Beauchamp, and K.C. Janda, *J. Chem. Phys.* **72**, 6805 (1980); M.P. Casassa, D.S. Bomse, and K.C. Janda, *J. Chem. Phys.* **74**, 5044 (1981).

[3] M.P. Casassa, C.M. Western, F.G. Celii, D.E. Brinza, and K.C. Janda, *J. Chem. Phys.* **79**, 3227 (1983).

[4] C.M. Western, M.P. Casassa, and K.C. Janda, *J. Chem. Phys.* **80**, 4781 (1984).

[5] M.P. Casassa, C.M. Western, and K.C. Janda, *J. Chem. Phys.* **81**, 4950 (1984).

[6] M.A. Hoffbauer, K. Liu, C.F. Geise, and W.R. Gentry, *J. Chem. Phys.* **78**, 5567 (1983); A. Mitchell, M.J. McAuliffe, C.F. Geise, and W.R. Gentry, *J. Chem. Phys.* **83**, 4271 (1985).

[7] W.-L. Liu, K. Kolenbrander, and J.M. Lisy, *Chem. Phys. Let.* **112** 585 (1984).

[8] D.S. King and J.C. Stephenson, *J. Chem. Phys.* **82**, 5286 (1985).

[9] G. Fischer, R.E. Miller, P.F. Vohralik, and R.O. Watts, *J. Chem. Phys.* **83**, 1471 (1985).

[10] F. Huisken, H. Meyer, C. Lauenstein, R. Sroka, and U. Buck, *J. Chem. Phys.* **84**, 1042 (1986); U. Buck, F. Huisken, Ch. Lauenstein, T. Pertsch, and R. Sroka, *Structure and Dynamics of Weakly Bound Molecular Complexes*, ed. A. Weber (Reidel, Dordrecht, 1987), p. 477; F. Huisken and T. Pertsch, *J. Chem. Phys.* **86**, 106 (1987); U. Buck, F. Huisken, Ch. Lauenstein, H. Meyer, and R. Sroka, *J. Chem. Phys.* **87**, 6276 (1987); U. Buck, Ch. Lauenstein, H. Meyer, and R. Sroka, *J. Phys. Chem.*, in press.

[11] M. Snels, R. Fantoni, M. Zen, S. Stolte, and J. Reuss, *Chem. Phys. Let.* **124**, 1 (1986); B. Heijmen, C. Liedenbaum, S. Stolte, and J. Reuss, *Z. Phys. D* **6**, 199 (1987).

[12] K.G.H. Baldwin and R.O. Watts, *Chem. Phys. Let.* **129**, 237 (1986).

[13] U. Buck, Ch. Lauenstein, A. Rudolph, B. Heijmen, S. Stolte, and J. Reuss, *Chem. Phys. Let.* **144**, 396 (1988).

[14] For a complete discussion of the ethylene dimer dissociation, see Chapter 2.

[15] M.P. Casassa, F.G. Celii, and K.C. Janda, *J. Chem. Phys.* **76**, 5295 (1982).

[16] U. Buck and H. Meyer, *Phys. Rev. Let.* **52**, 109 (1984), and references therein.

[17] K. Kolenbrander and J.M. Lisy, *J. Chem. Phys.* **85**, 6227 (1986).

Chapter 4

The Structure and Dissociation Dynamics of Ne_2Cl_2

Abstract

Ne_2Cl_2 and Ne_3Cl_2 are investigated using a laser pump-probe technique. Analysis of a rotationally resolved B←X excitation spectrum shows that Ne_2Cl_2 has a distorted tetrahedral structure with bond distances that agree with predictions of an additive atom-atom interaction model. Excitation spectral shifts predict a Ne_3Cl_2 structure with the neon atoms encircling the Cl_2 bond axis. The total van der Waals bond energy of Ne_2Cl_2 is found to be between 145.6 and 148.6 cm^{-1}. For Cl_2 stretching levels below $\upsilon = 10$, transfer of one Cl_2 vibrational quantum to the van der Waals vibrational modes is sufficient to dissociate both neon atoms from the complex. This indicates that the two neon atoms do not dissociate via independent, impulsive "half-collisions." The Cl_2 fragment rotational state population distributions for different initial vibrational levels are characterized using a simple rotational surprisal analysis. The extent of product rotational excitation is only weakly dependent upon the amount of energy available to the products.

4.1 Introduction

Recent studies have reported a variety of detailed information about the structure and dynamics of triatomic rare gas-halogen van der Waals molecules.[1-15] The simplicity of triatomic complexes makes them attractive for both experimental and theoretical studies. Even these simple systems exhibit a wide variety of dynamical behavior, including rotational rainbows,[6] quantum interference effects,[12] and sequential, vibrational energy redistribution.[13] Studies on slightly larger complexes may aid in understanding the behavior of weakly bound systems as their size progresses from triatomic complexes to large clusters that exhibit phase transitions,[16] and finally to the liquid phase. In this paper we present such a study of the Ne_2Cl_2 and Ne_3Cl_2 complexes. The pump-probe experiments described here determine the structure, the van der Waals bond energy, and the dissociation dynamics of Ne_2Cl_2, as well as a possible structure for the Ne_3Cl_2 complex.

The first experiments studying rare gas-halogen van der Waals molecules used laser-excited fluorescence of the halogen $B^3\Pi(0_u^+) \rightarrow X^1\Sigma_g^+$ transitions to observe vibrational predissociation on the B state potential energy surface.[17] Levy and coworkers examined the dissociation process for triatomic and larger complexes of I_2.[17] Although the

structures of the neon complexes were not determined, a proposed band-shift rule[18] indicated that the rare-gas atoms are in equivalent positions for Ne_nI_2 (n=1-6)[19] and He_nI_2 (n=1,3).[18] This is also true for the $Ar_mHe_nI_2$[20] and Ne_nBr_2 (n=1-3)[21] complexes, which were studied with the same technique. A structure that satisfies this requirement and is consistent with the observed T-shaped triatomic structures is a "belt" configuration with the neon atoms encircling the halogen bond axis.

In addition to fluorescence excitation spectra, the I_2 product vibrational states were measured for the He_nI_2,[18] Ne_nI_2,[19] and $He_mAr_nI_2$[20] complexes by dispersing the I_2 fragment fluorescence. For the Ne_2I_2 complex, two quanta of I_2 vibration are required to dissociate the complex. This mechanism is called the $\Delta v=-2$ channel. For the vibrational excitations studied, dissociation occurs via the $\Delta v=-2$ and $\Delta v=-3$ channels with approximately equal probability. Modeling the intensity of the $\Delta v=-3$ product spectra showed that, while the two neon atoms may dissociate sequentially, their dissociation is not independent.[19] For the He_2I_2 complex, dissociation occurred almost exclusively via the $\Delta v=-2$ channel, although the $\Delta v=-1$ channel is energetically open. For this complex, it appears that the two helium atoms dissociate independently, each requiring one quantum of energy from the I_2 vibration.[18] For both the ArI_2 and

$HeArI_2$ complexes, three quanta of Cl_2 stretching energy are required for dissociation. This observation indicates that the argon and helium dissociations are not independent.[20]

More recent experiments have applied a powerful laser pump-probe technique to rare gas-halogen van der Waals complexes.[1-6,10-13] In this method, the complex is first excited to the long-lived B (or $A^3\Pi$) electronic state, as in the fluorescence experiments described above. A short time after the complex vibrationally predissociates, the halogen fragment is probed by exciting the E←B (or E←A) transition. With this method, the rotational and vibrational states of the halogen dissociation fragments can be determined. With high-resolution lasers and advantageous rotational constants, state-to-state dynamics can be investigated.[11,12] The chlorine-containing complexes are particularly attractive. Their relatively large rotational constants enable more detailed information to be obtained than for the heavier halogen complexes. In addition, their smaller mass and larger vibrational frequencies makes three-dimensional quantum mechanical calculations feasible.[14]

This pump-probe technique has been applied to He-,[11,12] Ne-,[10,12] and $ArCl_2$[13] complexes. The geometries are T-shaped,[7,8,13] and the dissociation dynamics follow a

parity conservation selection rule that allows rotational states of the complex to dissociate only to fragment rotational states of the same parity.[11] This parity conservation is observed for all triatomic chlorine complexes and arises from the symmetry of the rare gas-Cl_2 potential.

The detailed dissociation dynamics differs for the rare gas-chlorine triatomic molecules. For the $HeCl_2$ and $NeCl_2$ complexes, the dissociation occurs predominantly by the $\Delta v=-1$ channel.[10-12] The product rotational state populations are relatively independent of the total number of vibrational quanta initially excited and the number of vibrational quanta lost in the dissociation. The average amount of rotational energy released in the dissociation does not change dramatically with the amount of available energy. For $NeCl_2$ excited to certain vibrational states, conservation of energy dictates the maximum observable Cl_2 rotational quantum number, j. This enables the van der Waals bond energy of the complex to be estimated.

The dissociation of $ArCl_2$ may proceed by a different mechanism from that of the neon complex.[13] For higher vibrational levels, the $\Delta v=-1$ channel is closed energetically. The product rotational state populations for the $\Delta v=-2$ channel are structured and dependent on the initial vibrational state of the complex. This result has been attributed to intramolecular vibrational energy

relaxation (IVR) prior to dissociation. This sequential IVR model differs from the presumably direct dissociation mechanism of $HeCl_2$ and $NeCl_2$.

In addition to the triatomic rare gas-chlorine molecules discussed above, the pump-probe technique has been used to study complexes containing two and three argon atoms.[13] As in the $NeCl_2$ case, the product rotational states are constrained by conservation of energy for some vibrational levels. This has allowed the van der Waals bond energies to be determined for Ar_nCl_2, n=1,2,3. These energies compare well with predictions of additive atom-atom interactions. The band shifts in the excitation spectra were used to predict structures for the Ar_nCl_2. Unlike Ne_nI_2 and Ne_nBr_2, the Ar_nCl_2 complexes do not follow a simple band-shift rule. The results suggest that the argon atoms are equivalent in Ar_2Cl_2 but not in Ar_3Cl_2.[13]

This paper extends these pump-probe experiments to the Ne_2Cl_2 and Ne_3Cl_2 dissociations. We have measured excitation spectra that allow us to determine the structure of Ne_2Cl_2 and surmise a structure for Ne_3Cl_2. Product rotational and vibrational distributions have also been measured for Ne_2Cl_2, which enable us to estimate the van der Waals bond energy. The Ne_2Cl_2 product state populations for several vibrational levels are analyzed using a simple rotational surprisal analysis. The

following section describes the pump-probe technique and the experimental apparatus. Section 4.3 outlines the results and their analysis. Finally, Section 4.4 discusses how Ne_2Cl_2 and Ne_3Cl_2 compare to the complexes described above.

4.2 Experiment

The laser pump-probe technique used in these experiments has been described previously.[1-5,10,11] In brief, the Ne_2Cl_2 complex is excited by a visible pump laser to an electronic state correlating to the $B^3\Pi(0_u^+)$ state of Cl_2. For convenience, we refer to this as the B state when discussing both the Ne_2Cl_2 complex and the Cl_2 molecule. The vibrationally excited complex can undergo vibrational predissociation to yield neon atoms and a Cl_2 molecule in a lower vibrational level. Because the dissociation process is fast compared to the B-state radiative lifetime of Ne_2Cl_2, the Cl_2 fragment remains in the B state. A probe laser pulse then excites the Cl_2 fragment to the $E(0_g^+)$ state. The subsequent E→B fluorescence of the Cl_2 fragment is the detected signal.

There are several different experiments that can be performed using this pump-probe scheme. By fixing the pump laser frequency at the maximum of the Ne_2Cl_2 absorption and scanning the probe laser, the spectrum of

the Cl_2 fragments is measured, giving product vibrational and rotational state population distributions. Alternatively, by fixing the probe laser frequency and scanning the pump laser, an excitation spectrum of the Ne_2Cl_2 complex is obtained. Fixing the probe laser to detect a specific E←B transition will select the parity of the levels that can be observed in the excitation spectrum. This allows the recording of parity-selected excitation spectra with reduced spectral congestion.

The apparatus used in these experiments has also been described previously.[10,11] The sample was obtained by passing a mixture containing 90% neon and 10% helium over liquid chlorine at -77°C. The mixture was expanded at 450-475 psi through a 150 μ pulsed solenoid valve into a vacuum chamber. The pump and probe laser pulses passed colinearly through the vacuum system, intersecting the jet at a 90° angle. The durations of the pump and probe pulses were each 20 ns; the delay between them was approximately 10 ns. A photomultiplier tube detected the Cl_2 E→B fluorescence perpendicular to the jet and laser axes. This signal was preamplified and recorded with a gated integrator. A $XeCl_2$ excimer laser pumped both the pump and probe dye lasers. The pump laser bandwidth was 0.2 cm^{-1}; for measuring higher resolution excitation spectra, addition of an intracavity etalon decreased the bandwidth to 0.05 cm^{-1}. The probe laser output was

frequency-doubled to produce UV pulses with a 0.2 cm^{-1} bandwidth. The synchronization of the laser and valve pulses, the laser scanning, and the signal averaging were all computer-controlled.

4.3 Results and Analysis

4.3.1 Excitation Spectra

Figure 4.1 shows a low-resolution excitation spectrum of the B←X, $v'=15 \leftarrow v''=0$ band of Cl_2 and Ne_nCl_2 complexes. The excitation band of Ne_2Cl_2 is blue-shifted approximately 6 cm^{-1} from the $NeCl_2$ band, which in turn is blue-shifted approximately 6 cm^{-1} from the Cl_2 band origin. Also observed is a weak Ne_3Cl_2 signal, shifted approximately 6.5 cm^{-1} to the blue of the Ne_2Cl_2 band. The assignment of these features was confirmed by their qualitative dependence on the beam source pressure and concentration. The shifts increase slightly as a function of Cl_2 vibrational excitation, but their relative values remain approximately equal.

Parity-selected excitation spectra of the Ne_2Cl_2 B←X 8←0 band are shown in Figure 4.2. The even and odd excitation spectra were measured by scanning the probe laser through the 8←0 band while detecting the P(10) and P(11) rotational lines of the Cl_2 E←B 0←6 band,

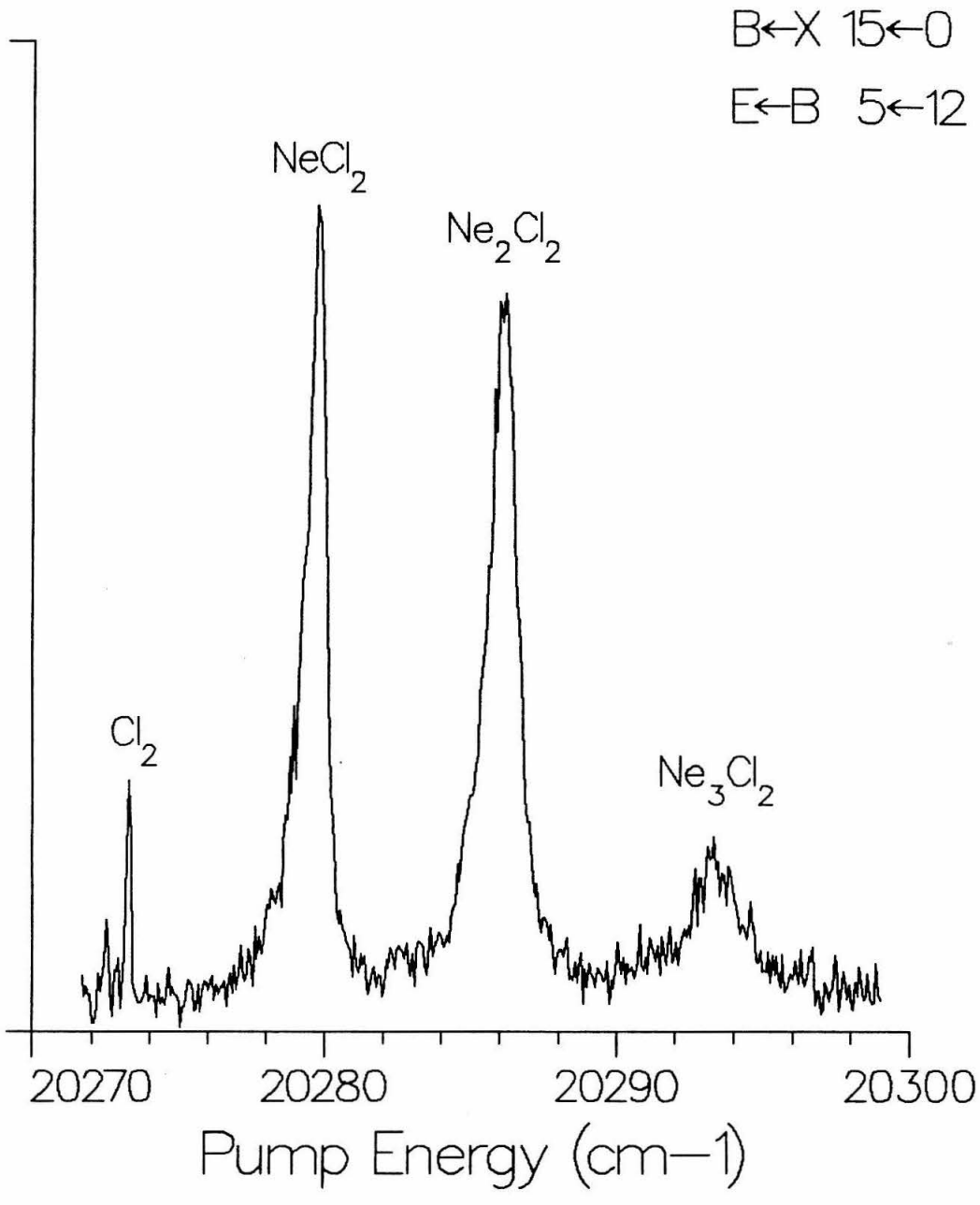

Figure 4.1. Low-resolution excitation spectrum near the B←X, 15←0 transition of Cl_2. To the blue of the Cl_2 excitation lie features assigned to $NeCl_2$, Ne_2Cl_2, and Ne_3Cl_2. The Cl_2 E←B, 5←12 transition is probed.

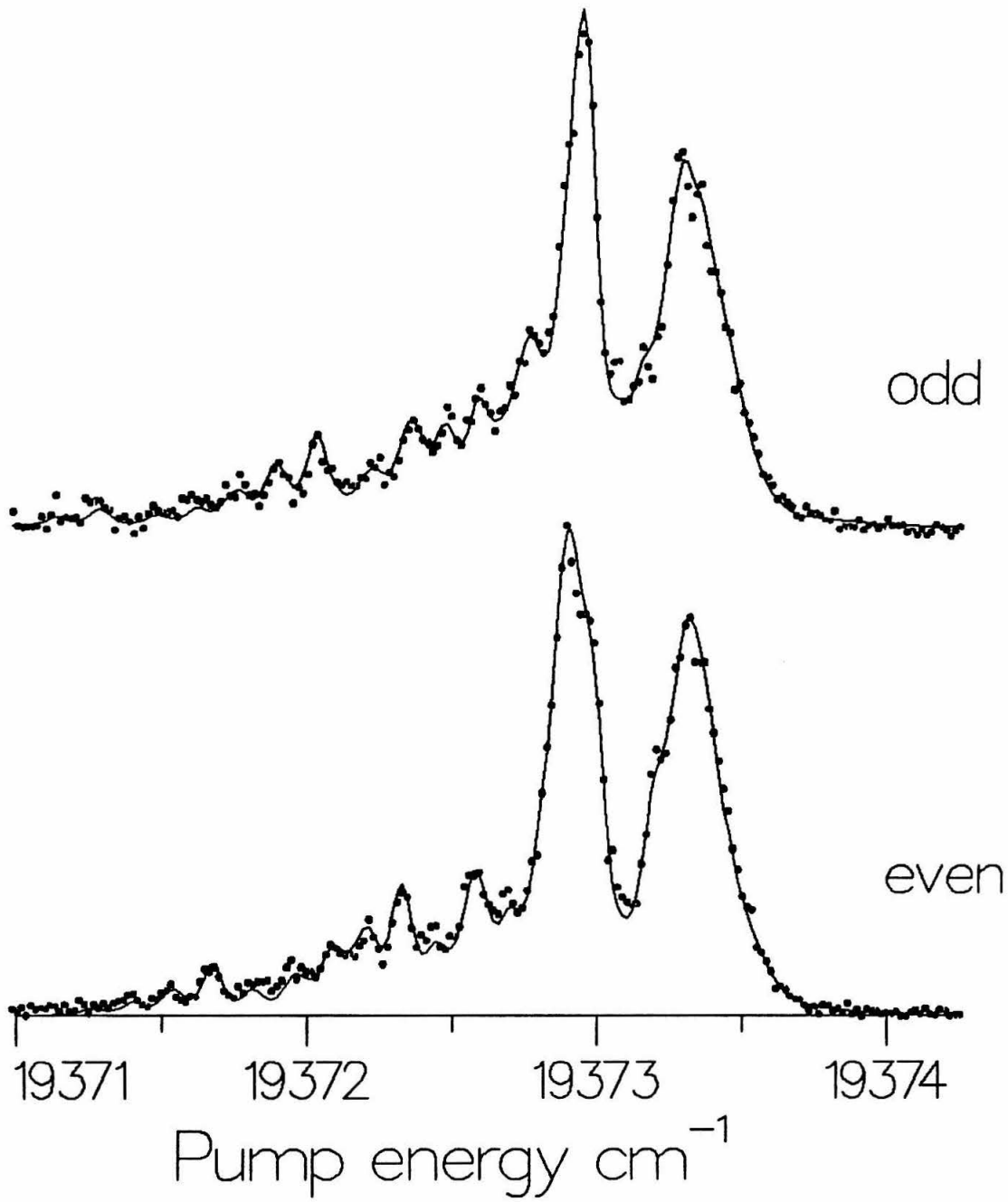

Figure 4.2. Parity-selected excitation spectra of Ne_2Cl_2. The pump laser is scanned through the Ne_2Cl_2 B←X 8←0 band, while the probe laser excites the Cl_2 E←B 6←0 transition. In the upper trace, the Cl_2 E←B 6←0 P(11) rotational line is probed, while in the lower trace the P(10) line is probed. The points represent the experimental data and the lines are calculated as described in the text. The pump laser bandwidth is 0.05 cm^{-1}.

respectively. The spectra shown by the solid lines are calculated from asymmetric top energy levels assuming rotational constants for the B and X states of the complex, a ground state rotational temperature, instrumental and homogeneous linewidths, and the band origin. The best fit was obtained with a rotational temperature of 1.6 K and a homogeneous linewidth of 0.043 cm^{-1}. The rotational constants determined by the fitting procedure correspond to a distorted tetrahedral structure, with the Cl-Cl axis perpendicular to the Ne-Ne axis. In both the X and B states, the Cl_2 bond distance is unchanged from the uncomplexed Cl_2 molecule. The Cl-Cl distances are 1.99 and 2.64 Å in the X and B states, respectively. The distances between the two neon atoms and between the neon-neon and chlorine-chlorine centers of mass are the same for the X and B states, within the error of the fitting procedure. The Ne-Ne distance is 3.12 Å, while the distance from the Cl_2 center of mass to the neon-neon center of mass is 3.23 Å. Other possible structures, such as a square planar configuration, could not reproduce the observed spectra.

Excitation spectra for two higher vibrational levels were also measured in order to observe differences in the homogeneous linewidths. The excitation spectra of the 11←0 and 13←0 bands of the complex were fit, using the

rotational constants determined from the 8←0 excitation spectra described above. The homogeneous linewidth increases with vibrational excitation: the 11←0 and 13←0 bands have linewidths of 0.12 cm^{-1} and 0.56 cm^{-1}, respectively. The three measured linewidths correspond to vibrational predissociation lifetimes of 123.7 ps for v=8, 44.4 ps for the v=11, and 9.5 ps for the v=13 band.

4.3.2 Fragment Rotational and Vibrational Distributions

The Cl_2 fragment vibrational and rotational state distributions for the vibrational predissociation of Ne_2Cl_2 were measured by fixing the pump laser frequency and scanning the probe laser. For lower vibrational levels ($v' \leq 9$), Ne_2Cl_2 can dissociate by transferring either one or two quanta of Cl_2 vibrational energy to the van der Waals modes. As v' increases, the energy of the Cl_2 vibrational quanta decreases, and the Δv=-1 channel closes. For example, following excitation of the complex to v'=7 (B←X, 7←0), Cl_2 fragments are observed with both v=6 and 5. Correcting the observed line intensities for the different Franck-Condon factors[12] shows that the Δv=-2 channel accounts for 21% of the observed Cl_2 fragments. For v'=9, Δv=-2 accounts for 81% of the observed Cl_2 products. For both the 9←0 and the 7←0 bands, the Δv=-3 channel was only weakly observed.

Measurement of the Cl_2 product rotational spectrum for a vibrational band close to the energetic closing of the $\Delta v=-1$ channel provides an estimate for the van der Waals bond energy of the complex.[12] Figure 4.3 shows the Cl_2 fragment spectrum measured by exciting the B←X 9←0 transition of the complex and scanning through the Cl_2 fragment E←B 1←8 transition. The spectrum shows a sharp cutoff at j=10, as marked in Figure 4.3. The sharp drop in intensity between j=10 and j=11 may indicate that a single Cl_2 stretching quantum provides sufficient energy to populate j=10 but is insufficient to populate j=11. The energies of the j=10 and j=11 levels can be used to estimate upper and lower limits for the total B state van der Waals bond energy. Using these limits, the B state bond energy of the complex falls between 145.6 cm^{-1} and 148.6 cm^{-1}.

The weakly observed j=11,12,13 lines in the spectrum can be attributed to dissociation via a different mechanism. The sharp drop in intensity at j=10 is caused by the energetic closing of the complete dissociation channel:

$$Ne_2Cl_2\ (v) \rightarrow 2\ Ne\ +\ Cl_2\ (v-1, j\leq 10)\ . \qquad (1)$$

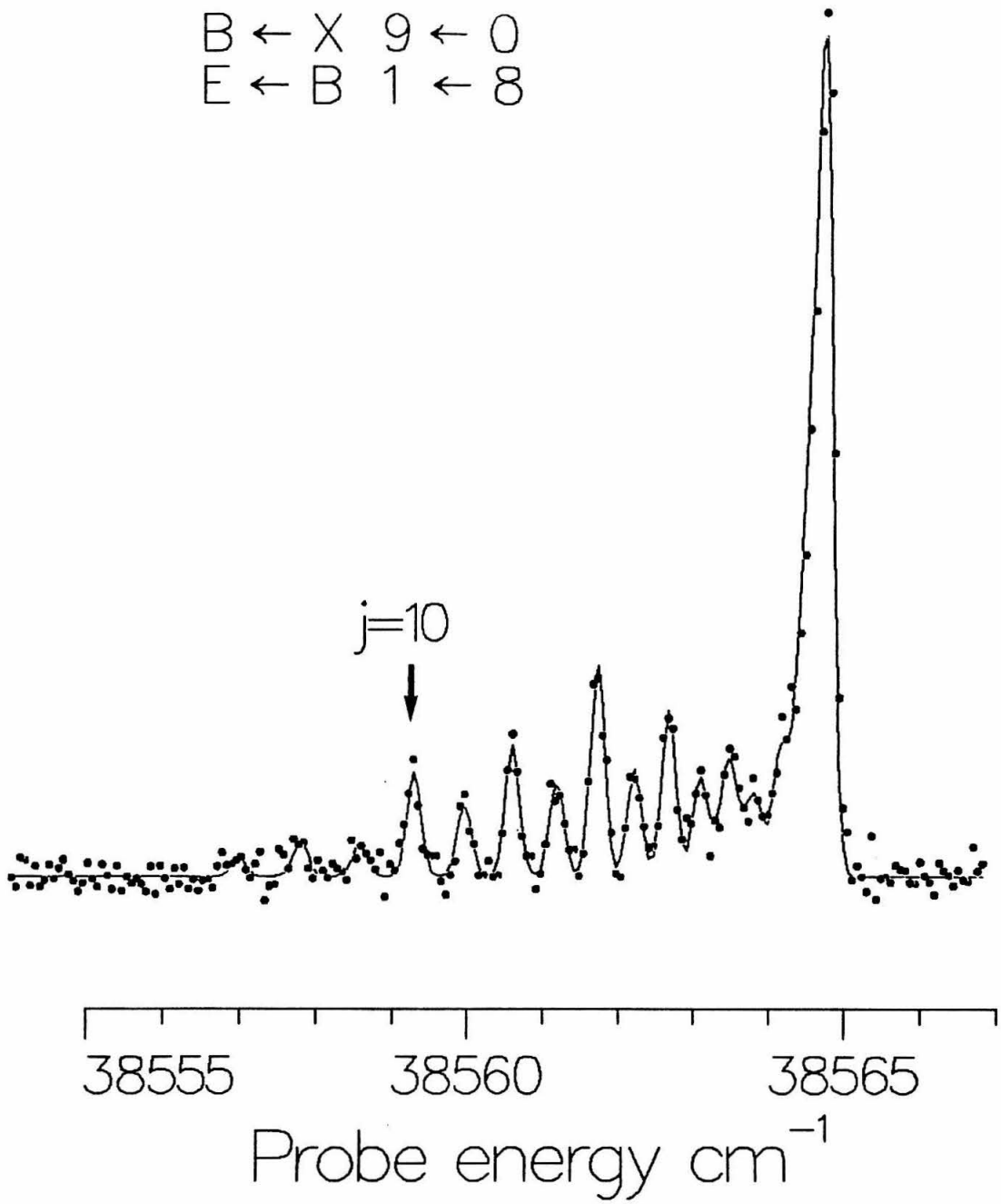

Figure 4.3. Cl_2 fragment E←B 1←8 spectrum, following excitation of the Ne_2Cl_2 B←X 9←0 transition. An arrow marks the highest strongly observed rotational line, j=10. The dots are the experimental data and the lines are a calculated Cl_2 spectrum. The band width of the pump laser is 0.2 cm^{-1}, enabling excitation of both even and odd levels.

For a dissociation to a Ne_2 fragment,

$$Ne_2Cl_2\ (v) \rightarrow Ne_2 + Cl_2\ (v-1, j \leq 13), \qquad (2)$$

approximately 16 cm^{-1} more energy is available for product rotation, making higher j levels accessible. Some excitation above the energetic closing of mechanism (1) can be expected because of the 1.5 K rotational distribution of the initial states. At this temperature, however, the initial energies cover a 1 cm^{-1} range, which would not account for the excitation of three additional j levels, 3.0, 6.3, and 9.9 cm^{-1} higher in energy than j=10.

The fragment rotational spectrum of a lower vibrational band illustrates another aspect of the Ne_2Cl_2 complex dissociation. Figure 4.4 displays the spectrum obtained by scanning the probe laser through the Cl_2 E←B 0←6 transition, while exciting the Ne_2Cl_2 B←X 7←0 transition. A broad feature is observed ~20 cm^{-1} to the red of the Cl_2 rotational spectrum. We attribute this feature to the excitation of $NeCl_2$ fragments resulting from an incomplete dissociation:

$$Ne_2Cl_2\ (B,\ v=7) \rightarrow Ne + NeCl_2\ (B,\ v=6). \qquad (3)$$

This assignment is confirmed by the observation of double resonance excitation of $NeCl_2$ (E ← B, v=6 ← X) at the same

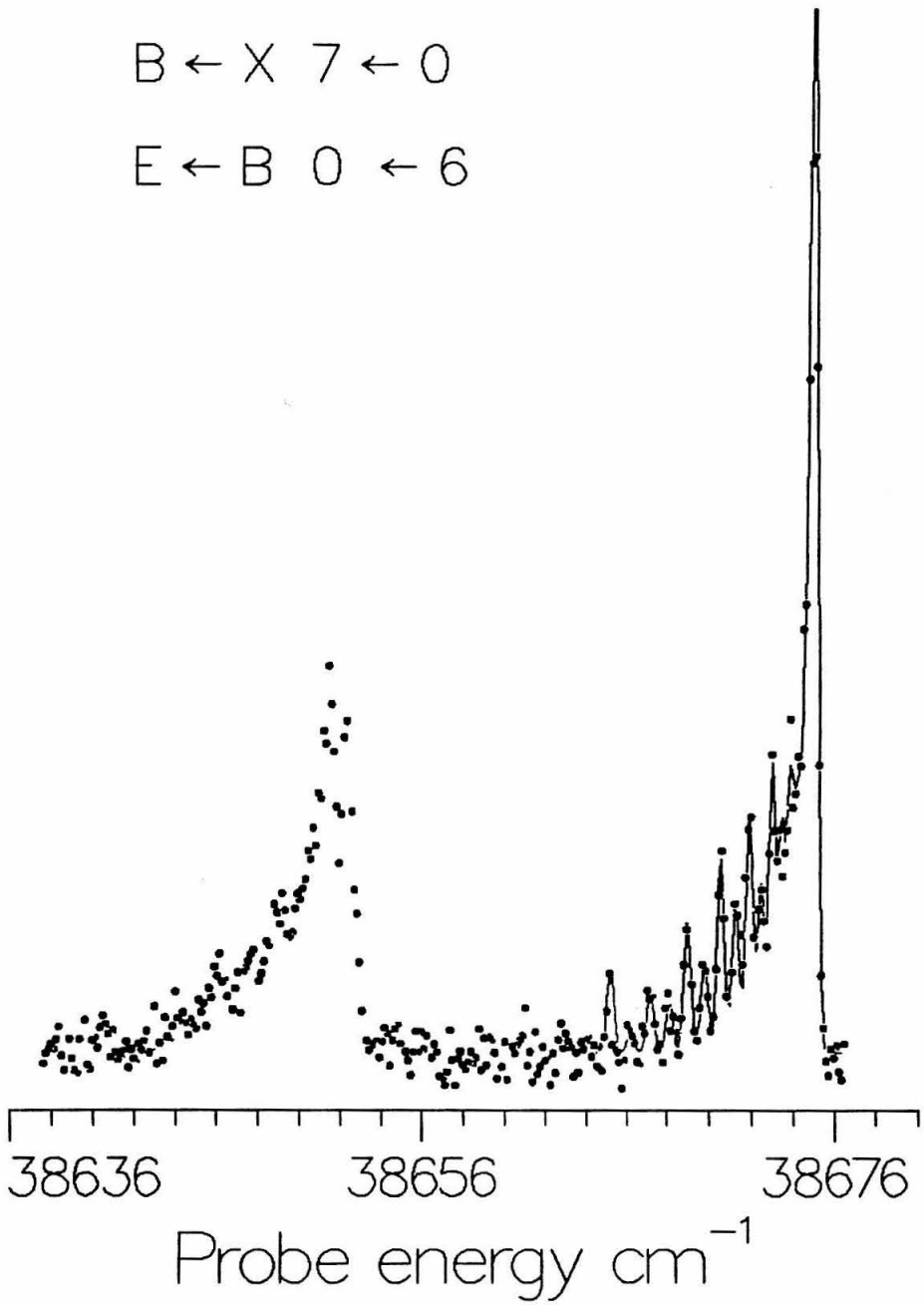

Figure 4.4. Cl_2 and $NeCl_2$ fragment E←B 0←6 spectrum, following excitation of the Ne_2Cl_2 B←X 0←7 transition. On the right lies the Cl_2 fragment rotational spectrum. The feature on the left is attributed to a $NeCl_2$ fragment excitation. The points represent the experimental data and the line is a calculated Cl_2 spectrum.

frequency. The direction of the band shift is consistent with that observed for a double resonance excitation of NeICl (E←A←X), although the magnitude is smaller.[2] This red shift indicates that the $NeCl_2$ E state binding energy is about 20 cm^{-1} greater than that of the B state, smaller than the 44 cm^{-1} difference observed for the NeICl complex.[2] For this E←B excitation to be observed, the lifetime of the $NeCl_2$ intermediate must be on the order of nanoseconds, the approximate delay between the start of the pump and probe pulses. The calculated lifetime for $NeCl_2$ (B, v'=6) is approximately 1.5 nanoseconds.[12] Theoretical predictions for $NeCl_2$ indicate that excitation of the van der Waals bends, likely to occur in reaction (3), may increase the lifetime, however.[12,14] This feature does not correspond to a transition of any Cl_2 isotope. In addition, the broadening observed in the feature would not be expected for a Cl_2 transition. The band is also shifted too far from the Cl_2 E←B, 0←7 transition to be attributed to an E←B excitation of Ne_2Cl_2 (B,υ=7).

4.3.3 Analysis of Fragment Rotational Distributions

The Cl_2 product rotational state populations can be extracted from the intensities of the rotational lines of the probe spectra.[12] The population distributions vary

smoothly with j, as do the distributions observed for $NeCl_2$[12] but unlike the structured distributions of $ArCl_2$.[13] Unlike the $NeCl_2$ and the $HeCl_2$ distributions,[12] no bimodal character is observed. The distributions do not change dramatically as the energy available for product rotation increases. Table 4.1 contains a summary of the results for several initial vibrational levels. Both the maximum-populated j state and the average rotational energy, $\langle E_{rot} \rangle$, increase slowly with the total available kinetic energy, E_{avail}. Considering the wide differences in the amount of available energy, the ratio between $\langle E_{rot} \rangle$ and E_{avail} does not vary strongly.

A more quantitative summary of these features of the Cl_2 rotational state population distributions is obtained by applying surprisal theory.[22,23] The method used here provides a quantitative comparison of the observed population distribution to a smooth prior distribution, P^o. This prior distribution assumes no dynamical constraints, and thus the probabilty of populating a given rotational level is proportional to an appropriate density of states. Using the degeneracy of rigid rotor levels and the density of translational energy states, the probability of populating a given j level of a given vibrational level of the Cl_2 fragment is[24]

$$P^o(j) \alpha \ (2j + 1) \ (E_{avail} - E_{rot}(j))^2 \ .$$

Table 4.1

Summary of Cl_2 fragment rotational state population distributions for the dissociation of Ne_2Cl_2. Energies are in cm^{-1}.

B←X	E←B	j_{max}	$E(j_{max})$	$\langle E_{rot} \rangle$ even	$\langle E_{rot} \rangle$ odd	$\langle E_{rot} \rangle / E_{avail}$ even	$\langle E_{rot} \rangle / E_{avail}$ odd	E_{avail}
$\Delta v=-2$								
13←0	4←11	24	75.46	18.71	19.00	.179	.182	104.24
9←0	0←7	29	122.74	26.03	28.08	.136	.147	191.36
8←0	0←6	31	143.29	28.02	28.46	.131	.134	213.12
7←0	0←5	30	137.38	24.01	22.63	.102	.097	234.50
$\Delta v=-1$								
9←0	1←8	10	15.17	6.21	4.90	.409	.323	15.17
8←0	0←7	12	22.06	7.70	6.36	.279	.230	27.60
7←0	0←6	16	39.37	8.02	6.77	.209	.177	38.34

Here, E_{avail} is the total energy available to the fragments and $E_{rot}(j)$ is the rotational energy of the fragments. The surprisal for a given j level gives a measure of the deviation between the prior and the observed distributions. Using the reduced rotational energy,

$$g = \frac{E_{rot}}{E_{avail}} ,$$

the rotational surprisal for a given vibrational level υ is defined as:

$$I(g;\upsilon) = -\ln \frac{P(g)}{P^{o}(g)} .$$

Here, P(g) is the observed distribution and $P^{o}(g)$ is the calculated prior distribution. In simple rotational surprisal analysis, I(g) is approximated as a linear function of g:

$$I(g) = \theta_o + \theta_r g .$$

The slope of the surprisal plot, θ_r, characterizes the observed population distribution. A positive value of θ_r

indicates that the observed distribution is "cold" in comparison to the prior distribution.

Figures 4.5-4.8 show prior and experimental distributions along with surprisal plots for four vibrational channels. The values of θ_r for these channels are summarized in Table 4.2. The even and odd j states are each treated separately, since the parity selection rule prevents mixing between them. The figures illustrate the analysis of the even j states, while the results in Table 4.2 include both even and odd levels. For some spectra, the population of the j=0 level is highly uncertain because of overlapping lines in the bandhead. For these spectra, the j=0 point was excluded from the determination of θ_r. All vibrational levels exhibit positive θ_r values, indicating that the observed populations as a function of reduced rotational energy are all colder than the prior distribution.

Figures 4.5, 4.6, and 4.7 compare the $\Delta\upsilon$=-2 channel for different amounts of initial vibrational excitation. The θ_r values increase as the number of vibrational quanta decreases. For the dissociation of Ne_2Cl_2 υ=13 (Figure 4.5), 87 cm^{-1} less energy is available than for υ=9 (Figure 4.6), which in turn has 43 cm^{-1} less energy available than the υ=7 (Figure 4.7). The trend in θ_r indicates that complexes with the most energy available for rotation have the coldest product distribution.

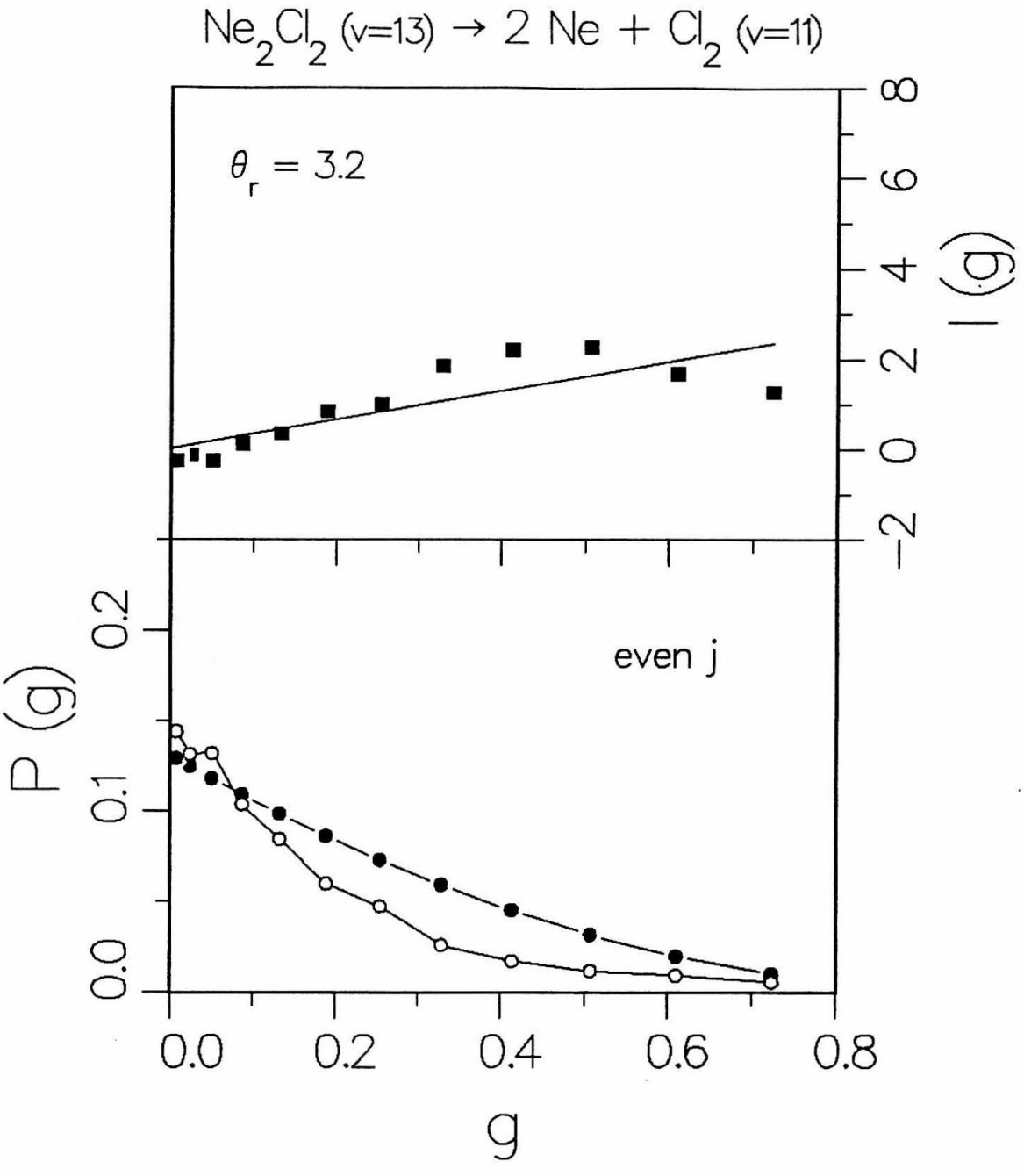

Figure 4.5. Rotational surprisal analysis of the υ=13, $\Delta\upsilon$=-2 dissociation channel. The lower plot shows the prior distribution (solid circles) and the experimental distribution (open circles) as a function of relative rotational energy, g. The upper plot shows the rotational surprisal as a function of g. The line is a best fit to the calculated surprisals.

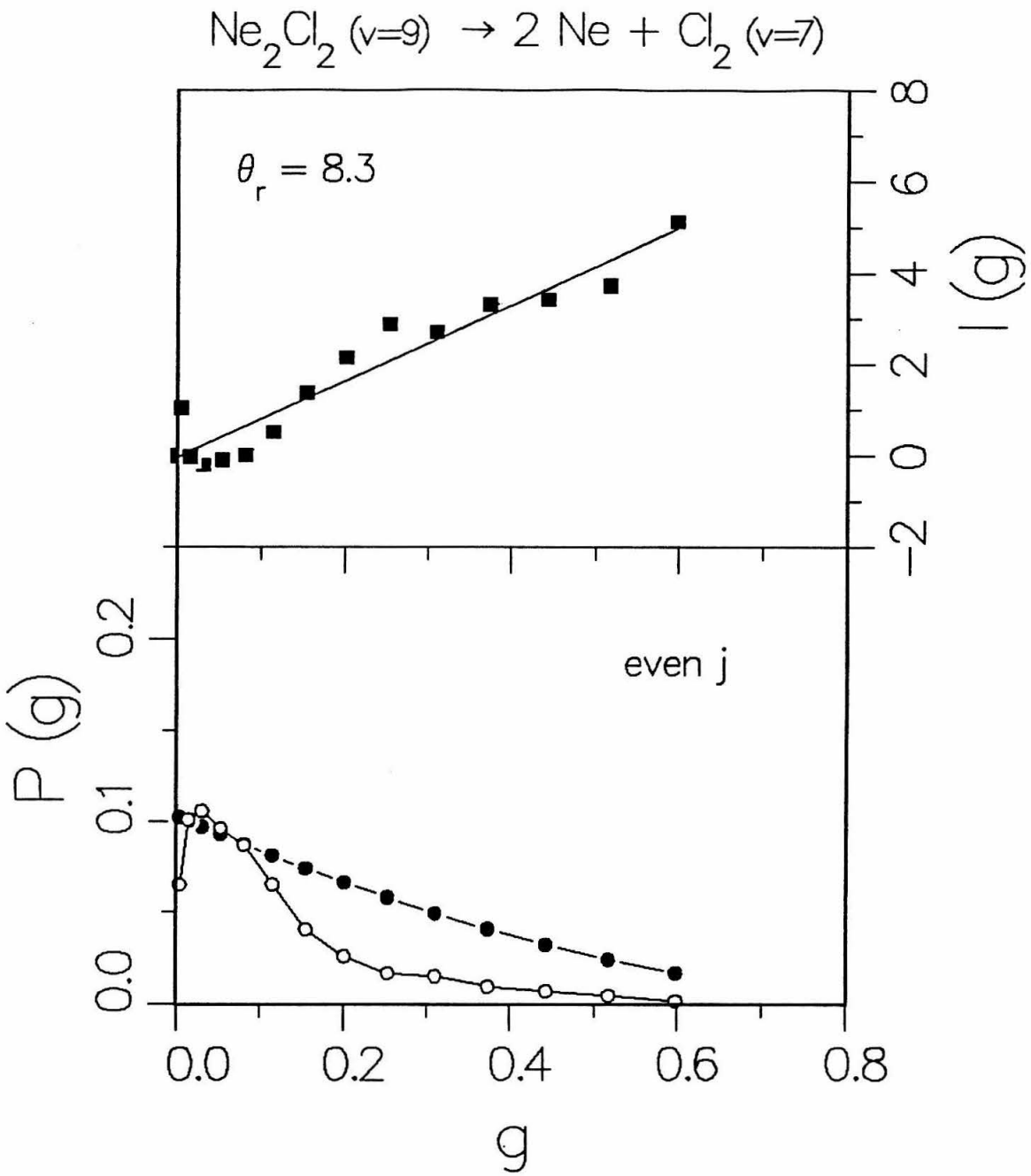

Figure 4.6. Rotational surprisal analysis of the υ=9, $\Delta\upsilon$=-2 dissociation channel. In the lower plot, the prior distribution (solid circles) and the experimental distribution (open circles) are displayed as a function of relative rotational energy, g. The upper plot shows the rotational surprisal as a function of g. A best fit to the calculated surprisals is also displayed.

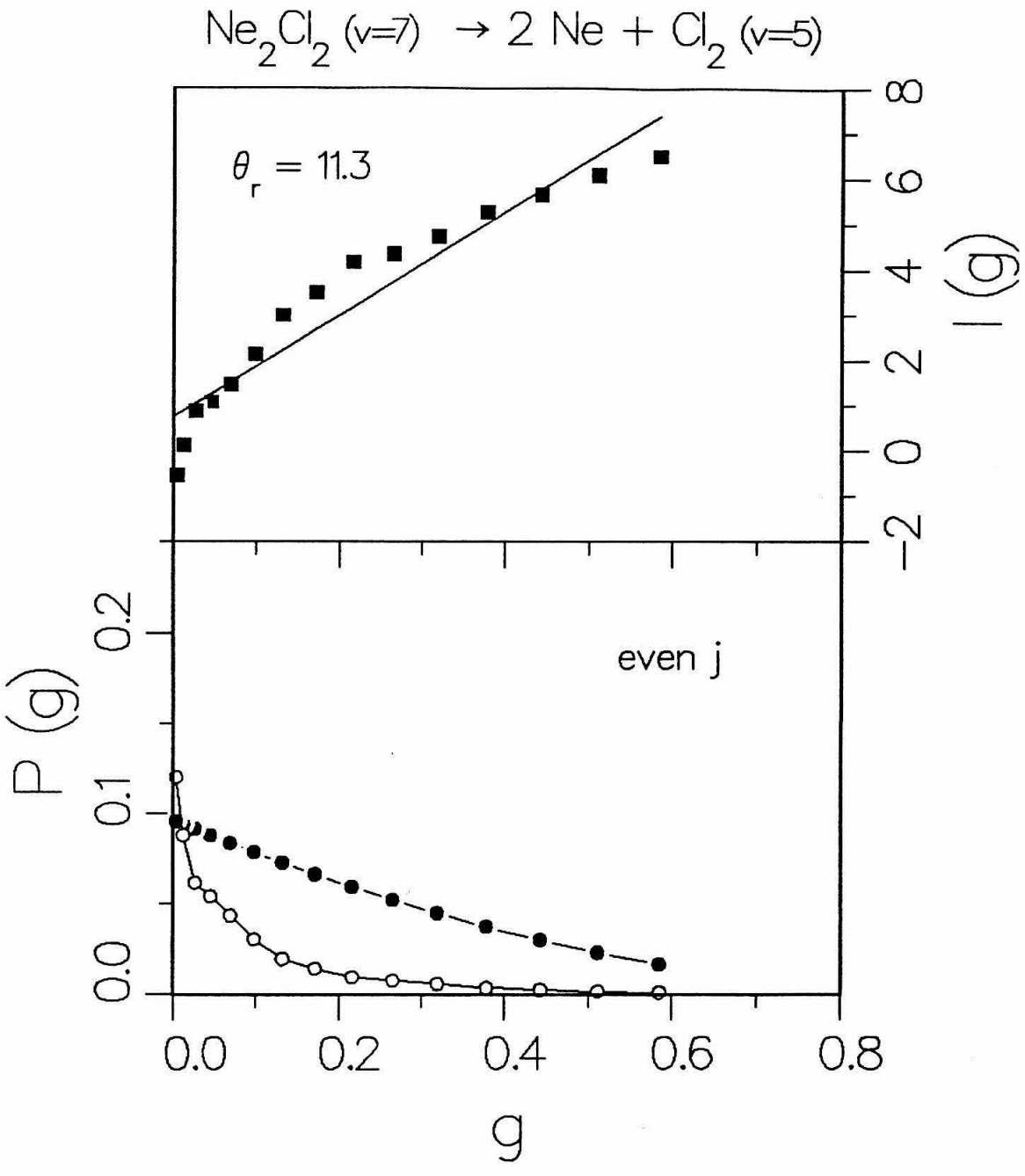

Figure 4.7. Rotational surprisal analysis of the υ=7, $\Delta\upsilon$=-2 dissociation channel. The lower plot shows the prior distribution (solid circles) and the experimental distribution (open circles) as a function of relative rotational energy, g. In the upper plot, the rotational surprisal is plotted as a function of g. The line is a best fit to the calculated surprisals.

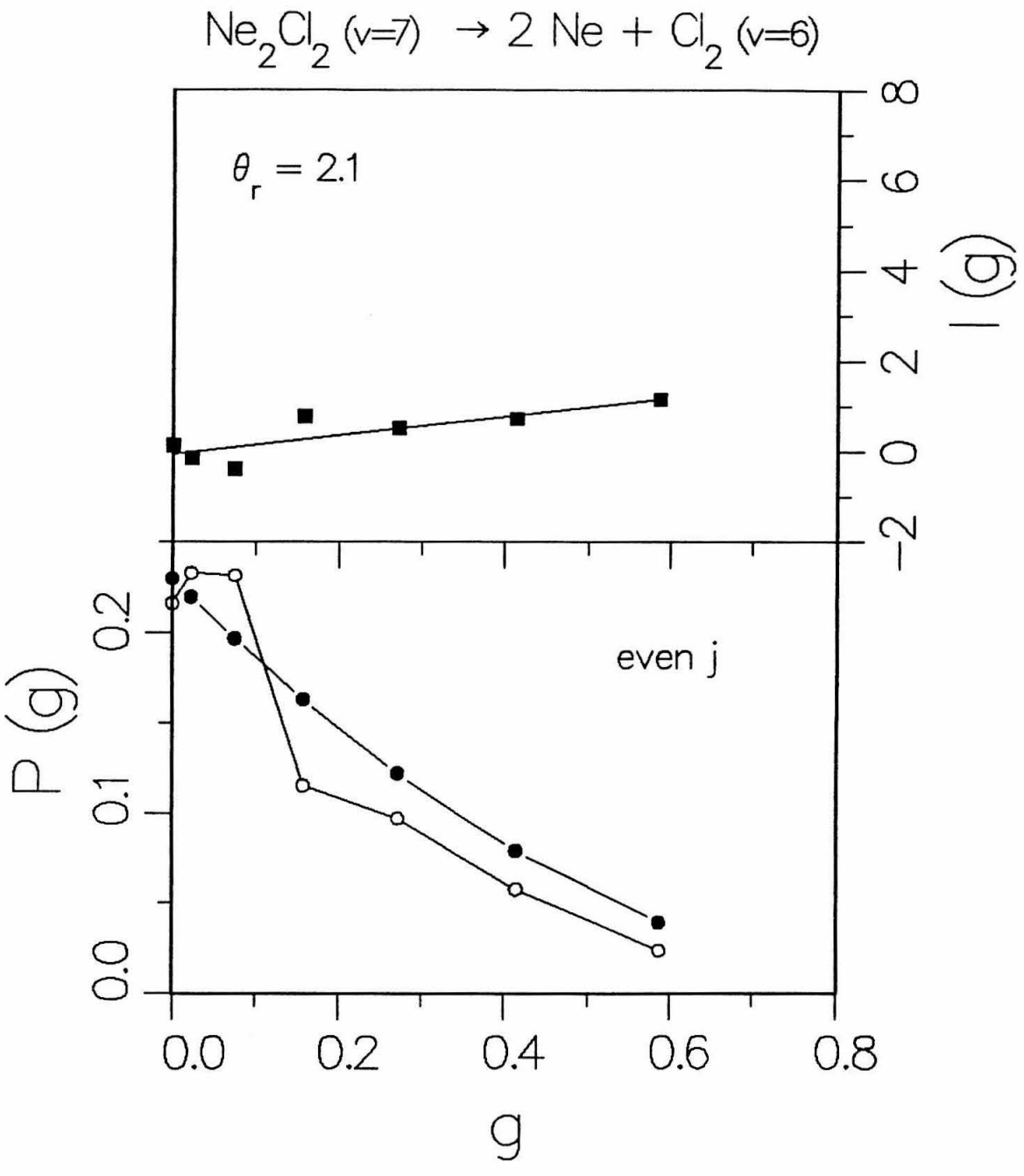

Figure 4.8. Rotational surprisal analysis of the υ=7, Δυ=-1 dissociation channel. The lower plot shows the prior distribution (solid circles) and the experimental distribution (open circles) as a function of g. The upper plot shows the rotational surprisal as a function of g. The line is a best fit to the calculated surprisals.

Table 4.2

Slope of rotational surprisal plots for the dissociation reaction $Ne_2Cl_2(v=n) \rightarrow 2\ Ne + Cl_2(v=m)$.

n	m	J parity	θ_r
13	11	even	3.19
		odd	3.15
9	7	even	8.33
		odd	7.57
8	6	even	8.80
		odd	8.49
7	5	even	11.27
		odd	12.42
8	7	even	0.82
		odd	0.45
7	6	even	2.10
		odd	0.86

Figures 4.7 and 4.8 compare the Δv=-1 and Δv=-2 channels for the dissociation of the Ne_2Cl_2 complex with seven quanta in the Cl_2 vibration. The slope of the Δv=-2 channel (Figure 4.7) is greater than that of the Δv=-1 channel (Figure 4.8). Once again, the channel with the most available energy, the Δv=-2 channel, appears to have a colder rotational distribution.

4.4 Discussion

The results presented for the Ne_2Cl_2 and Ne_3Cl_2 complexes can be compared to those observed for several rare gas-halogen complexes. In this section, we first compare the structural results for Ne_2Cl_2 and Ne_3Cl_2 to those of Ar_nCl_2, Ne_nBr_2, and Ne_nI_2. The bond energy determined for Ne_2Cl_2 is then compared to predictions of an additive atom-atom interaction model. Next, we discuss the dissociation dynamics of Ne_2Cl_2 in comparison to that of $NeCl_2$, NeICl, and Ne_nI_2. Finally, we present conclusions drawn from the results for the Ne_2Cl_2 molecule.

The distorted tetrahedral structure determined for the Ne_2Cl_2 complex agrees with predictions based on additive atom-atom interactions. The two neon atoms are each 3.59 Å from the Cl_2 center of mass, which is close to

the 3.54 Å bond distance observed for $NeCl_2$. In addition, the Ne-Ne distance (3.12 Å) is close to the minimum of the Ne_2 van der Waals potential (3.15 Å).[25] The equivalent positions of the two neon atoms agree with predictions of a simple band shift rule.[18-20] For Ne_nCl_2 (n=1-3) complexes, the increase in the shifts of the B←X excitation bands from the Cl_2 band is nearly linear with n. Although these shifts do not probe the van der Waals bonding in either the X or B state directly, they indicate that the difference in the total van der Waals binding energy in the X and B states changes by a constant amount with each additional rare gas atom. From this fact, it is reasonable to assume that the binding energy per rare gas atom in the X and B states does not vary with n.[18,19] Since nearly equal shifts are observed for the excitation features of Ne_nCl_2 (n=1-3), the neon atoms have almost equal binding energies and thus equivalent positions in the complex. For Ne_3Cl_2, the equivalent shifts suggest that the three neon atoms circle the Cl_2 bond axis. This agrees with the "belt" model predicted for Ne_nI_2 (n=1-6)[19] and Ne_nBr_2 (n=1-3).[21] The three neon-containing complexes all exhibit the same pattern of nearly equal shifts in the excitation spectra, but the Ar_3Cl_2 complex does not.[13] The predicted Ar_3Cl_2 structure is a triangle of argon atoms clustered near the Cl_2. This geometry includes an additional rare gas-rare gas

interaction not present for the n=3 complexes in the belt structure. The increased energy of the Ar-Ar attraction over the Ne-Ne attraction may account for the different structures predicted from the observed spectral shifts. Calculations for Ne_3Cl_2 using simple atom-atom potentials indicate that the minimum for the clustered structure, with three neon-neon interactions, is slightly higher in energy than that of the belt structure, with two neon-neon interactions.

As shown above, the structure determined for Ne_2Cl_2 agrees with predictions of atom-atom interactions; however, the total B state van der Waals bond energy determined for the Ne_2Cl_2 complex is greater than predicted using this model. The experimental value of the total Ne_2Cl_2 van der Waals binding energy ($D_o \sim 147$ cm^{-1}) is 20 cm^{-1} larger than 2 D_o $(Ne\text{-}Cl_2)$[12] + D_o (Ne_2)[25] = (2x54) + 16 = 124 cm^{-1}. There are three possible corrections to the two bond energy values that may reduce this descrepancy. First, the experimental bond energy determination neglects the effect of the centrifugal barrier to dissociation, which results from fragment angular momentum.[12] For the observed j states, we expect the barrier to be on the order of 2-3 cm^{-1}. Another source of disagreement may be the uncertainty of the small Ne-Ne D_o value.[25] Again, this uncertainty can account for only a few cm^{-1} of the discrepancy. Finally, the

zero-point energy of the complex may be responsible for part of the disagreement. If the attraction between atoms is additive, one would expect the sum of the atom-atom well depths, D_e, to predict the total interaction, rather than the sum of the D_o values. If the zero-point energy for Ne_2Cl_2 differs from the sum of the 2 $NeCl_2$ and Ne_2 zero-point energies (48 cm^{-1}), the prediction made with D_o values would be incorrect.

The dissociation dynamics of Ne_2Cl_2 exhibits many similarities to that of $NeCl_2$.[12] In both cases, the Cl_2 fragment rotational state populations vary smoothly with j and are very similar for different vibrational channels. Increasing the available energy by changing the initial vibrational excitation or by observing a different Δv channel does not drastically change the fragment rotational population distributions for either Ne_2Cl_2 or $NeCl_2$. The average rotational energy, $\langle E_{rot} \rangle$, and the ratio between $\langle E_{rot} \rangle$ and E_{avail} are slightly larger for Ne_2Cl_2 than for $NeCl_2$, but for each molecule the ratio does not change significantly with available energy. Unlike the $NeCl_2$ case, the Ne_2Cl_2 rotational state population distributions do not exhibit any bimodal behavior. Although the Ne_2Cl_2 distributions appear smooth, the prior distribution utilized by simple rotational surprisal analysis does not fit the experimental distributions. This prior distribution does

not include dynamical constraints that are necessary to describe the Ne_2Cl_2 dissociation. The rotational distributions of Ne_2Cl_2 and $NeCl_2$ both differ from the behavior exhibited by NeICl (υ=23).[5] The rotational distribution for the $\Delta\upsilon$=-1 channel of NeICl (v=23) is dominated by low j states, while that of the $\Delta\upsilon$=-2 channel is nearly uniformly populated up to rotational levels that account for 69% of the available energy.

The homogeneous, linewidth-derived lifetimes observed for Ne_2Cl_2 are shorter than those of $NeCl_2$. For example, in the υ'=11 level, the Ne_2Cl_2 lifetime is 44 ps, while that of $NeCl_2$ is 100 ps.[9] If the Ne_2Cl_2 dissociation occurs in two sequential steps, the line broadening will give the time of the first dissociation step. The linewidth comparison between Ne_2Cl_2 and $NeCl_2$ agrees with theoretical predictions for the Ne_2I_2 sequential dissociation.[15] This calculation, which assumed a linear Ne_2I_2 structure, predicted that the first neon dissociation would take half the time of the second.

The fragment vibrational distributions for Ne_2Cl_2 differ from those observed for He_2I_2,[18] Ne_2I_2,[19] and $HeArI_2$.[20] For the He_2I_2 complex, dissociation occurs almost exclusively via the $\Delta\upsilon$=-2 channel, even though the $\Delta\upsilon$=-1 channel is energetically available. This suggests a mechanism consisting of two independent, sequential helium atom dissociations. For Ne_2I_2, both the $\Delta\upsilon$=-2 and $\Delta\upsilon$=-3

channels are observed. The Δv=-3 channel appears to a greater extent than predicted by an independent, sequential mechanism, however. The $HeArI_2$ complex also seems to dissociate in an interdependent manner, since both the ArI_2 and $HeArI_2$ complexes dissociate via the Δv=-3 channel. Unlike these I_2-containing complexes, Ne_2Cl_2 dissociates via the Δv=-1 channel, when energetically possible. This indicates that the dissociation of the two neon atoms does not occur independently, although a sequential mechanism is still possible. The possibility of dissociation to a Ne_2 fragment (Equation 2) underscores the interdependence of the neon atom dissociations.

For dissociation of Ne_2Cl_2 via the Δv=-2 channel, we cannot conclude whether the dissociation of the two neon atoms is independent. The direct E←B excitation of $NeCl_2$ indicates that a sequential mechanism (Equation 3) is important for the Δv=-2 channel, however.

Clearly, the dissociation dynamics of the Ne_2Cl_2 complex is not simple enough to be described as two successive $NeCl_2$ dissociations. Nor is the Ne_2Cl_2 complex large enough to behave in a statistical manner. While our results cannot conclusively determine the importance of different possible dissociation mechanisms, they do suggest several important mechanistic features.

4.5 Conclusions

The results presented here determine the structure of Ne_2Cl_2 to be a distorted tetrahedron, as predicted by additive atom-atom interactions. The shifts in the excitation features predict a Ne_3Cl_2 structure with the three neon atoms encircling the Cl_2 bond axis. The total B state van der Waals bond energy of Ne_2Cl_2 is found to be between 145.6 cm^{-1} and 148.6 cm^{-1}, 15% greater than predicted by adding $D_o(Ne_2)$ and 2 $D_o(Ne\text{-}Cl_2)$. The Ne_2Cl_2 complex dissociates via the $\Delta v=-1$ channel, as well as the $\Delta v=-2$ channel, indicating that the dissociation of the two neon atoms is interdependent. For Ne_2Cl_2, the fragment rotational population distributions are only weakly dependent on the initial Cl_2 vibrational excitation and the Δv of the channel. A simple rotational surprisal analysis shows that the observed rotational distributions are all cold relative to a random prior distribution, and become colder as the total available energy increases. Finally, observation of a $NeCl_2$ fragment E←B excitation points out the importance of a sequential dissociation mechanism. This result suggests the possibility of directly monitoring the time evolution of cluster evaporation as a function of size.

4.6 References

[1] J.M. Skene and M.I. Lester, *Chem. Phys. Let.* **116**, 93 (1985).

[2] J.C. Drobits, J.M. Skene, and M.I. Lester, *J. Chem. Phys.* **84**, 2896 (1986).

[3] J.M. Skene, J.C. Drobits, and M.I. Lester, *J. Chem. Phys.* **85**, 2329 (1986).

[4] J.C. Drobits and M.I. Lester, *J. Chem. Phys.* **86**, 1662 (1987).

[5] J.C. Drobits and M.I. Lester, *J. Chem. Phys.* **88**, 120 (1988).

[6] J.C. Drobits, J.M. Skene, and M.I. Lester, poster presentation, Conference on the Dyamics of Molecular Collisions; July, 1987, Wheeling, WV.

[7] J.I. Cline, D.D. Evard, F. Thommen, and K.C. Janda, *J. Chem. Phys.* **84**, 1165 (1986).

[8] D.D. Evard, F. Thommen, and K.C. Janda, *J. Chem. Phys.* **84**, 3630 (1986).

[9] D.D. Evard, F. Thommen, J.I. Cline, and K.C. Janda, *J. Phys. Chem.* **91**, 2508 (1987).

[10] J.I. Cline, N. Sivakumar, D.D. Evard, and K.C. Janda, *J. Chem. Phys.* **86**, 1636 (1987).

[11] J.I. Cline, N. Sivakumar, D.D. Evard, and K.C. Janda, *Phys. Rev.* **A 36**, 1944 (1987).

[12] J.I. Cline, Ph.D. Thesis, California Institute of Technology, 1988; Janda and coworkers, manuscripts in preparation.

[13] D.D. Evard, Ph.D. Thesis, California Institute of Technology, 1988; D.D. Evard, C.R. Bieler, J.I. Cline, N. Sivakumar, and K.C. Janda, manuscript in preparation.

[14] N. Halberstadt, J.A. Beswick, and K.C. Janda, *J. Chem. Phys.* **87**, 3966 (1987); B.P. Reid, K.C. Janda, and N. Halberstadt, *J. Phys. Chem.* **92**, 587 (1988).

[15] G.C. Schatz, V. Buch, M.A. Ratner, and R.B. Gerber, *J. Chem. Phys.* **79** 1808 (1983); M.A. Ratner and R.G. Gerber, *J. Phys. Chem.* **90**, 20 (1986).

[16] J. Bösiger and S. Leutwyler, *Phys. Rev. Let.* **59**, 1895 (1987), and references therein; D. Eichenauer and R.J. Le Roy, *J. Chem. Phys.* **88**, 2898 (1988), and references therein.

[17] For a review see D.H. Levy, *Adv. Chem. Phys.* **47**, 323 (1981).

[18] W. Sharfin, K.E. Johnson, L. Wharton, and D.H. Levy, *J. Chem. Phys.* **71**, 1292 (1979).

[19] J.E. Kenny, K.E. Johnson, W. Sharfin, and D.H. Levy, *J. Chem. Phys.* **72**, 1109 (1980).

[20] K.E. Johnson, W. Sharfin, and D.H. Levy, *J. Chem. Phys.* **74**, 163 (1981).

[21] B.A. Swartz, D.E. Brinza, C.M. Western, and K.C. Janda, *J. Phys. Chem.* **88**, 6272 (1984).

[22] For a general discussion of surprisal theory, see R.D. Levine and J.L. Kinsey, *Atom-Molecule Collision Theory: A Guide for the Experimentalist*, ed. R.B. Bernstein (Plenum, New York, 1979); R.B. Bernstein, *Chemical Dynamics via Molecular Beam and Laser Techniques* (Oxford University Press, New York, 1982).

[23] Examples of the application of surprisal theory can be found in R.D. Levine and R.B. Bernstein, *Accts. Chem. Res.* **7**, 393 (1974); E. Zamir, R.D. Levine, and R.B. Bernstein, *Chem. Phys.* **55**, 57 (1980).

24 The rotational prior for the Ne_2Cl_2 dissociation differs from that given in Reference 22, because the density of translational states includes contributions from three dissociating fragments. For a binary collision, with one relative velocity vector, the density of translational states is proportional to the square root of the translational energy. For three separating particles, there are two relative velocity vectors, and the translational density of states goes as

$$\int_0^{E_{tr}} E_1^{1/2} (E_{tr} - E_1)^{1/2} \, dE_1 \quad \alpha \quad E_{tr}^2 \, ,$$

where E_{tr} is the total translational energy, E_1 is the translational energy corresponding to one relative velocity vector, and $(E_{tr} - E_1)$ is the translational energy of the second relative velocity vector.

25 K.P. Huber and G. Herzberg, *Molecular Spectra and Molecular Structure IV. Constants of Diatomic Molecules* (New York, Van Nostrand Reinhold, 1979).